
University of Strathclyde

Renewable Energy Marine Structures - Centre for Doctoral Training

Department of Naval Architecture, Ocean, and Marine Engineering

# Fracture Mechanics Analysis of Offshore Wind Turbine Monopile Structures for Lifetime Extension

Ayodele Fajuyigbe

A thesis submitted in partial fulfilment of the requirements for the degree of Doctor of Engineering

2022

Supervisor: Professor Feargal Brennan

## DECLARATION OF AUTHENTICITY AND AUTHOR'S RIGHTS

This thesis is the result of the author's original research. It has been composed by the author and has not been previously submitted for examination which has led to the award of a degree.



Ayodele Fajuyigbe

September 2022

## STATEMENT ON PREVIOUSLY PUBLISHED WORK

In the course of this thesis, a number of papers are published in scientific journals or are still under review at the time of writing. The author of this thesis was and is in all these publications - even if the paper is co-authored - the main responsible person. The author's contributions to the publications, thus, comprise conceiving the works, administering the studies, realising the works, performing literature studies, developing the methodologies, performing the researches, developing and applying the approaches, working with and extending the software, curating the data, verifying and validating the methods and results, analysing and investigating the data and results, post-processing and visualising the results and findings, writing the papers and preparing the original drafts, interacting with the journals' editors and reviewers, as well as reviewing and editing the papers for the final publications.

Ayodele Fajuyigbe

September 2022

## ABSTRACT

As more early offshore wind farms reach the end of their design life, the wind industry needs to prepare for end-of-life decision making for offshore wind turbine (OWT). One idea gaining traction is lifetime extension, that is, operating an OWT monopile beyond its original lifetime if it can be shown that the monopile possesses structural reserves. Currently, the industry practise is to establish the extent of structural reserves by repeating the initial S-N fatigue calculation with updated actual environmental data, turbine operational data and improved simulation tools. However, this approach does not allow the integration of inspection results as the S-N calculation encapsulates the three stages of a structure's fatigue life into a single value.

Monopiles are large, welded structures. Thus, it is likely that an aged monopile already has a crack initiated. There may actually be multiple cracks on the same plane due to manufacturing defects from the time of fabrication or due to loading. Therefore, later life fatigue calculation must focus on the crack propagation phase. Crack propagation is analysed using fracture mechanics. It requires the calculation of stress intensity factor (SIF) which is a function of structure geometry, crack geometry and the applied load. The SIF can be obtained from handbook solutions for simple cases or by finite element analysis for complex cases. However, SIF by finite element analysis (FEA) is not practical for fatigue load cases because the procedure is computationally expensive. It has been shown that the SIF provided in handbooks is imprecise for large diameter pipes.

This thesis investigated fracture mechanics approach to assessing the integrity of OWT monopiles with multiple cracks. The thesis proposes that suitability of cracked OWT monopile be assessed using a failure assessment diagram (FAD). The FAD simultaneously assesses both brittle failure and plastic collapse. The core of this thesis is twofold:

1) the development of an efficient and accurate method to calculate the SIF of an OWT monopile containing a semi-elliptical external surface crack subjected to arbitrary stress loading. The SIF is integral to the assessment of brittle failure. The approach proposed in this thesis is based on the theory of weight functions.

2) the development of a simplified and accurate methodology for calculating the plastic collapse (limit) bending moment load of an OWT monopile with external circumferential flaws. The limit load is integral to the assessment of plastic collapse. The proposed methodology is based on net section collapse (NSC) theory.

Both methods allow the assessment of multiple cracks. For SIF, a new equation for the interaction of SIF between co-planar, circumferential, semi-elliptical, external surface flaws located in offshore wind turbine monopile is also derived. The effect of multiple cracks on plastic collapse is explicitly captured in the methodology for obtaining the limit load.

As part of this thesis an application was written using the Visual Basic .Net programming language that incorporates the proposed methods. The new application is tested with two case studies to demonstrate its performance. The case studies demonstrate fast and accurate assessment of the integrity of cracked OWT monopiles. The results of this thesis provide a clear demonstration of the fracture mechanics approach to assess OWT monopiles for lifetime extension.

## ACKNOWLEDGEMENTS

***

"No man is an island entire of itself".

***

The completion of this thesis owes a debt of gratitude to many wonderful individuals.

I would like to thank my supervisor, Professor Feargal Brennan for his guidance, patience and being an inexhaustible ocean of calmness.

I would like to thank Robel Yoseph for being an ally in the battle against VB .net.

I would like to thank Kingsley Sunday for always being there.

I would like to thank Charley Fajuyigbe for listening to four years of my wind turbine rants.

I would like to thank everyone on the Renewable Energy Marine Structures centre for doctoral training.

Most importantly, I give thanks to God, through whom all things are possible

***

Wisdom seeks Knowledge

****

This thesis is dedicated to Master Ifeoluwa Fajuyigbe in whom my hope for the future finds nourishment.

## TABLE OF CONTENTS

## LIST OF FIGURES

## LIST OF TABLES

# 1 NOMENCLATURE

## 1.1 Symbols

| | |
|---|---|
| $\alpha$ | Wind shear exponent |
| $a$ | Crack depth |
| $a/c$ | Crack Aspect ratio |
| $a_c$ | Critical crack depth |
| $C$ | Crack growth parameter |
| $da$ | Crack growth for a given number of stress cycles |
| $dN$ | Number of cycles |
| $E$ | Youngs' modulus |
| $Hs$ | Significant wave height |
| $\Delta K$ | Difference in SIF at the maximum and minimum stress positions. |
| $K_r$ | Brittle ratio |
| $L_r$ | Load ratio |
| $m$ | material coefficient |
| $n_i$ | number of cycles at stress level i |
| $N_i$ | fatigue life cycles at stress level i |
| $P_L$ | Plastic Limit load |
| $r_i$ | Monopile inner radius |
| $r_o$ | Monopile outer radius |
| $\sigma$ | Stress |
| $\sigma_{ref}$ | Reference stress |
| $\sigma_u$ | Ultimate tensile strength |
| $\sigma_y$ | Yield strength |
| $S$-$N$ | Stress range - number of cycles |
| $\vartheta$ | Crack half angle |
| $t$ | Monopile thickness |
| $T_p$ | Peak period |
| $T_z$ | Average zero up-crossing period |
| $Y$ | Shape function |
| $z$ | Elevation |

## 1.2 Abbreviations

| | |
|---|---|
| ACFM | Alternating Current Field Measurement |
| ADCP | Acoustic Doppler Current Profilers |
| CDF | Critical Driving Force |
| DNV | Det Norske Veritas |
| DNVGL | Det Norske Veritas - Germanischer Llyod |
| EC | Eddy Current |
| ECA | Engineering Critical Assessment |
| FAD | Failure Assessment Diagram |
| FAL | Failure Assessment Line |

| | |
|---|---|
| FE | Finite Element |
| FEA | Finite Element Analysis |
| FEM | Finite Element Method |
| FMD | Flooded Member Detection |
| IEC | International Electrotechnical Commission |
| LEFM | Linear Elastic Fracture Mechanics |
| MPI | Magnetic Particle Inspection |
| NASA | National Aeronautics and Space Administration |
| NDT | Non Destructive Testing |
| NREL | National Renewable Energy Laboratory |
| NSC | Net Section Collapse |
| OWT | Offshore Wind Turbine |
| PoD | Probability of Detection |
| RUL | Remaining useful life |
| SCADA | Supervisory control and data acquisition |
| SIF | Stress Intensity Factor |
| WFD | Widespread Fatigue Damage |
| X-FEM | Extended finite element method |

# 2 INTRODUCTION

## 2.1 Background and Problem Statement

On the 6th of March 2021 Denmark met 99% of its demand for electricity with wind power [1]. A Similar impressive uptake of wind power can be observed in many countries in Europe and in the world. This makes it abundantly clear that wind energy is and will continue to play a key part of our energy landscape.

The rise of wind power has its origins in the oil shortages of the 1970s which sparked interest in alternative energy sources for commercial purposes. Between 1970 to 1990, several experiments in wind energy generation were undertaken under the direction of NASA, leading to invaluable research results that culminated in the construction of the first commercial offshore wind farm in Vindeby, Denmark, in 1991. According to WindEurope [2], the use of offshore wind has steadily increased, with leading countries such as Denmark, England and Germany generating up to 50% of their wind power from offshore.

Typically, wind turbines are designed for 20-25 years of operation, which means that the turbines installed in the 1990s have reached the end of their service life. Ziegler [3] comments that with the increased installation of offshore wind turbines in the late 90s and early 2000s, the wind industry needs to prepare for upcoming challenges, such as maintenance of aging assets, assessment of structural integrity, lifetime extension decision making, and decommissioning of turbines.

For an OWT structure approaching its end of life, there are typically three options available: repowering, decommissioning, and lifetime extension (Figure 2.1). Decommissioning is the least desirable option as it removes the value of the asset. The most attractive of these three options is probably lifetime extension, i.e. operating the monopile beyond its original lifetime. The option of extending the life of an offshore wind farm is growing in popularity as many of the structural and logistical issues associated with repowering are explored.

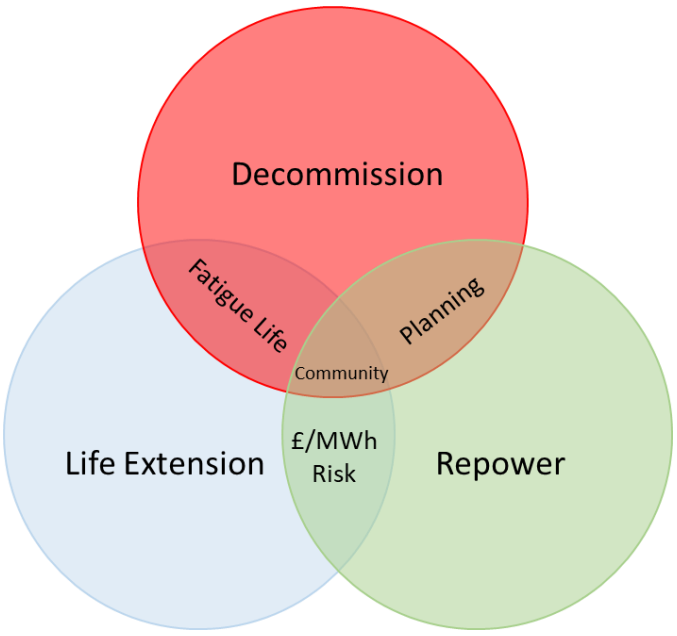


**Figure 2.1 – End-of-Life Decision Making**

Monopile support structures represent the largest portion of currently installed OWT support structures [4]. OWT monopiles are fabricated by rolling and then welding thick structural steel plates longitudinally to create “cans” that are then welded together circumferentially to achieve the desired length. OWT monopiles are exposed to constant cyclic loading causing fatigue to be the driving limit state. As such, lifetime extension is only possible if the monopile has fatigue structural reserves at the end of the design lifetime.

## 2.2 Research Gap and Objectives

There is little experience in the re-assessment of OWT monopiles to support operation beyond the initial design lifetime. In 2016, certification body DNVGL produced a general guideline DNVGL-ST-0262 [5] on lifetime extension of the entire wind turbine. The guideline proposes a two-part process: the first is an analytical part involving new and/or additional damage calculation for the wind turbine, considering the site-specific installations and its local conditions. The second is a practical part consisting of assessment by inspection of the wind turbine taking into account the maintenance/operational history and the turbine type related field experience. DNVGL has also produced a guideline, DNVGL-SE-0263 [6], for the certification of lifetime extension of wind turbines. However, the guidelines do not provide a specific structural analysis framework for completing the lifetime extension process.

Recent research work such as that by Pakenham et al. [7], Rubert et al. [8] and Nielsen et al. [9] focuses mainly on economic decision making methods for lifetime extension. There is scant work exploring a reasonable and reliable methodology for structural assessment of a monopile nearing the end of its design life with the view of lifetime extension. This is because most research assume that structural fatigue analysis component of lifetime extension simply involves repeating the initial S-N fatigue assessment with actual site conditions, actual turbine operation and environmental loads. This approach ignores some inherent issues (discussed subsequently) in using S-N data to design monopiles. Key among these is the inability to integrate fatigue assessment by S-N approach with inspection capabilities. Inspection results are critical for validating the integrity of monopiles operating beyond their initial certified design life. The importance of a coherent inspection planning strategy in the prolonging of life of key wind turbine components such as welds is discussed by Munoz [10]. The integration of inspection with fatigue calculation further enables the development of the damage tolerance capability of a wind turbine. Design for damage tolerance is already well established in other fatigue-susceptible industries such as aviation as discussed by Swift [11].

There is some work; Ziegler [12] , Amirafshari et al. [13] examining the structural framework for remaining useful life of monopiles using fracture mechanics. However, these only provide brief description of the analysis methodology. Furthermore, Ziegler [12] as with other work on fatigue damage of monopiles consider fatigue failure due to a single dominant crack. An aged structure is likely to contain multiple cracks. Any serious consideration of operation beyond initial design life must assess these structures with multiple cracks. The effect of multiple cracks on an aged structure is well known in other industries such as aerospace, where it is referred to as ‘widespread fatigue damage (WFD)’. The inclusion of multiple cracks is a novelty for the fatigue assessment of offshore wind turbine monopiles.

The continued operation of a wind turbine monopile beyond its initial design life requires continuous verification of its structural integrity. It must be clearly demonstrated to all stakeholders that the monopile can continue to withstand imposed loads for the period of the lifetime extension. While metals may be subject to a myriad of material damage mechanisms, the key damage mechanism of OWT monopiles considered in this work is fatigue eventually leading to failure by fracture or plastic collapse. Therefore, the aim of this work is to provide an accurate framework/tool for assessing the integrity of cracked structures subject to fatigue loading taking, account of the recommendations in DNVGL-ST-0262 [5]. To deliver this aim, the following objectives are defined for this thesis:

1) Propose a methodology for assessing the fatigue crack growth of OWT monopiles containing multiple flaws.

2) Propose a methodology for assessing the susceptibility of the monopile to plastic collapse considering multiple flaws.

3) Propose a methodology for assessing the susceptibility of a monopile to fracture considering multiple flaws.

## 2.3 Thesis Structure and Publications

This thesis consists of a portfolio of work addressing the above objectives which have been published in peer-reviewed journals. The publications form the basis of the various sections of this thesis as described below

Section 2 introduces the problem at the core of the thesis as well as the research objectives. A literature review is presented in Section 3.

Section 4 of this document is based on the paper examining the procedure for flaw acceptability assessment through a case study of a semi-elliptical surface crack in an offshore monopile as it grows till it forms a through thickness crack. Using the procedure prescribed in an industrial standard (BS 7910), the fracture ratio, $K_r$ is shown to increase monotonically with increasing crack depth. The load ratio, $L_r$, is initially insensitive to the crack depth. However, there is a rapid increase in $L_r$ when the crack depth to thickness ratio exceeds 80%. $L_r$ values obtained from detailed 3D FE limit analysis using elastic perfectly-plastic material behaviour do not exhibit the asymptotic behaviour predicted by BS 7910 as the flaw transitions from deep crack to through-thickness crack. Furthermore, $K_r$ predicted by BS 7910 is shown to be imprecise for the typical dimensions of offshore monopiles. The findings suggest that a surface breaking defect may be identified as unacceptable based on BS 7910 when there may still be a non-trivial amount of structural residual life. This is a concern for monopiles where crack growth as a large flaw forms a significant part of the total life.

Section 5 of this document is based on the paper proposing a methodology for calculating the plastic collapse (limit) bending moment load of a pipe with a circumferential flaw with an emphasis on its application for use in the assessment of cracked offshore wind turbine monopile using failure assessment diagrams. The proposed methodology is based on the theory of net section collapse (NSC) but differs from existing approaches in that it does not

need idealisation and categorisation of the crack before assessment. The proposed methodology is validated against results presented in literature and also finite element analysis results. Although it is possible to obtain limit loads using FEA, this is computationally expensive and time consuming. The proposed approach allows for near instantaneous calculation of limit load for any arbitrary crack configuration and loading direction.

Section 6 of this document is based on the paper proposing a methodology for calculating the stress intensity factor (SIF) of an offshore monopile containing a semi-elliptical external surface crack subjected to a combination of bending and tensile stress distribution. The approach is based on the theory of weight functions. The proposed methodology is validated against results presented in literature and also bespoke FEA The proposed methodology is significantly faster than conventional finite element fracture mechanics analysis.

Section 7 is based on the paper investigating the interaction between co-planar, circumferential, semi-elliptical, external surface flaws located in OWT monopiles. The interaction is characterised through its influence on the stress intensity factor (SIF) obtained from linear elastic fracture mechanics (LEFM). SIF is a key parameter in assessing the suitability of cracked monopiles as it is used in the plotting of the fracture ratio, Kr on a failure assessment diagram (FAD).

The VB.net application developed based on the methodologies proposed in sections 5 and 6 is introduced and discussed in section 8. The application is tested with some case studies discussed in section 9 and 10. Conclusions and recommendations from the research work are presented in section 11.

# 3 LITERATURE REVIEW

## 3.1 OWT Foundations

Every OWT requires a support structure whose basic function is to keep it in place. The support structure is divided into two parts: the turbine tower and the foundation. Offshore foundations can either be fixed or floating. For fixed OWT foundations, there are several available concepts such as tripod and jacket (steel structures) or concrete gravity bases. The selected concept for any wind turbine is generally based on the operational water depth.

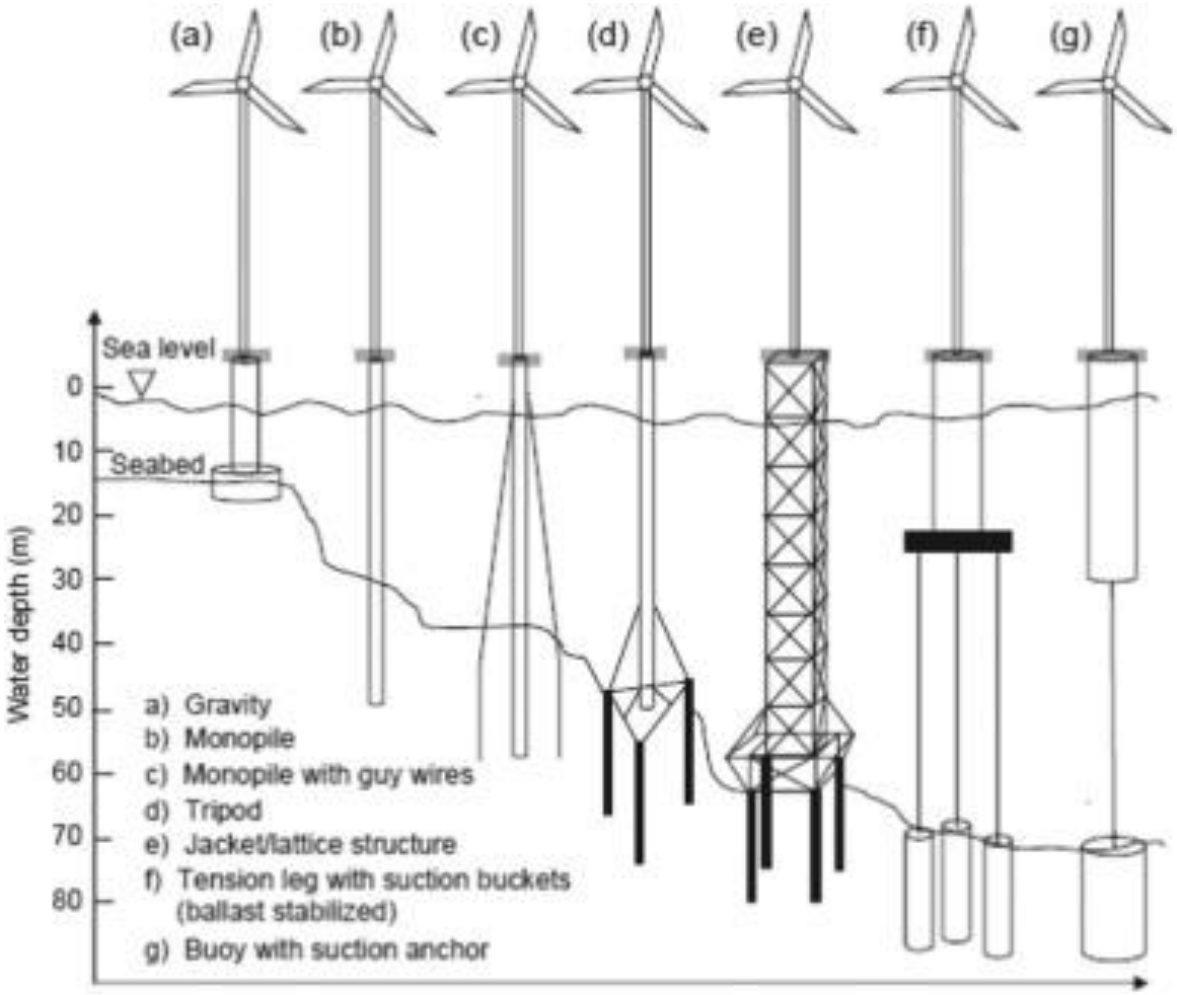


**Figure 3.1 – Typical Foundations of Offshore Wind Turbines [14]**

The development of onshore wind quickly revealed a bottleneck in the availability of suitable locations on land. For many countries, the logical step was to explore suitable locations near-shore in shallow water. The commercial offshore industry grew out of this move such that most offshore wind farms are located on the continental shelf. Wu et al. [15] state that the majority of offshore wind farms are located on the continental shelf, about 10km off the coast in shallow water depths. Floating OWT provide access to deeper water than fixed-bottom wind turbines, but a review of floating offshore wind turbines by Muskulus and Stewart [16] found that most floating turbines are in development stage. However, due to a mix of favourable government policies and increasing investments, the floating wind sector is making the transition from pre-commercial to commercial projects.

At present, fixed-bottom OWT represent the largest market. As shown in Figure 3.1, the main types of fixed foundations are gravity, tripods, jackets and monopile foundations. Nogueira et al. suggest [17] that gravity foundations are potential solutions for OWT located in shallow water depths with hard soils which are difficult to penetrate. Gravity bases are typically simple reinforced concrete caisson structures designed according to their self-weight, which must be sufficient to resist extreme overturning moments. Additional checks on soil bearing capacity and horizontal sliding resistance are also required. Gravity foundations were used in early wind farms such as Vindeby (1991), Tunø Knob (1995), Middelgrunden (2001), Nysted (2004) and Sprogø (2009) in Denmark, Lillgrund (2008) in Sweden, and Thorntonbank (2009) and Belwind (2011) in Belgium [15].

A tripod structure comprises a main pipe and three legs. Tripod foundation structures are constructed in transitional water depths (between 30 and 50m). Zaaijer [18] compared a number of turbine foundation designs and found that tripods are less resonant with waves and provide more opportunities to tune the natural frequency. Jacket foundations are also used in similar water depths to tripods. They comprise of steel framework usually anchored in the seabed with piles and are often preferable to the tripod concept in terms of scour, ship collision and deflection at tower top. Whilst they may be used in deeper waters than gravity foundations, both tripods and jacket create complicated geometry at the intersection of members [19]. Examples of wind farms utilising tripod foundations are Alpha Ventus, Germany (2010) [19] and Nogersund, Sweden (1990) [20]. Examples of wind farms utilising jacket foundations are Alpha Ventus, Germany (2010), Beatrice, UK (2006), and Ormonde, UK (2012).

Installation in a shallow water and the simplicity in design, fabrication and installation perhaps explains why monopiles are the most common type of fixed-bottom foundations used for OWT. Approximately 90% of existing offshore wind turbine foundations are monopiles as reported by Ho et al. [21]. OWT monopiles are fabricated by rolling and then welding thick structural steel plates longitudinally to produce “cans” which are then welded together circumferentially to achieve the desired length. The diameter, thickness, and length of the monopile is the output of the foundation design process conducted by a foundation or geotechnical engineer. Guidance on the design of the support structure is given in industry codes such as DNVGL-ST-0126 [22]. An example design procedure for OWT monopiles is provided by Arany et al. [23]. In summary, the key parameters of the monopile are broadly obtained from the following considerations:

1) LeBlanc et al. [24] state that the length of the monopile is typically governed by the overturning capacity under extreme conditions, or the maximum allowable tilt of the turbine over its lifetime due to accumulated rotations from cyclic loads

2) Kallehave et al. [25] find that the diameter of the monopile is driven by the required fundamental frequency of the turbine. This frequency is dependent on the interaction of the pile and soil

3) The wall thickness is governed by two factors:
   a) The required value to prevent shell buckling during installation and/or extreme events

b) The required value to generate the desired fatigue life for the structure under fatigue loads.

There are various research work and publications into the design considerations of monopile foundations. For instance, Gupta and Basu [26] compare accuracy and computational efficiency of typical analytical theories employed in the design of monopiles, Brennan and Tavares [27] discuss the origins fatigue analysis methodology for monopiles and Bryne et al. [28] present some recent advances in the modelling of soil-monopile interaction arising from the Pile Soil Analysis (PISA) project.

According to DNVGL-ST-0126 [22], the design of a monopile (OWT support structure) must satisfy four limit states; ultimate, accidental, serviceability, and fatigue. A limit state is a condition beyond which a structure or structural component will no longer satisfy the design requirements. The ultimate limit state corresponds to the maximum load-carrying resistance of the monopile. This typically refers to the capability of the monopile to withstand loads imposed under extreme events. The accidental limit states correspond to failure due to rare accidental loads, for instance collision with boats. The serviceability limit state corresponds to tolerance criteria applicable to normal use. For monopiles, this may mean a limit of the acceptable deflection of the structure under imposed loads. The fatigue limit state corresponds to failure due to dynamic loads. Fatigue is the slow deterioration of the monopile steel due to continuous varying loads over time.

While the initial design of a monopile must satisfy the ultimate, serviceability and accidental limit states, the calculation of remaining lifetime of a monopile can only depend on the fatigue limit state as it is the only limit state that is cumulative in nature.

## 3.2 Monopile Fatigue Loads

OWT monopiles are exposed to three key environmental loads: wind, waves and current. Design standards such as DNVGL-ST-0437 [29] and IEC 61400-3 [30] provide guidance on the combination of these loads to be considered under fatigue assessment. Since the required lifetime of the turbine is 20-25 years, long-term distributions of these loads are required. The design conditions are typically summarised and provided in a design basis such as the exemplar provided by Natarajan et al. [31].

The wind data is gathered in bins to minimise the number of load cases. Typical bin sizes cover a range of 2m/s. The binning of the data is done such that the windspeed corresponding to a bin of specific value, for instance 4m/s, contains all wind speed observations ranging from ≥3m/s to <5m/s as shown in the Upwind design basis produced by Fischer et al. [32]. The wind speed is usually given for a particular elevation, for example at hub height, the wind speed at any other elevation is determined by:

$$V(z) = V_{targ}\left(\frac{z}{z_{targ}}\right)^{\alpha} \quad 3.1$$

Where:
$V(z)$ is the wind speed at elevation z
$z$ is the elevation
$V_{targ}$ is the known wind speed at the known height (typically the turbine hub)

$z_{targ}$ is the elevation of the known $V_{targ}$
$\alpha$ is the wind shear exponent for the turbine location.

The wind speed values are for static conditions. Fatigue analysis requires stochastic wind, so an appropriate turbulence model is required to generate a stochastic wind time series. IEC 61400-3 [30] recommends a normal turbulence model (NTM) with the details of that model provided in IEC 61400-1 [33].

The long-term wave loads are usually gathered in tables (scatter diagrams) showing significant wave height ($H_s$) and period ($T_p$ or $T_z$). An example of a scatter diagram is shown in Figure 3.2. Tempel [34] notes that such a wave scatter diagram is available for every wind speed bin. A 3D scatter diagram showing the simultaneous occurrence of wave height, period and wind speed can also be generated. The scatter diagrams do not account for directionality; therefore, additional diagrams are needed to show the spreading of wave directions per wave height bin. The wave directions are typically assembled in a wave rose which show the number of waves for various cardinal directions. An example of a wave rose taken from the Upwind design basis [32] is shown in Figure 3.3. Similar rose diagrams are created for the wind data.

| $H_s$ (m) | $T_z$ (s) | | | | | | | | Sum |
|---|---|---|---|---|---|---|---|---|---|
| | 0–1 | 1–2 | 2–3 | 3–4 | 4–5 | 5–6 | 6–7 | 7–8 | |
| 6.5–7.0 | | | | | | | | | 0.0 |
| 6.0–6.5 | | | | | | | | 0.1 | 0.1 |
| 5.5–6.0 | | | | | | | 0.1 | 0.1 | 0.2 |
| 5.0–5.5 | | | | | | | 0.1 | 0.1 | 0.2 |
| 4.5–5.0 | | | | | | | 1 | | 1.0 |
| 4.0–4.5 | | | | | | | 4 | | 4.0 |
| 3.5–4.0 | | | | | | 4 | 5 | | 9.0 |
| 3.0–3.5 | | | | | | 19 | 0.1 | | 19.1 |
| 2.5–3.0 | | | | | 0.1 | 38 | | | 38.1 |
| 2.0–2.5 | | | | | 27 | 43 | | | 70.0 |
| 1.5–2.0 | | | | 0.1 | 115 | 5 | | | 120.1 |
| 1.0–1.5 | | | | 6 | 220 | 1 | | | 227.0 |
| 0.5–1.0 | | | | 236 | 145 | 1 | | | 382.0 |
| 0.0–0.5 | 1 | | 1 | 113 | 14 | 0.1 | | | 129.2 |
| Sum | 1.0 | 0.0 | 1.0 | 355.1 | 521.1 | 111.1 | 10.4 | 0.3 | 1000 |

**Figure 3.2 – Wave Scatter Diagram with Occurrence in Parts per Thousand [34]**

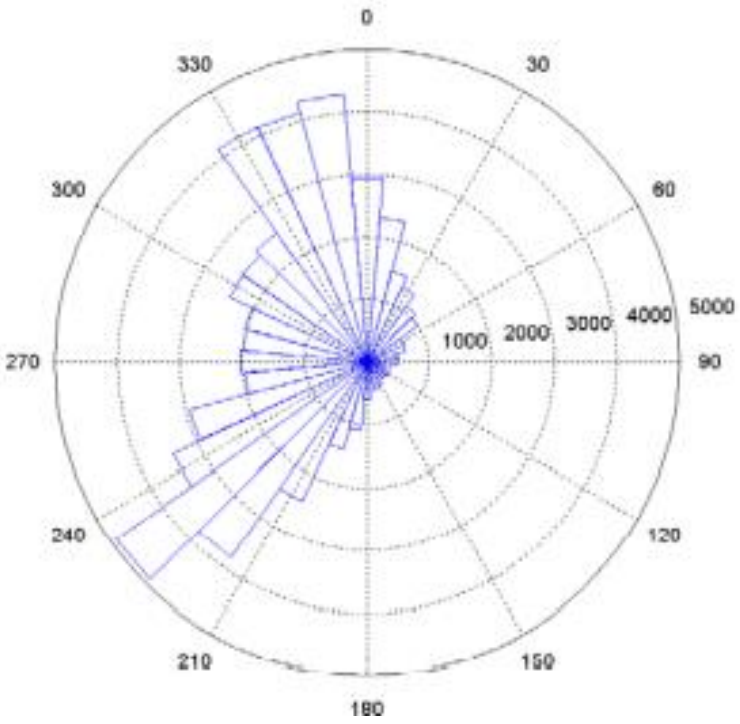


**Figure 3.3 – A Typical Wave Rose [32]**

For each $H_s$, $T_p/T_z$ combination, irregular waves are generated using empirical spectral relationships such as the Joint North Sea Wave Project (JONSWAP) spectrum proposed by Hasselmann et al. [35]. The various combinations of wave height, wave period, wave direction, irregular seed realisations, wind speed, wind direction as well as differing environmental conditions and bathymetry across the wind farm can lead to a very large number of numerical analyses. Typically, the amount of data is reduced by binning. Ziegler at al. [36] further note that the turbines in a wind farm are clustered around conservative design positions. This inevitably leads to some conservatism in the numerical solution for individual turbines.

To calculate the fatigue life of the structure, the loads presented above must be run through some form of numerical simulation software to generate stress time histories at locations of interest. Typically, numerical finite element simulations are used to determine the stress loads on an OWT monopile for a set of site-specific conditions (wind, wave, soil). For large wind parks, the site-specific conditions are typically clustered to minimise the size of the design envelope as noted in various publications on the simulation of OWT wind turbine loads by Ziegler at al. [36], Vorpahl et al. [37] and Seidel [38]. OWT design is typically completed using two models. The first model comprises the turbine and tower structure and is developed by the turbine manufacturer. The second model is of the foundation and is developed by the foundation designer. The response of turbine depends on the monopile and vice versa. The interaction between the two models is represented by a cold link, containing loads, stiffness, or equivalences. Several iterations of the analysis are required to optimise the solution. Fischer and Vries [39] note that an integrated model may improve this process but requires the turbine and foundation designers to work on the same model which may not be commercially practical when they are two independent contractors. There are various codes and tools for performing fully coupled aero-hydro-servo-elastic

simulations of an OWT in an integrated manner such as Bladed [40] and OpenFast (formerly known as Fast) [41].

As the initial fatigue design is looking into the future, the fatigue design of an OWT monopile is based on forecasted future aerodynamic and hydrodynamic loads. There are inherent uncertainties associated with forecasting. Therefore, for lifetime recalculation, it is preferable to update the environmental loads with measured loads where available for the period up to the time of re-calculation. However, uncertainties in the forecast of future load conditions still remain. There are several methods for obtaining the actual environmental loads experienced by an OWT monopile. General wind conditions can be measured using anemometers and wind vanes mounted on meteorological masts. Individual turbines are equipped with a supervisory control and data acquisition system (SCADA) which record environmental (wind speed, direction), electrical and turbine control parameters (blade angles, rotational speed). Wymore et al. [42] provide a survey of health monitoring systems for wind turbines. Udo and Muhammad [43] discuss the specific use of SCADA data to perform predictive maintenance of wind turbines whilst Gonzalez et al. [44] provide exemplar statistical assessment of SCADA data for three wind farms. Wave and current data can be measured using a range of technologies such as wave rider buoy, acoustic doppler current profilers, high frequency radar. Emmanuel et al. [45] provide an overview of recent technologies for wave and current measurement. Rossi et al. [46] discuss the various techniques involved in the measurement of sea waves.

An alternative approach to FE simulation is the direct monitoring of the moments and stresses at target locations of the OWT monopile. Axial, bending, and torsional stresses may be obtained using an array of strain gauges installed at positions of interest. While there is a direct and reliable correlation between the measured strain data and fatigue loads, cost implications prohibit the installation of strain gauges at all locations of interest. Faulkner et al. [47] discuss the challenges of installing structural health monitoring systems in challenging environments. Furthermore, although new monopiles are now being fitted with strain measurements from installation, and therefore enabling data to be generated from day one, it is impractical to fully instrument monopiles already installed in the seabed. Further practical challenges to the fatigue monitoring of offshore monopiles is discussed by Brown et al. in [48]. Luengo et al. [49] discuss statistical analysis of structural health monitoring data including pattern recognition.

Pattern recognition often forms the basis of various virtual sensing techniques that may be used to estimate loads at unmeasured hotspots for individual turbines and across the wind farm. Ziegler at al. [50] provide a strain based extrapolation algorithm for load estimation for non-instrumented hotspots based on data recorded from more accessible locations. Henkel et al. [51] and Iliopoulos et al. [52] achieve similar stress estimation using multi-band modal expansion and a calibrated finite element model to reconstruct the full-field response based on accelerometers and strain sensors installed at a few easily accessible locations. Noppe et al. [53] compare the modal expansion to a technique based on a Kalman filter and find both to produce a good match in the time domain. Bouty et al. [54] take a wider view to examine the possibility of extrapolating the results from fatigue assessment of wind turbines at selected design positions to other wind turbines in the farm.

For lifetime assessment of OWT support structures, it is likely that a combination of numerical simulations calibrated with long term direct measuring campaigns will be required as suggested by Loraux and Brühwiler [55]. Furthermore, it is the author's expectation that while numerical analysis to predict possible lifetime extension may be conducted, operation beyond the initial design life would need a process for continuous validation of predicted behaviour. There are uncertainties and changes to design parameters that cannot be reasonably determined from numerical analysis. For example, results from a measurement campaign at the Walney Offshore Wind Farm by Kallehave et al. [25] discovered that there was an under-prediction of system natural frequency due to inaccuracies in the evaluation of the pile-soil stiffness. More recently, research by Ma et al. [56] suggests that under numerous load cycles during the lifespan of the monopile, the foundation stiffness may change. The foundation stiffness affects the natural frequency of the system and has a significant impact on fatigue life.

## 3.3 S-N Fatigue Design

Once the stress signal for locations of interest is established, the corresponding fatigue damage can be determined. There are three stages to the fatigue life of any structure: *crack initiation* (caused by microstructural process), *crack propagation* (steady growth due to continued cyclical stresses) and *crack failure* (accelerated growth leading to fracture) as laid out by Stephens et al. [57]. As specified in DNVGL-ST-0126 [22], the initial fatigue design of support structures such as monopiles is completed using S-N curve analysis typically following guidelines set out in industry standard DNVGL-RP-C203 [58]. S-N curves define the number of cycles to failure (N) when a material is repeatedly cycled through a given stress range (S). Most S-N curves are determined in laboratories where small-scale test specimens are subjected to constant amplitude stress until failure. Given a suitable number of tests, it is then possible to fit a curve to the test dataset with the formula:

$$log_{10}N = log_{10}a - mlog_{10}S \tag{3.2}$$

Typically, the curves are drawn to ensure a probability of survival of 97.7% corresponding to 2 standard deviations above the mean of the test data. Standard S-N curves that are classified into groups which take into account the type of material, weld geometry stress direction, and the surrounding environment are available in industrial standards such as BS 7910 [58]. The double sided butt welds used to join the "cans" together to form the monopile are typically of 'class D' as specified in DNVGL-RP-C203 [58].

The OWT monopile is subject to stochastic stress loading due to dynamic variations in the wind and wave loads. The time history of stress loading is counted to obtain corresponding stress ranges and number of cycles. There are various possible cycle counting techniques but by far the most popular is the rainflow counting technique first introduced in 1968 by Matsuishi and Endo [59], and mathematically defined by Rychlik [60]. The "rainflow" is named in comparison to flow of rain falling down a pagoda roof and is the first accepted method used to extract closed loading reversals or cycles.

The accumulated damage for each stress range is the ratio of the counted number of cycles to the total number of cycles to failure predicted by the S-N curve for that stress range. The total damage (D) is determined according to Palmgren-Miner rule:

$$D = \sum_{i}^{k} \frac{n_i}{N_i} \qquad 3.3$$

Where:
$k$ is the number of stress ranges
$n_i$ is the number of cycles at stress level $i$
$N_i$ is the fatigue life cycles at stress level $i$

The Palmgren-Miner rule is based on linear damage accumulation. This allows the simplification of stochastic load time series into a single damage equivalent load (DEL). DEL is a constant load range such that when it is applied for a specific number of reference cycles, it causes the same amount of fatigue damage as the stochastic load time series. This approach is sometimes further extended into lumping the environmental loadcases to select a reduced set of loadcases that captures the OWT dynamics and fatigue damage whilst reducing computational efforts as discussed in Katsikogiannis et al. [61].

Based on equation 3.3, the structure is deemed suitable if D<1 for the design lifetime. It is noted that multiplication factors, termed Design Fatigue Factors (DFF), are typically applied to the characteristic cumulative fatigue to ensure that, even at the end of the design life, the probability of failure is below a target level. DFF is applied to individual structural details to account for inspection/repair plan and the reliability of inspection method, failure mechanism, and associated consequences. Furthermore, for fatigue analysis using S-N approach, DFF may be used to account for uncertainties in random loading and the assumption of linear damage accumulation that is inherent in the Palmgren-Miner rule. Equation 3.3 assumes that the damage accrued is independent of the load sequence. It has been observed experimentally that crack growth slows after high stress cycles. Work by researchers such as Newman [62] suggest that the crack growth retardation may be due to crack-closure effects. Other researchers, such as Wheeler [63], suggest it may be down to the size of the plastic zone in front of the crack tip. For either explanation, the net effect is that the location of the occurrence of high stresses in the stress time history may impact the crack growth.

For lifetime extension, D must remain below 1/DFF for the duration of the lifetime extension. Since the initial design of the monopile is likely to have used D=1/DFF as the target design lifetime, the reassessment of an OWT turbine for lifetime extension such as specified in DNVGL-ST-0262 [5] is predicated on the turbine being operated under operating and environmental conditions that comply with, or are more benign than, the original design conditions. However, large uncertainties are normally associated with fatigue life assessments and thus conservatisms in the selection of DFF in the initial fatigue design that may be grounds for lifetime extension. This is to say that, although the initial fatigue design of the monopile may have considered the achievement of D=1/DFF at the end of the 20 year design life, a conservative DFF used to counteract uncertainties in the design data or process

may mean that the monopile may be at a value of D < 1/DFF at the end of the initial design life.

Another source of conservatism may be in the S-N curve data itself. Brennan and Tavares [27] identified several issues with the use of historic S-N curve data for the design of monopiles. These include questions on the applicability of the specimen sizes and the out-of-date information on improvements in advanced fabrication, quality control, and inspection techniques. Brennan and Tavares [27] argue that S-N curve original designed for small diameter oil and gas systems may not be appropriate when applied to the fatigue design of OWT monopiles.

Monopiles are welded structures so are likely to spend most of their lives in the crack propagation stage due to the ready initiation of cracks caused by weld defects. Furthermore, a candidate for lifetime extension (aged structure) is expected to be well in the crack propagation phase. It is therefore necessary to be able to assess the crack propagation phase and lead up to brittle fracture without the need to consider the time spent at crack initiation. Fracture mechanics provides a useful tool for assessing the crack propagation of a flawed structure using models derived from experimental test results.

## 3.4 Fracture Mechanics Fatigue Design

Fracture mechanics is the field of mechanics concerned with the study of the propagation of cracks in materials. It uses methods of analytical solid mechanics to calculate the driving force on a crack and those of experimental solid mechanics to characterise the material's resistance to fracture. There is interesting background to the development of the field of fracture mechanics in various literature such as [64-66]. Anderson [64] discussed the theory and applications of linear and nonlinear fracture mechanics. His initial technical report on the matter is expanded into a popular and comprehensive book by the same title which is currently on its 4$^{th}$ edition. Gross [65] provides an interesting and concise history of the field of fracture mechanics mainly starting from the work of A.A. Griffith on the theory of rupture but also with some musings on evidence of scientific consideration of fracture from the Renaissance period. More recently, Ritchie and Liu's book [66] on introduction to fracture mechanics informs the reader on how fracture mechanics work and provides practical direction for the use of fracture mechanics in damage-tolerant design.

A crack grows under the application of cyclic loading. There are several proposed fracture mechanics models to capture the relationship between the applied loading and the crack growth. The most widely used of these models is Paris' law which defines the relationship between crack growth and the stress intensity factor (SIF) [67]. There are various representation of Paris' law, but the simplest version is as follows:

$$\frac{da}{dN} = C(\Delta K)^m \qquad 3.4$$

Where:

$da$ is the crack growth for a given number of stress cycles
$dN$ is the number of cycles
$C$ is the crack growth parameter

$m$ material coefficient
$\Delta K$ is the difference in SIF at the maximum and minimum stress positions.

$C$ and $m$ are obtained experimentally. The SIF describes the stress state at the crack tip. The SIF depends on the applied load and gross geometrical features of the cracked structure. The general form of the SIF as described in industry standard BS 7910 [68] and Newman [69] is:

$$K = \sigma . Y \sqrt{\pi a} \quad 3.5$$

Where:
$\sigma$ is the remotely applied stress
$Y$ is the geometry factor

There are three modes of fatigue considered in fracture mechanics: Mode I, Mode II, and Mode III. Each mode has an independent stress intensity factor. These are shown in Figure 3.4. Mode I is termed the opening mode and is caused by tensile stress normal to the plane of the crack. Mode II is the sliding mode caused by shear stress acting parallel to the plane of the crack and perpendicular to the crack front. Mode III is the tearing mode caused by shear stress acting parallel to the plane of the crack and parallel to the crack front. The nature of the critical loading on an offshore monopile (bending moment due to wind and wave shear loads) means that Mode I fatigue failure is dominant and is the focus of this thesis.

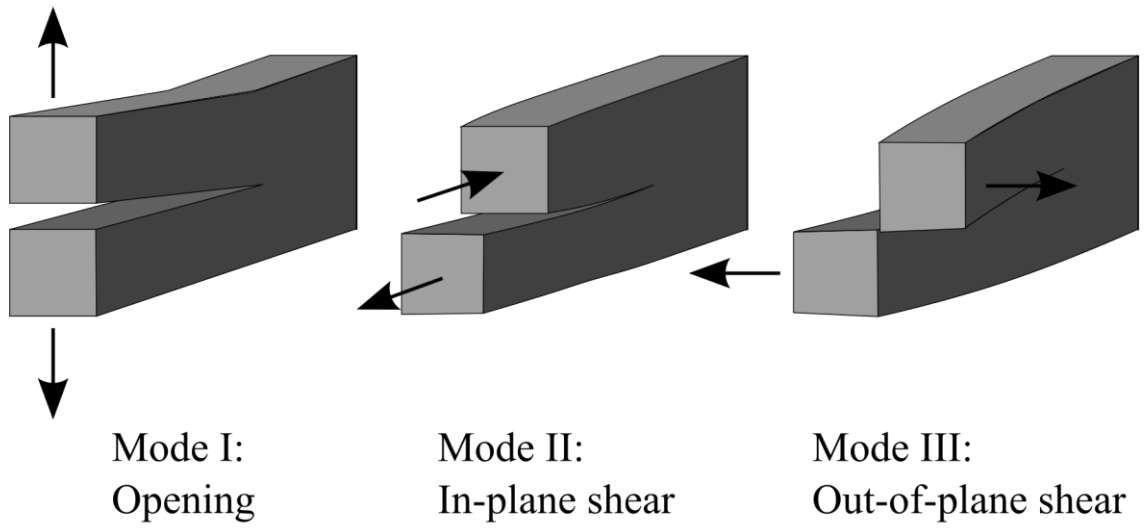


**Figure 3.4 – Fracture Mechanics Failure Modes**

For simple loading, SIF can be obtained from hand-book solutions available in various publications such as those presented by Tada et al. [70], Rooke and Cartwright [71], Sih et al. [72], and Murakami and Keer [73]. In general, the most wide-ranging of SIF solutions are available in industry standards R6 [74] and BS 7910 [68]. SIF provided in handbooks are not specifically for the type of structures used in monopiles (large diameter pipes). For instance, the SIF solution in BS 7910 [68] for a circumferential external surface crack in a cylinder is based on the flat plate solution underpinned by the empirical SIF equation for a semi-elliptical surface crack in a finite plate proposed by Newman and Raju [75, 76]. It was shown

in work by Bocher et al. [77] and later by Fajuyigbe [78] that for typical monopile sizes, these solutions provide an inaccurate estimate of the shape function.

Another option is to obtain the SIF using FEA. The methodology for obtaining SIF from FE analysis is well established. The monopile and crack geometries are modelled in the FE software. The relevant loads are applied, and the SIF is obtained through the calculation of contour integrals. This approach requires special techniques and meshing in the vicinity of the crack tip. This is computationally expensive and time consuming for fatigue situations where the crack is growing and is subject to a lengthy time series of changing loads.

As indicated above, the evaluating of fatigue crack growth by conventional finite element method (FEM) is challenging due to the need for conformal meshing in the model around the crack even with the use of modern adaptive meshing software such as ZenCrack™ [79] and FEACrack [80]. In recent years, new methodologies broadly termed as extended finite element methods (X-FEM) have been developed to address some of these issues. X-FEM is a numerical method based on a standard Galerkin procedure and uses the concept of partition of unity to accommodate the internal boundaries in a discrete model. Therefore, allowing the boundaries, such as holes or cracks, to be modelled without the need for specialised meshing. The basic ideas and mathematical foundation of the partition of unity finite element method is presented by Melenk and Babuška [81] and builds on the work of Duarte and Oden [82] on meshless methods for solving boundary value problems.

Belytschko and Black [83] proposed a method of enrichment of nodes that enriches the standard finite element approximations so that minimal remeshing is required to solve crack growth problems. Moes et al. [84] and Dolbow et al. [85, 86] introduced a much more elegant technique by adapting an enrichment that includes the asymptotic near-tip field and a Heaviside function H(x). The extension of this concept to the three-dimensional static crack modelling was proposed by Sukumar et al. [87]. Belytschko et al. [88] unified the modelling of functions with arbitrary discontinuities and discontinuous derivatives in finite elements.

As noted in Budyn et al. [89] X-FEM is particularly suitable for modelling crack propagation because it does not require the definition of the crack growth path. However, the advantages provided by partition of unity (PU) enrichment often come at the price of numerical problems. Most notably, ill-conditioning can render the solution of the resulting systems of equations problematic or even impossible as shown by Agathos et al. [90]. A state-of-the-art review on the applications of X-FEM in the modelling of elastoplastic crack growth is presented in Kanth et al. [91].

The implementation of X-FEM is still limited in commercial FEA software and has not seen widespread acceptance. Crack propagation fracture mechanics is a very important engineering field so it is expected that work will continue on X-FEM due to its major promise. For now, classical FEM with suitable mesh refinement is used for most fracture analysis.

Through the application of equations 3.4 and 3.5, it is possible to calculate the crack growth for an applied stress history for a cracked structure with known material constants. Therefore, when considering an OWT monopile for lifetime extension, a key input is the

identification of cracks present in the structure. According to DNV guideline [5], the assessment of the monopile for remaining life requires a practical part as well as an analytical part. The practical part in this instance is the inspection of the monopile to detect any fatigue damage. The inspection of the monopile can be used to identify and characterise the flaws present. The growth of the flaws under the applied loading may then be assessed using a suitable empirical model.

There is a lack of specific industry guidelines on the inspection and detection of cracks in OWT monopiles. There is general recommended practice on the inspection of fatigue cracks in offshore structures provided in DNVGL-RP-C210 [92]. According to DNVGL-RP-C210 [92], the most common non-destructive techniques (NDT) for crack detection are: flooded member detection (FMD), eddy current (EC), magnetic particle inspection (MPI), and alternating current field measurement (ACFM).

It is noted that not all the listed techniques are appropriate for use with OWT monopiles either due to accessibility, risks to health and safety and effectiveness. For instance, FMD is only suitable for scenarios where the presence of through thickness cracks (required for fluid ingress) does not itself constitute a failure of structural integrity. The key parameter in assessing the reliability of an inspection process is the probability of detection (PoD) defined according to DNVGL-RP-C210 [92]as:

$$PoD(a) = 1 - \frac{1}{1 + \left(\frac{a}{X_0}\right)^b} \qquad 3.6$$

Where:

$a$ is the crack depth in mm

$X_0$ is the distribution parameter( = 50% median value for the PoD)

$b$ is a distribution parameter

Inspection techniques are constantly evolving and improving. However, in the absence of contractor specific data, the following values for PoD parameters for cracks below the water line provided in DNVGL-RP-C210 [92] are presented Table 3.1. The corresponding PoD curves are shown in Figure 3.5. The curves show that the probability of detection is greater than 90% for crack depths greater than 15mm. According to Arany et al. [23], the typical wall thickness of existing monopile in various wind farms across Europe is 60-100mm. Therefore, one might expect a monopile nearing its end of life to have developed cracks with depths that have a high chance of detection.

**Table 3.1 – PoD Distribution Parameter**

| NDT | Distribution Parameters | |
|---|---|---|
| | $X_0$ | $b$ |
| EC, MPI, ACFM | 1.16 | 0.9 |
| UT | 0.410 | 0.642 |

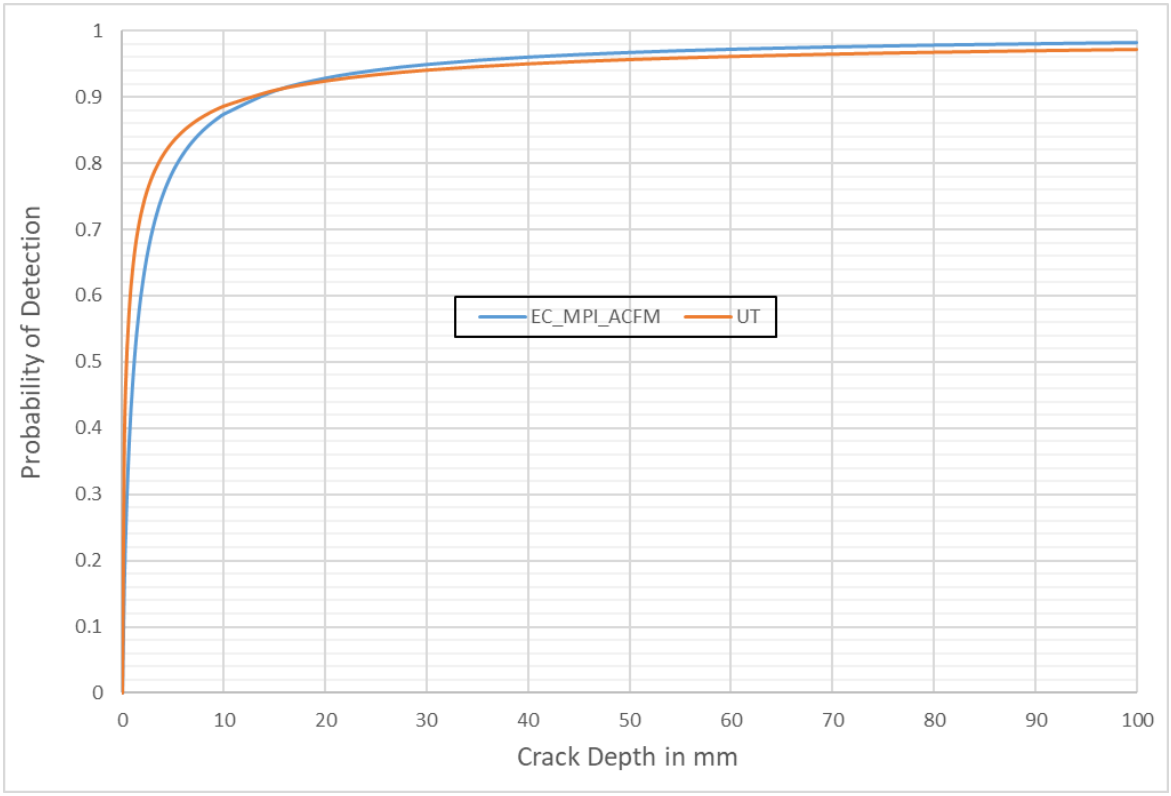


**Figure 3.5 – PoD Curves (Inspection under water)**

## 3.5 Failure Assessment Diagram

Fatigue failure in fracture mechanics analysis is based on a critical crack depth ($a_c$). $a_c$ may be specified as either a function of the monopile thickness or based on other empirical considerations. One approach to fracture mechanics fatigue assessment for OWT monopiles, is to take failure as the point when the dominant crack grows through the thickness of the pipe. This is a reasonable approach because SIF for circumferential through-wall cracks in cylinders calculated using BS 7910 [68] or from closed-form SIF solutions provided by Shim at al. shows that crack growth significantly increases once the crack is through the wall thickness.

However, this approach only considers brittle failure (where the SIF of the crack becomes greater than the fracture toughness of the material). It does not consider failure due to plastic collapse under extreme loads. The failure assessment diagram (FAD) is a widely accepted method for assessing both the fracture failure and plastic collapse of a cracked structure. The FAD approach is established and enshrined within international standards and design guidance, such as BS 7910 [68]. The FAD is a plot which delineates regions of safe operation based on empirical data for different materials. The ordinate plots fracture ratio, $K_r$: a measure of the susceptibility of the structure to unstable brittle fracture failure. The abscissa plots load ratio, $L_r$: a measure of the susceptibility of the structure to plastic collapse (as is typical of less brittle or ductile materials where the microstructure allows for deformation/flow of the material). For any loading condition, if $K_r$ and $L_r$ fall below the failure assessment line (FAL), the flaw is deemed acceptable (see Figure 3.6).

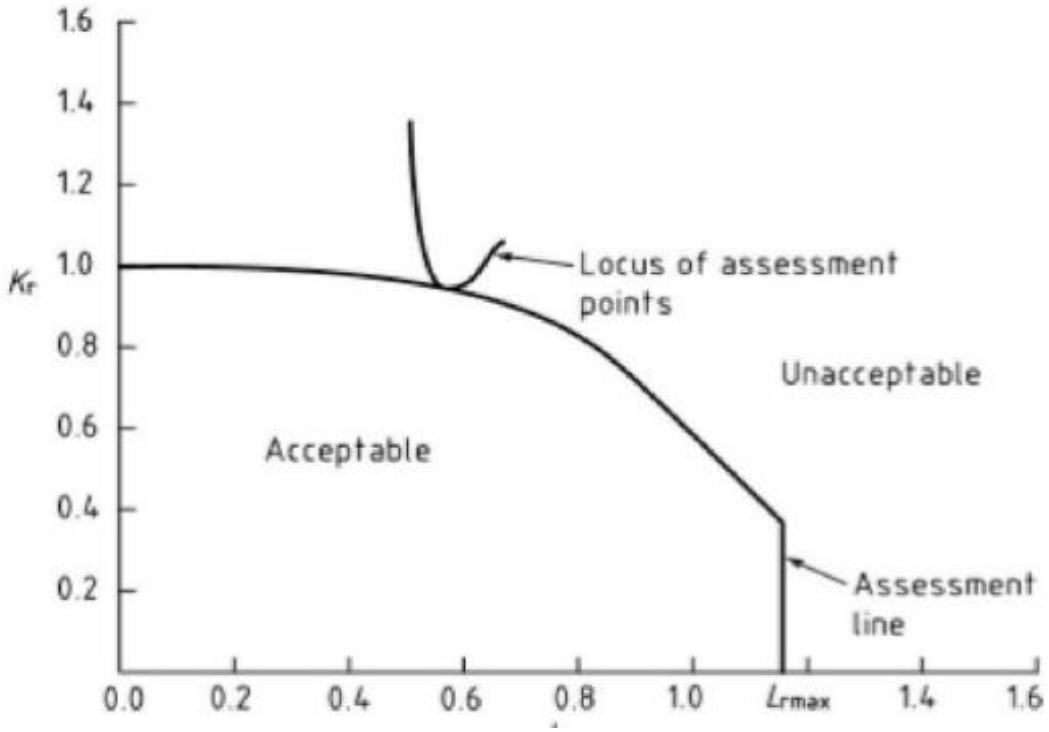


**Figure 3.6 – Failure Assessment Diagram [68]**

The FAL describes the interaction between plastic and fracture failure. The key benefit of the FAD is that $K_r$ and $L_r$ can be determined independently but their effects are then combined when plotted on the FAD. As noted by Hadley [93], whilst there are other alternatives to the FAD approach such as crack driving force (CDF) methods, it is this simplicity that has led to the popularity of FAD and wide implementation in engineering critical assessment (ECA) procedures. A failure assessment curve specific to a particular material, geometry and loading type may be determined using both elastic and elastic-plastic analyses of the flawed structure as a function of the loads give rise to primary stresses. FAL may also be generated using simple conversative procedures that do not require detailed material data and analysis. An example of this is the "option 1" FAL provided in BS 7910 [68] which only requires knowledge of the Young's modulus, yield strength, and ultimate tensile strength of the material.

Although there may be significant difference in the assessment of some FAD parameters between various assessment codes, as highlighted by Eren et al. [94], the FAD method is widely accepted to evaluate the extent to which cracks may affect structural safety. The reader is directed to research such as Ainsworth et al. [95] and Kouzoumis [96] for some experimental validation results.

## 3.6 Assessing Multiple Cracks

The consideration of multiple cracks is a novelty for the fatigue assessment of OWT monopile. To the author's knowledge, there is no published work that addresses the assessment of multiple cracks in OWT monopiles. Aged structures as a monopile nearing the end of its design life may have multiple cracks on the same plane due to manufacturing defects or loading history. The failure of a structure due to the presence of multiple cracks

known as widespread fatigue damage (WFD) is well known in other industries, such as aerospace and nuclear. Tan et al. [97] propose a methodology to assess the development of WFD and its effect on the residual strength of aircraft structure. Bombardier et al. [98] developed fracture mechanics models to be used in quantitative risk assessment of aircraft structural integrity. Ruiz-Muñoz [99] proposed a method to analyse multiple site damage fatigue before and after crack coalescence. WFD in a structure is characterised by the simultaneous presence of cracks at multiple points that are of sufficient size and density. Whilst each crack may be individually acceptable, interaction between the cracks may cause failure.

There was the failure of the Aloha 737 airplane in 1988 due to the linking of numerous small cracks at a number of fastener holes, as discussed in Hendricks [100]. The report by Dawson and Brooks [101] into the failure of the reboiler at the ESSO plant in Longford was also caused by multi-site cracks/flaws in the weld and a similar problem leading to the loss of seven bulk carriers off the coast of Western Australia during the period January 1990 to August 1991 [102].

For a structure with multiple cracks, the question to answer is two-fold: the first is to determine the influence of the cracks on each other (interaction), and the second is to determine if the cracks may join together (coalescence). The finite element method (FEM) is widely used in the analysis of 3D multiple crack problems. There are a significant number of publications into the use linear elastic fracture mechanics to examine the interaction and coalescence of multiple cracks. Jiang et al. [103] presented work on the SIF of two parallel 3D surface cracks. Lin and Smith [104] simulated multiple surface cracks in plates subjected to various combinations of tension and bending loads to examine interaction and coalescence. This built on the work of Soboyejo et al. [105] and Kishimoto et al. [106] on the interaction and coalescence of twin coplanar cracks. There is also research work on the use of X-FEM methodologies for the analysis of multiple cracks. Dundar et al. [107], Price et al. [108], and Liu at al. [109] used enriched finite elements to examine the crack propagation of multiple cracks in different 2D and 3D geometries. Pierres at al. [110] used extended finite element method to simulate 3D fatigue propagations. The pros and cons of XFEM were discussed earlier.

This literature review suggests that the analysis of multiple cracks is typically performed with FEM with some form of element enrichment to facilitate the simulation of crack propagation. This is a computationally expensive approach and may not be suitable for large number of loadcases associated with the fatigue design of OWT monopiles.

In any case, the acceptability of a monopile with multiple cracks may still be assessed using the FAD. Suitable methodologies are needed to determine the SIF of the various cracks (considering various interaction and coalescence effects) and the plastic limit load of the multi-cracked structure. These may then be used to calculate appropriate $K_r$ and $L_r$ for plotting on the FAD.

## 3.7 Conclusions

Presently, the adopted approach for lifetime extension is to repeat the S-N fatigue design of the monopile using state-of-the-art numerical tools and the true operating conditions of

the OWT, as discussed by Ziegler and Muskulus [111]. However, this approach ignores some inherent limitations in fatigue design using S-N curves. Firstly, S-N curves are obtained from the test of small standard specimens under laboratory conditions. The tests cannot capture the actual operations conditions of the monopile. Brennan and Tavares [27] maintain that the choice of fatigue test specimen is critical to the resulting S-N curve so test specimens and conditions need to be as representative of the true situation as is possible.

Another issue is the probabilistic nature of fatigue failures. Carefully machined specimens from the same stock material will fail at different number of cycles even for the same applied stress. This variability is often addressed through the use of design curves generated by applying reductions and safety factors to the test data, as discussed in Barbosa et al. [112]. This means that the failure point predicted by the S-N curve is unlikely to correlate to true structural failure.

Perhaps the most significant limitation of fatigue design using the S-N curve is that the process encapsulates the three stages of a structure's fatigue life into a single value. It is not possible to separate the various stages because any value of D, other than D=1 (failure), does not correspond to a physical state of the structure. The lack of detail on the behaviour of the structure at intermediate points (D<1) inhibits operational decision making such as integrating inspections that may further extend the life of the structure.

These issues may be circumvented through the use of fracture mechanics for the fatigue assessment following an inspection to determine and characterise the flaws present in the aged structure. Presently, LEFM is performed using FEA to determine the SIF of a single dominant crack. This is then combined with a crack growth model (typically Paris's law) to determine the time taken for the crack to grow to a critical size under the applied loading. This approach is time consuming and also ignores the effect of multiple cracks on both brittle and plastic failure.

Based on the literature review, it is clear that a framework/tool is required for assessing the integrity of monopiles for lifetime extension purposes. The process should be capable of assessing the growth of cracks under applied load. The approach should be based on fracture mechanics to allow the integration of inspection results. The calculation of SIF of the cracked monopile should be more accurate than current handbook solutions and the solutions process should be faster and less computationally expensive than conventional FEA. The framework should allow for concurrent assessment of brittle failure and plastic collapse and should account for multiple cracks.

Jacob et al. [113] and Mehmanparast et al. [114] indicated that for monopiles, fatigue crack initiation and growth occur primarily at circumferential welds due to cyclic loads from wind and waves. The most significant source of Mode I fatigue crack growth are the bending moment loads applied to the monopile. The stresses due to bending loads are greatest at the outer fibre so it may be logical that cracks in monopiles start at the external surface and grow surface inwards. However, it is noted that high stresses at the outer fibres is not the only possible cause of crack initiation. The misalignment of the monopile "cans" may also readily lead to cracks on the internal surface. Corrosion can also lead to crack initiation and amplify crack growth.

Whilst a crack may initiate as an irregular shape, Lin and Smith [115] showed that an initially non semi-elliptical cracks develops rapidly into approximate semi ellipses. It is for this reason that most seminal research work, such as Newman and Raju [116], focus on semi-elliptical cracks in pipes and hollow cylinders.

Taking consideration of the above, this thesis focusses exclusively on semi-elliptical external surface circumferential cracks. However, it is noted that much of the framework developed may be applicable to other types of cracks.

# 4 ASSESSING FITNESS FOR PURPOSE - FAILURE ASSESSMENT DIAGRAM

*Fajuyigbe A., and Brennan F. (2021), "Fitness-for-purpose assessment of cracked offshore wind turbine monopile" Marine Structures 77: 102965.*

*Sections of the content presented below are reproduced from the published peer-reviewed paper.*

## 4.1 Paper Synopsis and Additional Notes

A key requirement identified from the research objective is to determine a suitable process/methodology for assessing the integrity of a monopile. The literature review suggests that a failure assessment diagram (FAD) may be a suitable tool for assessing the acceptability of a cracked structure. This paper examines the current state-of-the-art methodology for generating a FAD based on the procedure outlined in the industry standard BS 7910 [68] which is one of the prominent engineering critical assessment (ECA) procedural guidelines widely used in many industries.

The procedure in BS 7910 [68] is examined through a case study of a semi-elliptical surface crack in an offshore monopile as it grows till it forms a through thickness crack. The findings suggest that a surface breaking defect may be identified as unacceptable based on BS 7910 when there may still be a non-trivial amount of structural residual life. This is a concern for monopiles where crack growth as a large flaw forms a significant part of the total life.

## 4.2 Introduction

In 2016, 12% of the installed wind turbine capacity in Europe was older than 15 years. This share increases to 28% by 2020. These wind turbines will soon reach the end of their designed service life, which is typically 20 years. As a consequence, the wind industry needs to prepare for upcoming challenges, such as maintenance of aging assets, assessment of structural integrity, lifetime extension decision making, and decommissioning of turbines [3].

There is little experience in the re-assessment of wind turbines to quantify remaining useful life. Recommendations from recently published industry standard [22] suggest a two-part process. The first is an analytical part involving damage re-calculation for the wind turbine, considering the site-specific installations and its local conditions. The second is a practical part consisting of assessment through inspection of the wind turbine considering the maintenance/operational history and the turbine type related field experience. As an aged structure is likely to already contain a flaw either due to manufacturing defects or through system loading, it is necessary to assess the fitness for service by ascertaining if a known crack is likely to cause a monopile to fail under applied load.

Linear-elastic fracture mechanics (LEFM) models are used to characterise crack growth as a function of stress cycles, structural and crack geometry, and material parameters. The models allow the investigation of the second fatigue phase (crack propagation) to ascertain the conditions under which a crack will grow to a point at which further crack growths are

unrestricted. There are several industrial standards outlining recommendations for the use of LEFM models in determining the acceptability of flaws in metallic structures such as BS 7910 - Guide to methods for assessing the acceptability of flaws in metallic structures [117] and API 579 – Fitness for Service [118].

This paper examines the approach laid out in BS 7910. BS 7910 was driven by the need of the oil and gas industry in the 1960s and 1970s to provide a technically sound, transparent, accurate, user-friendly, and free from commercial bias approach for assessing flaws in welded structures using a fracture mechanics approach rather than rules based on workmanship. A brief history of and background to BS 7910 may be found in several publications such as [119, 120].

Using an exemplar OWT monopile foundation as a case study, a surface flaw growing under the action of fatigue loads is assessed to investigate the failure mode of the structure. The remainder of this section is organized as follows: Section 4.3 presents a brief exposition into the primary tool used to assess acceptability of flaw in BS 7910. The parameters of the OWT and the adopted methodology are presented in section 4.4 to 4.7. The results are discussed in section 4.8. The conclusions and outlook are presented in section 4.9.

## 4.3 Failure Assessment Diagrams

For BS 7910 [68], the acceptability of a flaw is based on its position on the failure assessment diagram (FAD), as discussed in section 3.5. FADs provide a methodology, or framework, for demonstrating the proximity to failure of components containing crack-like defects. The FAD delineates regions of safe operation based on empirical data for different materials. The ordinate plots $K_r$: a measure of the susceptibility of the structure's unstable brittle fracture failure in the presence of a crack calculated using linear elastic fracture mechanics. The abscissa plots $L_r$; a measure of the susceptibility of the structure to plastic collapse as is typical of less brittle or ductile materials where the microstructure allows for deformation/flow of the material. The assessment line is cut-off at the point $L_r = L_{r,max}$ to prevent plastic collapse. For any loading condition, if $K_r$ and $L_r$ fall below the assessment line, the flaw is deemed acceptable.

The generation of the assessment line is heavily dependent on the amount of information available about the material. BS 7910 [68] provides 3 levels of calculation, the so-called options 1 to 3. The complexity of the information required to generate the assessment line increases with the levels, however, the level of conservatism in the analysis decreases. Option 2 is based on the use of a material-specific stress-strain curve. Option 3 uses numerical analysis to generate a FAD and is not confined to use with materials showing ductile tearing. Option 1 is adopted for this paper. It is a conservative procedure that is relatively simple to employ and does not require detailed stress/strain data for the materials being analysed. It is assumed that the material does not exhibit yield discontinuity in line with recommendations provided in clause 7.1.3.6 of BS 7910 [68].

Option 1 failure assessment line (FAL) is used in this work. From BS 7910, option 1 FAL is plotted based on the following governing equations:

$$K_r = f(L_r) = \begin{cases} \left(1 + \frac{1}{2}L_r^2\right)^{-1/2} \left[0.3 + 0.7e^{-\mu L_r^6}\right] & L_r \leq 1 \\ f(1)L_r^{(N-1)(2N)} & 1 < L_r < L_{r,max} \\ 0 & L_r \geq L_{r,max} \end{cases} \quad 4.1$$

$$\mu = min\left[0.001\frac{E}{\sigma_Y}, 0.6\right] \qquad N = 0.3\left[1 - \frac{\sigma_Y}{\sigma_u}\right]$$

$$L_{r,max} = \frac{\sigma_Y + \sigma_u}{2\sigma_Y}$$

$\sigma_Y$ is the lower of yield or 0.2% proof strength, $\sigma_u$ is the tensile strength and $E$ is the elastic modulus. $f(L_r)$ is the graph ordinate value as is the same as $K_r$ when used to plot the failure assessment line. $f(1)$ is the value of $f(L_r)$ at the point $L_r$=1.

### 4.3.1 Fracture and Load Ratio

For each crack geometry and loading conditions the fracture ratio, $K_r$ ratio is calculated as:

$$K_r = \frac{K_I^p + VK_I^s}{K_{mat}} \quad 4.2$$

$K_I^p$ is the stress intensity factor (SIF) at the current crack size due to the primary stresses. Primary stresses are defined as those that can contribute to plastic collapse such as internal pressure and external loads

$K_I^s$ is the stress intensity factor at the current crack size due to secondary stresses. Secondary loads are self-equilibrating loads necessary to satisfy compatibility of the structure such as thermal and residual stresses. Secondary stresses are not considered in this paper.

$K_{mat}$ is the fracture toughness taking account of any ductile tearing following initiation.

$V$ is a function of the primary and secondary loads and accounts for plasticity interaction.

The load ratio, $L_r$ is calculated as:

$$L_r = \frac{\sigma_{ref}}{\sigma_Y} = \frac{P}{P_L}\left(= \frac{applied\ load}{limit\ load}\right) \quad 4.3$$

$\sigma_{ref}$ is the reference stress calculated in accordance to Annex P of BS 7910. Alternatively, plastic limit loads $P_L$, may be derived from finite element analysis as discussed later.

## 4.4 Geometry Definition

### 4.4.1 Monopile Geometry

A flaw in an OWT monopile is selected as a case study for this paper. Monopile support structures represent approximately 90% of commissioned offshore wind structures [4].

OWT monopiles are fabricated by rolling and then welding thick structural steel plates in a longitudinal direction to produce "cans" which are then welded together circumferentially. The monopile has an outer radius ($r_o$) of 3m, inner radius ($r_i$) of 2.9m, wall thickness ($t$) of 100mm, and mean radius ($r_m$) of 2.95m. These are in line with typical sizes of existing monopiles in various wind farms across Europe as reported by Arany et al. in [23]. The length of the monopile is set as 40m which is the typical water depth of monopile foundation installations [77].

S355 steel is the most common material used in the fabrication of monopile support structure [121]. The material properties for S355 steel are as follows: the minimum yield strength ($\sigma_Y$) is taken as 335MPa, the tensile strength ($\sigma_u$) is taken as 470MPa, the modulus of elasticity (E) is 210GPa [122]. The fracture toughness of S355 steel is taken as $38MPa\sqrt{m}$ [123]. For the calculation of limit load, the onset of plasticity is set as the yield strength. This is in line with values recommended in ASME III Section NG-3224.1 [124] for limit load calculations.

## 4.5 Crack Geometry

Cracks in monopiles typically start from a surface flaw situated at the weld/parent metal interface. The crack grows gradually as a semi-elliptical flaw until it penetrates the wall thickness (Figure 4.1a). At this point, it begins to propagate in the circumferential direction until two crack lines meet (Figure 4.1b).

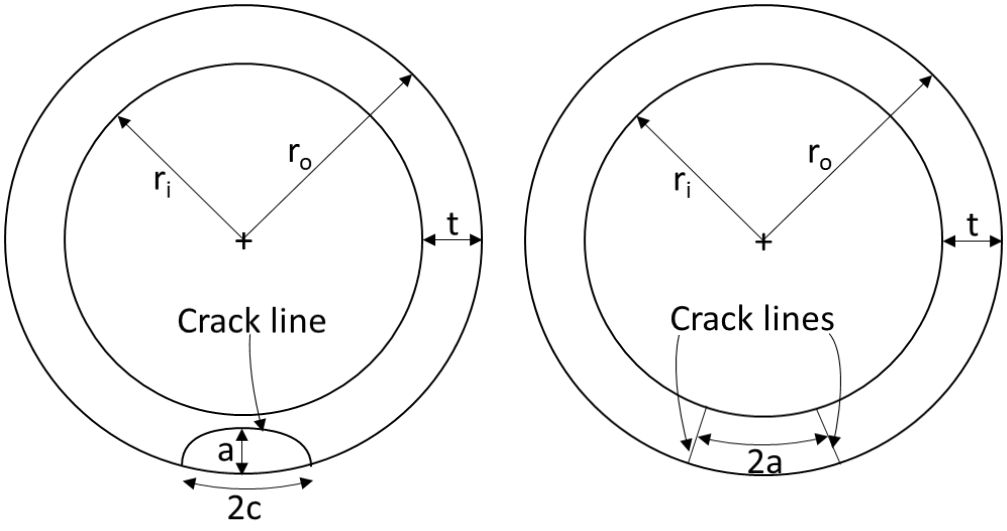


**(a) Semi Elliptical Surface Crack** **(b) Through Crack**

**Figure 4.1 - Crack Definition**

The crack aspect ratio (crack depth/crack half length, a/c) is assumed as 0.4 based on recommendations in [92]. It is generally assumed that a semi-elliptical crack grows according to Paris law. Numerically, it is clear that for growth at all points along the crack line to obey the Paris relation, the crack growth at different points must be different to account for the variation in stress field triaxiality. Some research work such as [125] and [126] studied the evolution of aspect ratio and thus establish numerical solutions for the

shape change of cracks during fatigue growth but the body of work in this field is light. For simplicity it is assumed that aspect ratio remains constant during crack growth.

## 4.6 Finite Element Modelling

The monopile is modelled in the finite element software package, ABAQUS [127]. The FE model is fixed at one end with a symmetry boundary condition in the Z direction (longitudinal axis of the cylinder). This allows a pure bending loading to develop in the monopile. The moment load is applied to a reference point coupled to free surface of the monopile. The axis of the moment load is oriented to cause crack opening under the applied load. It is noted that a reduced half model (partition line passing through the centre of the crack) could also be used to take advantage of the symmetry of the model.

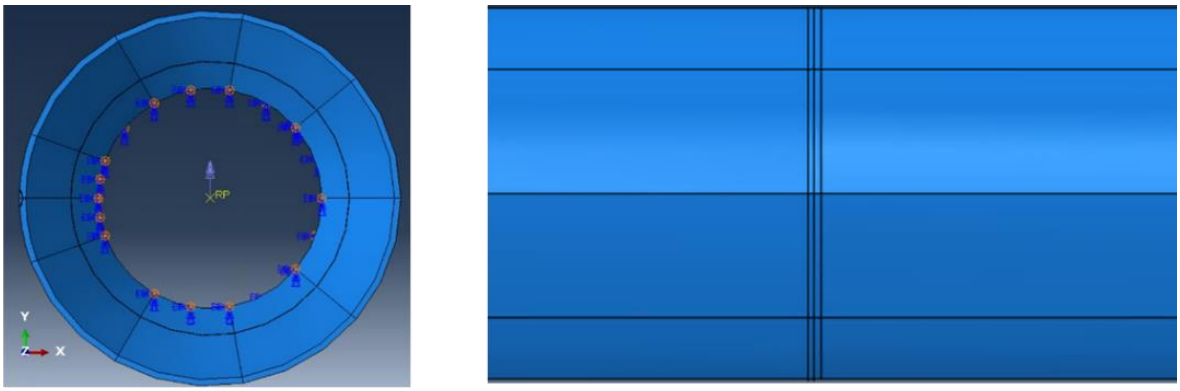

(a) Reference point and Boundary Condition

(b) Global Model Partitioning

**Figure 4.2 – Finite Element Model**

The model is partitioned for ease of meshing and locating of the crack. The monopile is partitioned into nine sectors to facilitate a swept mesh. One sector is further partitioned to create a line through the centre of the intended cracked region (Figure 4.2a). The model is then partitioned at mid length to create a surface to locate the crack. Two further partitions above and below the partition at mid-length are created to form region surrounding the crack for finer meshing (Figure 4.2b).

### 4.6.1 Surface Crack Definition

A semi-elliptical partition is extruded through the length of the monopile. The edge created at the intersection of this extrusion and the mid-length partition is the crack line. Two additional semi-elliptical partitions are created: one towards the centre of the cylinder, and the other towards the surface. These form the bounding region of the crack front in the thickness direction.

The region around the crack is seeded with approximate element size of 5mm. Bias seeding with a minimum size of 0.1m and a maximum size of 2m is applied along the length of the monopile with the bias towards the crack region (shown in Figure 4.4c). Away from the cracked region, the rest of the monopile is seeded with an element size of approximately 0.5m in the circumferential direction and the thickness of the pipe is split into four elements. An example of the seeding is shown in Figure 4.3.

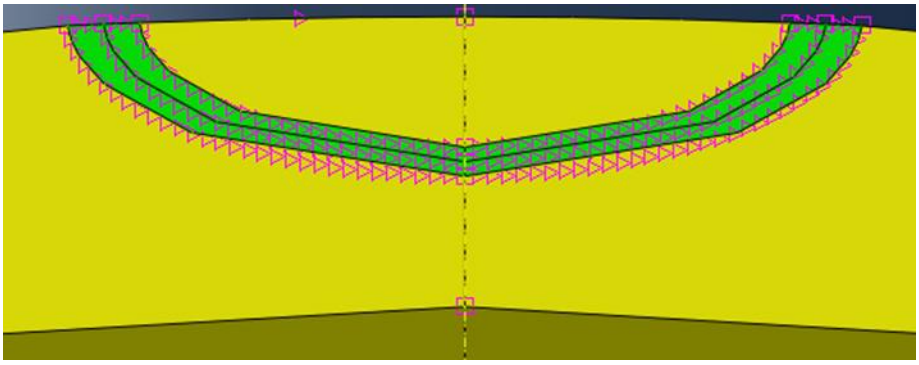

**Figure 4.3 – Element Seeding of Semi-Ellipses**

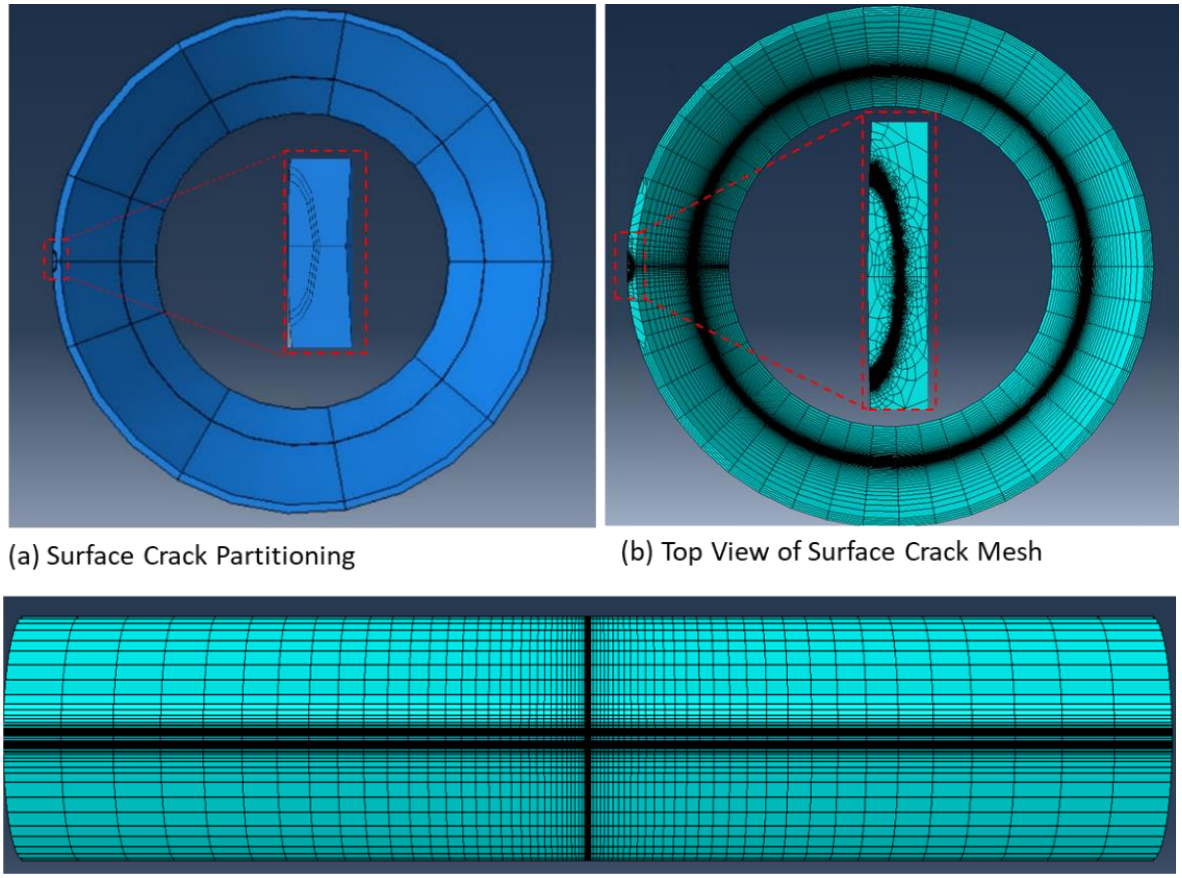


**Figure 4.4 – Surface Crack Definition**

### 4.6.2 Through-thickness Crack Definition

A through-thickness crack has two crack lines. One crack is advancing in the clockwise direction, the other in the anti-clockwise as shown in Figure 4.5.

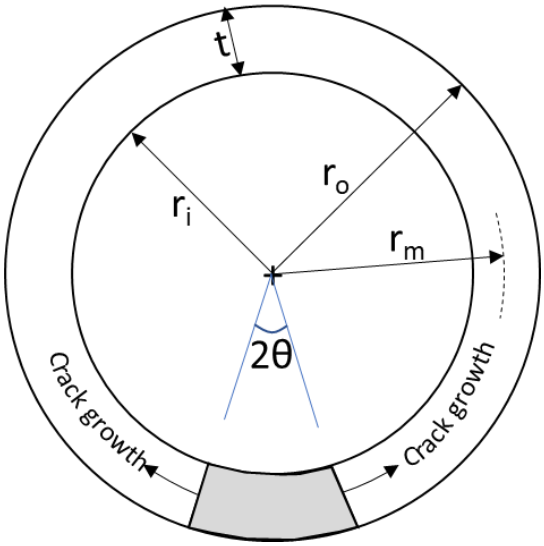


**Figure 4.5 - Through Thickness Crack Geometry**

To model the crack region in the FE software, six radial lines (3 per crack line) are extruded along the length of the monopile. One radial partition is the crack line whilst the remaining two partitions define the crack front region used in contour integral calculations (Figure 4.7a). The position of the radial lines is dependent on the half angle (θ) of the crack being analysed.

The region around the crack is seeded with an approximate element size of 5mm. Bias seeding with a minimum size of 0.1m and a maximum size of 2m is applied along the length of the monopile with the bias towards the crack region (shown in Figure 4.4c). Away from the cracked region, the rest of the monopile is seeded with an element size of approximately 0.5m in the circumferential direction and the thickness of the pipe is split into four elements. Element seeding around the crack region is shown in Figure 4.6.

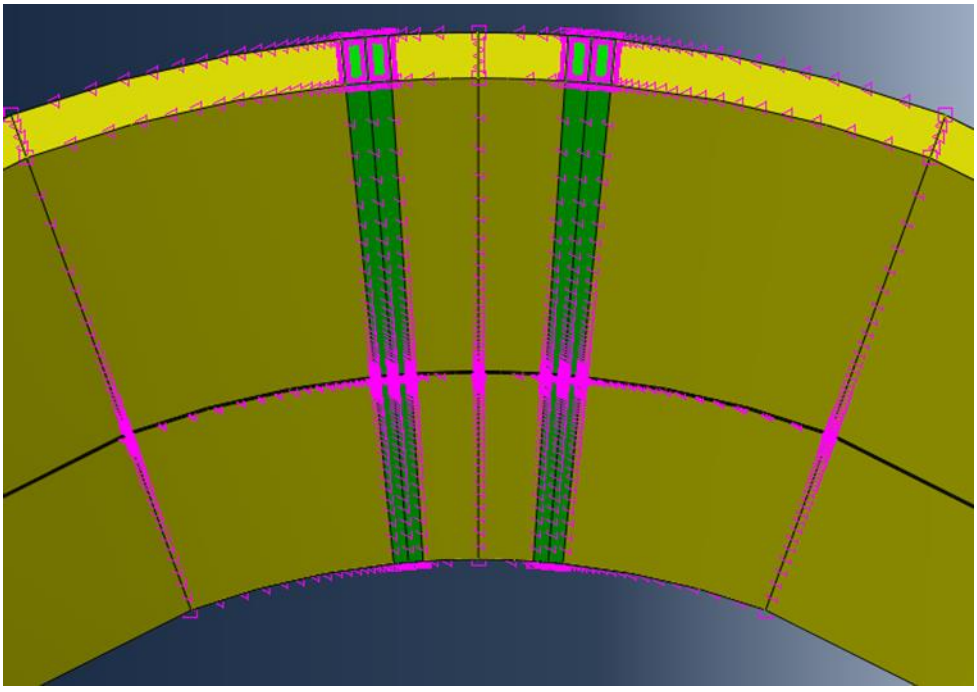

**Figure 4.6 – Element Seeding for Through-Crack**

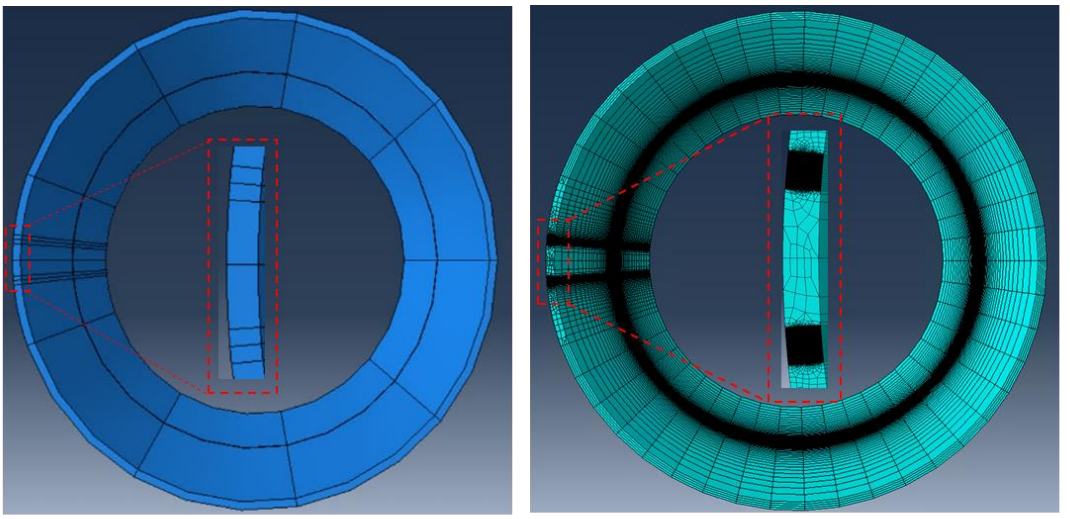

(a) Through-thickness Crack Partitioning (b) Top View of Through-thickness Crack Mesh

**Figure 4.7 – Through-thickness Crack Definition**

### 4.6.3 Cracks Analysed

$K_r$ and $L_r$ values are extracted for the following surface crack depths: from 10 – 80mm in increments of 10mm, and 80 – 95mm in increments of 5mm. $K_r$ and $L_r$ values are extracted for through cracks with half angles (θ) of 0.083rads, 0.1rads, 0.12rads, 0.14rad, and 0.18rads. The analysis is terminated at a half angle of 0.18rads as the structure is expected to have crossed into the unsafe region of the FAD at this point. The starting half angle of 0.083rad is the half angle subtended by a surface crack with an aspect ratio (a/c) of 0.4 growing to through thickness of 100mm:

$$\theta = \frac{\left(t/\frac{a}{c}\right)}{r_o} = \frac{100/0.4}{3000} = 0.083rads \quad 4.4$$

## 4.7 Methodology

### 4.7.1 Abaqus SIF Evaluation

The commercial FEA software Abaqus™ is used throughout this research for numerical simulations. Abaqus™ is one of the most popular FE software in academic and commercial purposes. Stress intensity factor for cracks is analysed using the integrated fracture mechanics module. The implementation of crack and fracture mechanics modelling is detailed in the software manual [127] but a brief overview of the process is presented subsequently.

The structure is modelled in FE space with suitable geometry partitioning to define the location and orientation of the crack to be assessed. Cracks are defined in the interaction module of Abaqus. A crack in a 3-D model is a region containing faces that are free to move apart. These faces form the seam and Abaqus creates duplicate overlapping nodes on the seam which are free to move apart as the seam separates. Contour integral estimates are performed around the seam to obtain key parameters such as J-integral, $C_{t\text{-integral}}$ (for creep), T-stress or SIF.

For integral calculations, the crack line and the crack extension direction must be defined. The cracks line is a series of connected edges along the crack front. The crack front is the forward part of the crack. The crack extension directions specified as q vectors which are normal to the crack plane at the different nodes along the crack line.

Abaqus integrates around the ring of element (contour) enclosing the crack line to determine the stress intensity factor. Using the divergence theorem, Abaqus expands the one-dimension contour integral into an area integral in two dimensions or volume integral in three-dimensions. These integrals are evaluated for multiple rings of elements surrounding the crack tip node. The first contour is formed from elements directly connected to the crack tip node. Each subsequent contour is created by offsetting one element away from the previous contour.

The Abaqus manual specifies a detailed, focused mesh around the crack tip for accurate contour integral evaluation. However, as noted by Brocks and Scheider [128], SIF estimates should be independent of the domain used, that is, the calculation of the SIF should not be path independent. Numerical variations in the values of SIF obtained from the integral evaluation of each contour may be due to the implementation of the calculations in the FE software. Abaqus manual recommends that large variations in SIF values between successive contour integrals may be addressed by mesh refinement and computing a minimum of two contour integrals. This is because the accuracy of the results from the first contour are heavily influenced by the crack tip. There is no hard limit to the number of contours to be evaluated, the number of contours should be high enough to check if a saturated far-field value of the contour integral has been reached.

Finite element simulation is performed on monopiles with various surface and through-thickness cracks respectively to obtain the stress intensity factor (SIF) solution. The finite element model is meshed with linear hexagonal elements with reduced integration (C3D8R). The C3D8 Abaqus element class are general purpose linear brick elements commonly used in stress analysis. C3D8R is the 8-noded brick element with reduced integration (1 integration point). The shape functions are the same as for the C3D8 but due to the reduced integration, the locking phenomena observed in the C3D8 element do not show. Abaqus also implements automatic hourglass control for this element. Stress intensity factors are obtained in ABAQUS through the calculation of contour integrals. Only SIF for mode I – opening mode is considered as the applied tensile stress is normal to the plane of the crack.

### 4.7.2 Stress Intensity Factor – BS 7910

From various literature such as [64] and supported by Annex M.1 of BS 7910, the general form of the stress intensity factor for load applied normal to the crack plane (crack face) of an external surface crack oriented circumferentially growing in the thickness direction is described as:

$$K_I = (Y\sigma)\sqrt{\pi a} \qquad 4.5$$

$\sigma$ is the global applied stress.
$a$ is the crack depth.
$Y$ is the shape function which is dependent on the geometry of the cracked structure.

There are existing empirical equations for the shape function for a semi-elliptical surface crack in a finite plate such as those proposed by [75]. Annex M.1 of BS 7910 provides an expression for the calculation of shape factor for a structure subjected to primary stresses:

$$(Y\sigma)_p = Mf_w\{k_{tm}M_{km}M_mP_m + k_{tb}M_{kb}M_b[P_b + (k_m - 1)P_m]\} \quad 4.6$$

$P_m$ and $P_b$ are the primary membrane and through-wall bending stresses respectively. $M, f_w, M_m, M_b$ are given for different types of flaws in different configurations in the standard. $M_{km}$ and $M_{kb}$ apply when a flaw is in a region of local stress concentration. $k_m$, $k_{tm}$, $k_{tb}$ account for stress concentration due to structural discontinuities or misalignment. For simplicity, $M_{km}$, $M_{kb}$ $k_m$, $k_{tm}$, $k_{tb}$ are set to a value of 1 as stress concentrations and discontinuities are not included.

### 4.7.3 Reference Stress – BS 7910

For practical engineering applications, thin-walled assumption is adopted for pipes with ratio of diameter to thickness (D/t) greater than twenty. The monopile in the case study has a D/t=60. Hence the reference stress is computed in accordance with the following BS 7910 clauses:

Clause P.10.4 for external surface flaw in thin-walled pipe:

$$\sigma_{ref} = \frac{P_m\left[\pi(1 - a/t) + 2\left(\frac{a}{t}\right)\sin(c/r_o)\right]}{(1 - a/t)[\pi - (c/r_0)(a/t)]} + \frac{2P_b}{3(1 - \alpha^{"})^2} \quad 4.7$$

Clause P.10.1 for through thickness flaw in thin-walled pipe:

$$\sigma_{ref} = \frac{\pi(p_{m,a} + P_{m,p})}{\pi - \frac{a}{r_i} - 2arcsin\left(\frac{1}{2}sin\frac{a}{r_i}\right)} + \frac{\pi P_{m,b}(r_o^4 - r_i^4)}{\left[\pi - \frac{a}{r_i} - 2\frac{sin^2\left(\frac{a}{r_i}\right)}{\pi - \frac{a}{r_i}} - \frac{sin\left(\frac{2a}{r_i}\right)}{2}\right](4r_o r_m^2 t)} + \frac{2P_{b,l}}{3\left(1 - \frac{2a}{\pi r_i}\right)} \quad 4.8$$

$P_{m,b}$, $P_{m,a}$, $P_{m,p}$ are membrane stresses due to external bending, axial loads, and internal pressure respectively. $P_{b,l}$ is the primary through-wall bending stress. $\alpha^{"} = \frac{a/t}{[1+(t/c)]}$ for $\pi r_o \geq c + t$ or $\frac{a/t}{(c/r_o)}$ for $\pi r_o < c + t$.

### 4.7.4 Limit Load

Limit load analysis is a well-established method for predicting margins against plastic collapse. The limit load is defined as: the load that causes local yielding (ligament collapse) or causes net section yielding (global limit load).

An option for determining limit load is the twice-elastic-slope (TES) method as used in the ASME III design code [129]. The TES criterion, discussed in Mackenzie and Li [130], involves plotting a load parameter against a deformation parameter. A straight line with a slope that is half of the initial elastic response of the characteristic curve relative to the load axis is drawn from the origin of the curve to the point it intersects with the characteristic curve. The corresponding load at the intersection point is taken as the plastic load. The difficulty with this approach is in the selection of the appropriate deformation parameter because it needs to accurately represent the nature of the plastic failure mechanism.

Another option for determining the limit load is the tangent intersection (TI) method as discussed in Moffat et al. [131]. The TI criterion is similar to the TES in that it also uses a characteristic curve of a load parameter against a deformation parameter. Two straight lines: one tangent to the initial elastic response, and the second tangent to the plastic deformation region are drawn. The corresponding load at the intersection of these lines is taken as the plastic load. One major difficulty with the TI criterion is the lack of clarity on where to draw the tangent to the plastic deformation part of the curve.

The limit load of a cracked structure may also be determined directly from elastic-perfectly-plastic 3D finite element analyses which is the methodology adopted in this work. As discussed in Booth [132], this is done by applying an elastic-perfectly-plastic material curve to the monopile with the onset of plasticity set as the yield strength. Incremental load is applied to the structure until the magnitude of the applied load cause global plastic collapse. This is signalled by the loss of static equilibrium due to excessive plasticity. The limit load is the maximum load satisfying equilibrium between external and internal forces when an elastic-perfectly plastic material model and small deformation theory are assumed. The load applied at the final converged increment is the limit load. It is noted that the limit load determined is only applicable to a specific geometry, including specific crack geometry and loading condition. Therefore, the analysis must be repeated for all crack geometries of interest.

For this work the analysis is performed using ABAQUS [127]. Kim et al. [133] performed finite element analysis to determine limit loads for cylinders with part through-surface cracks under combined loading, and recommend the use of quadratic reduced integration elements within ABAQUS (element type: C3D20R) to avoid problems associated with incompressibility. The reliability of the limit loads established from the finite element analysis is evidenced through comparison with theoretical solutions for uncracked pipes.

Care must be taken when interpreting limit load for failure of real structures as the purpose of the limit load criteria is to define the load at which plastic deformation becomes excessive, and not when actual physical collapse occurs. Furthermore, the elastic-perfectly-plastic approach ignores material strain hardening which may allow a structure to support

stresses greater than yield. Real structures may also experience large deformations which may alter the structural load path affecting the structure load carry capacity.

### 4.7.5 Structural Loads

OWT support structures are commonly designed according to loadcases specified in the IEC standard [134]. The list of Design Load Cases (DLCs) prescribed in the standard cover the various operating regimes of the wind turbine. A crack can experience three types of loading: Mode I (opening mode), Mode II (shearing mode) and Mode III (tearing mode). The crack is assessed for Mode I loading which is typical for most fractures. For a crack subject to Mode I loading, the principal load is applied normal to the crack and tends to open the crack. Although the monopile is subject to various types of loads (compressive loads, shear forces, and torsion), the primary Mode I crack opening loading is due to applied bending moment.

Morató [135] performed comprehensive aero-elastic analysis to determine the most onerous load case for mudline overturning moment and blade root moments. The analysis shows that for a NREL 5MW wind turbine [136] based in a shallow water site in the Dutch North Sea [32], a combination typically assessed in research work, the maximum and minimum mudline overturning moment are 1.769E5 kNm and 1.230E5 kNm for the typical design load cases. A bending moment load of 1.230E5 kNm induces a membrane stress of 45MPa in the outer fibres of the monopile and is considered for the assessment. For simplicity the through-wall bending stress is ignored in the analysis and can be shown to be small for thin-walled structures.

## 4.8 Results and Discussion

### 4.8.1 BS 7910 Results

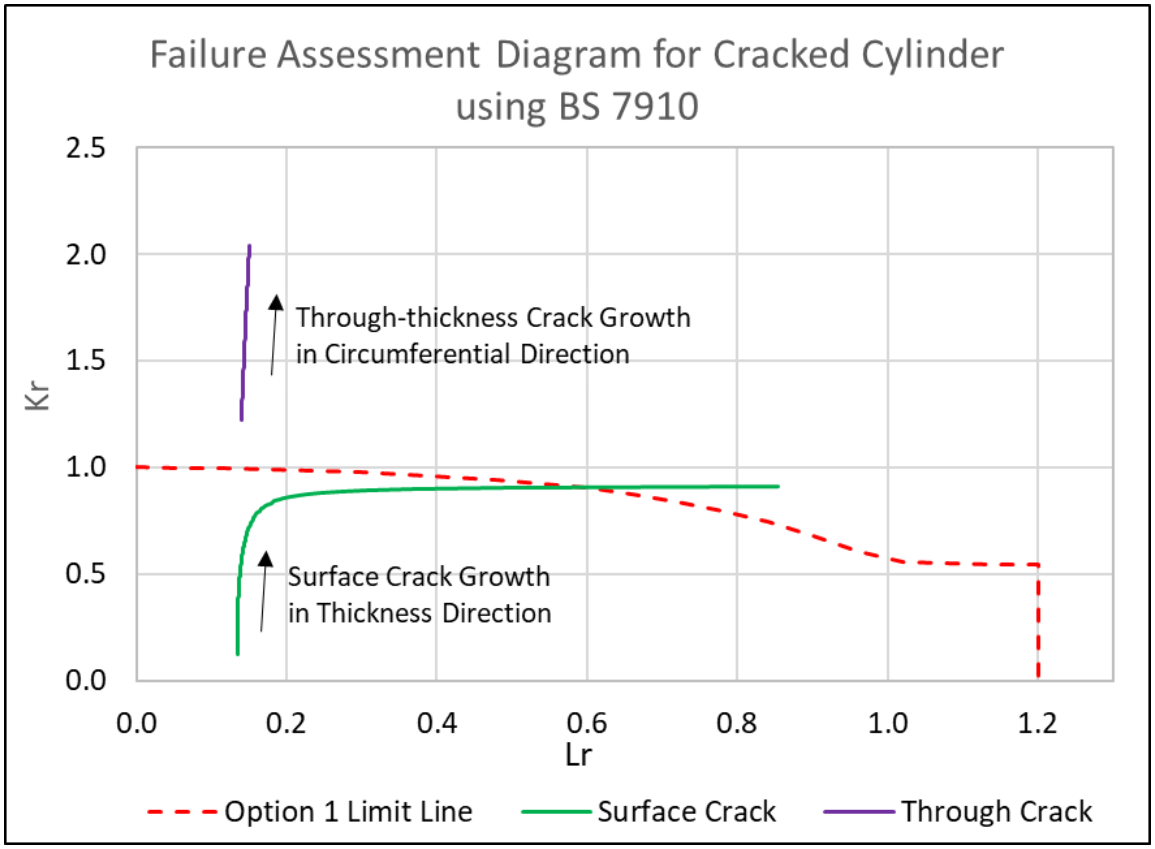


**Figure 4.8 – FAD for growing Circumferential Surface Crack and Through-thickness Crack**

The failure assessment diagram of a flaw growing from a surface crack until through thickness and for a through-thickness crack growing circumferentially is presented in Figure 4.8. The results show that for the applied stress, there is a surface crack depth which is unacceptable as it results in a combination of plastic collapse and brittle failure ratio that exceeds the FAD line.

However, examining the trends of the plastic collapse and brittle failure ratios reveals an anomaly. For the surface crack, the brittle failure ratio, $K_r$, is shown to increase monotonically with increasing surface crack depth. The plastic collapse ratio is initially insensitive to the crack depth. This is expected given the small size of the crack relative to the monopile, that is, there is sufficient intact ligament such that the monopile should not experience net section collapse due to loss of load bearing in the crack zone. However, the results show a rapid increase in the plastic collapse ratio as the crack depth to thickness ratio exceeds 80%.

The asymptotic trend is not present in the plastic collapse ratio for the through thickness crack. Whilst a discontinuity is expected in the jump from surface crack to through-thickness crack due to the additional ligament lost as the crack transitions from semi-elliptical to through thickness for the same depth to crack length ratio, it does not explain the rapid increase in the plastic collapse ratio for the semi elliptical crack.

It is clear that there is an issue with the calculation of plastic collapse ratio for a semi-elliptical crack for crack depths close to the value of the section thickness. A critical probing of the equation for reference stress suggests a purely numerical explanation for this behaviour. For a/c = 0.4, the maximum value of $c/r_0$ for this case study is 0.08. Therefore, as crack depth, a, approaches section thickness, t, the equation for reference stress for an external surface flaw may be simplified to:

$$\sigma_{ref} \approx P_m \left[1 + \frac{2c/r_0}{\pi}\left[\frac{a/t}{1-a/t}\right]\right] \qquad 4.9$$

The key component of equation 4.9 is $\frac{a/t}{1-a/t}$ which is plotted in Figure 4.9. The plot shows the exponential growth behaviour of the equation of values of a/t greater than 0.8. Figure 4.9 indicates an inherent flaw in the calculation of reference stress for cases where the crack has penetrated more than 80% of the monopile thickness.

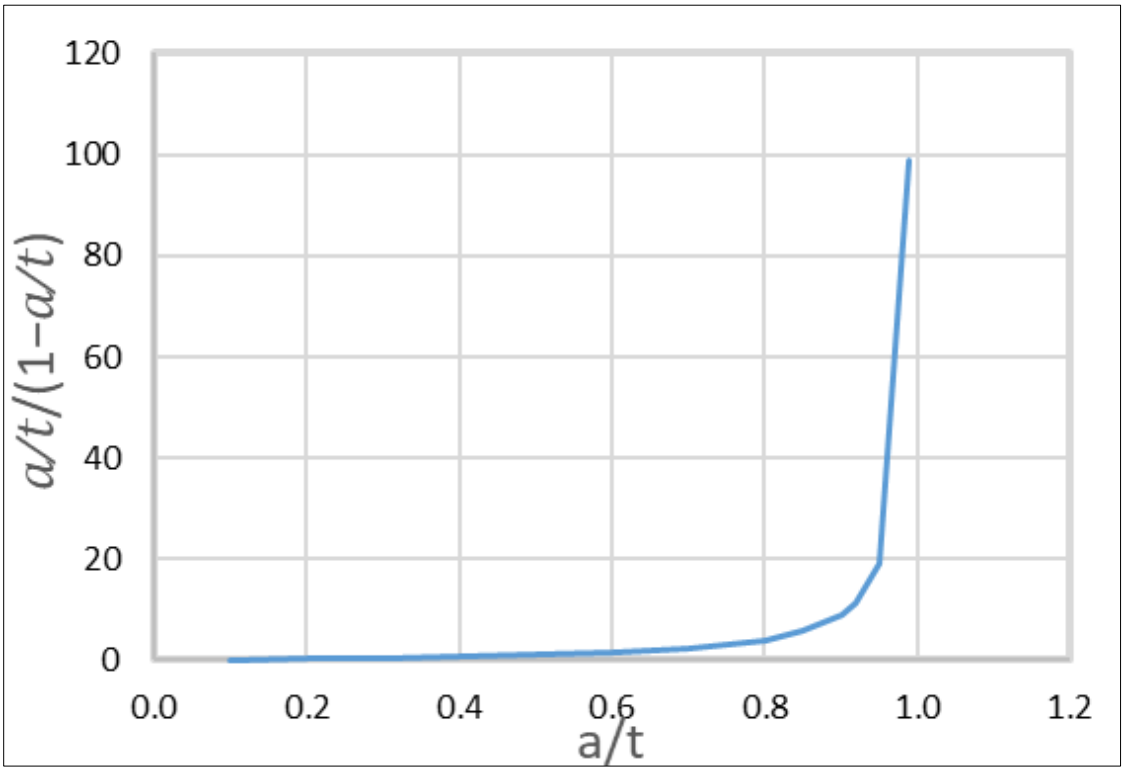


**Figure 4.9 – Plot of $\frac{a/t}{1-a/t}$ against a/t**

This behaviour is of less concern for cylinders where there is little margin between 80 – 100% of thickness. However, for monopiles, this range may cover a value of 20mm or greater. Crack growth as a large flaw, e.g. when the crack depth exceeds half the thickness of the monopile thickness, forms a significant part of the total life.

The invalidity of the reference stress equation for surface crack depths greater than 80% of section thickness is not explicitly stated in clause P.10.4 of BS 7910. The only specified limit of 80% is on the ratio of crack half-length to the pipe radius, c/ $r_o$. The cracks considered for this case study are well below this limit.

Taking the findings together, it is possible that a monopile with a circumferential surface flaw may be identified as close to plastic collapse failure when there may still be significant residual life for a situation where the ratio of crack depth to section thickness, a/t is greater than 80%.

### 4.8.2 FEA Results

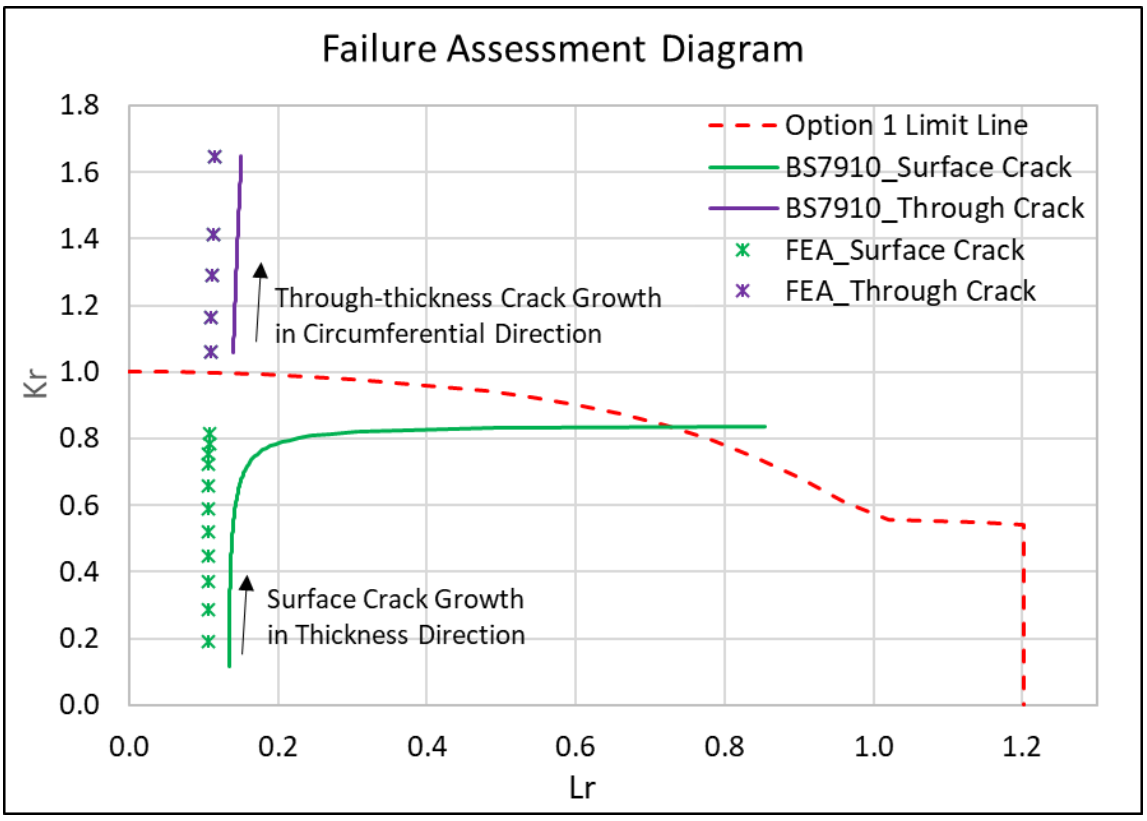


**Figure 4.10 – FAD for Circumferential Surface Crack and Through-thickness Crack**

A plot of the fracture and load ratios obtained from the FE analyses against the values calculated for the same geometry using the equations prescribed in the industrial standard BS 7910 [117] is presented in Figure 4.10. The fracture ratio, $K_r$, and the load ratio, $L_r$, are calculated based on stress intensity factor and limit loads obtained from FE analyses of various cracked geometry. The findings from the comparison are presented subsequently.

### 4.8.3 Load Ratio Comparison

Figure 4.10 shows agreement between both FE analysis and BS 7910 that there is little impact initially on the load ratio as the crack grows. This is expected as there is significant connected ligament in the rest of the structure such that the crack has little impact on the static load bearing capacity of the structure. This is in line with experimental observations by Martinez-Luengo et al. [137].

Figure 4.10 also shows that the load ratio obtained by FE analysis is slightly smaller than the value predicted by BS 7910. This is unsurprising as one would expect the results obtained from the application of a general code to be conservative compared to a bespoke analysis

due to the necessary assumptions involved in collating the equations for BS 7910. However, the major difference in the FE results and BS 7910 arise as the surface crack approached through thickness. The FE results do not exhibit the asymptotic behaviour as shown in the BS 7910 calculations. Figure 4.10 shows that the FE results proceed with the same trend as the surface crack transitions to a through thickness crack.

### 4.8.4 Fracture Ratio Comparison

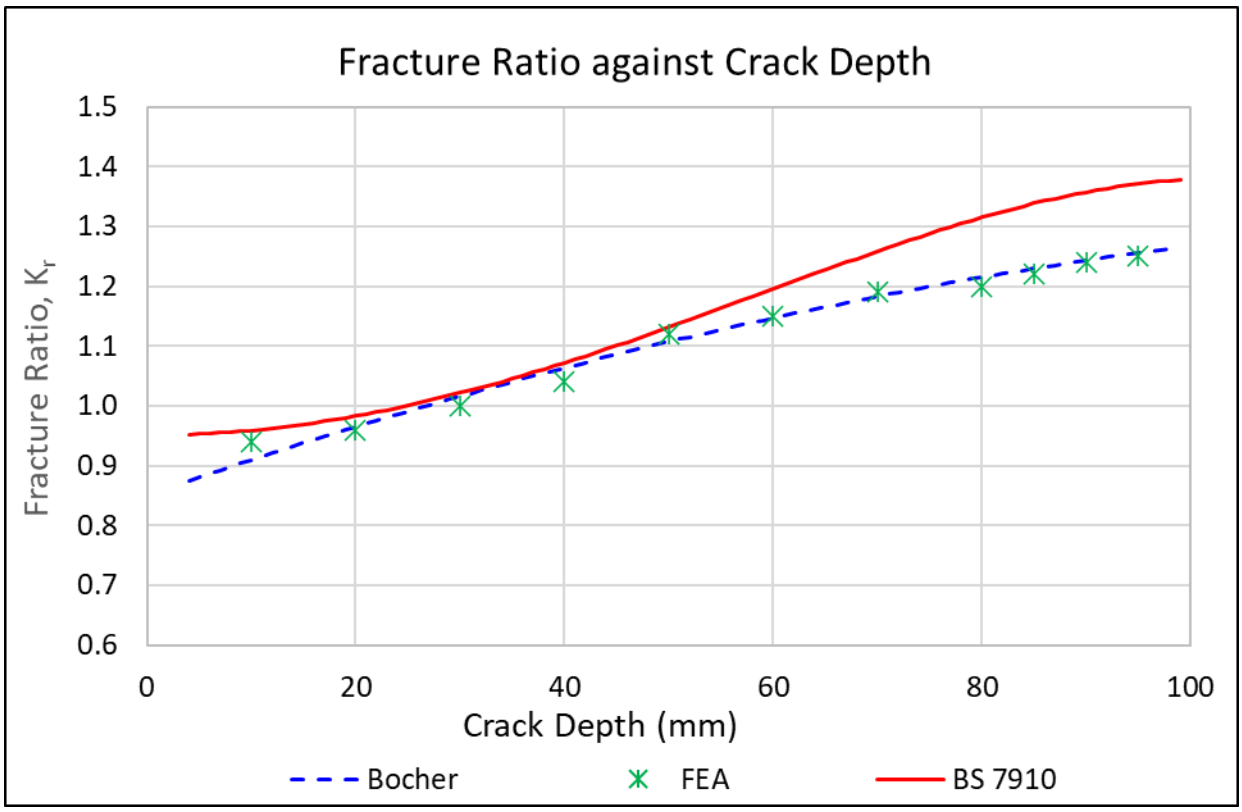


**Figure 4.11 – Fracture Ratio against Crack Depth**

The SIF solution in BS 7910 for a circumferential external surface crack in a cylinder is based on the flat plate solution underpinned by the empirical stress intensity factor equation for a semi-elliptical surface crack in a finite plate proposed by J.C. Newman and I.S. Raju [75] and [76].

It is shown in recent work by Bocher et al. [77] that for pipes with large radius/thickness ratios (as is common in monopiles), these solutions provide inaccurate estimation of the shape function. The results presented in Figure 4.11 show that there is alignment between the current work and the results presented by Bocher et al. [77].

Figure 4.10 shows a minor discontinuity between the $K_r$ value for a surface crack depth of 95mm and a through-crack with a half angle of 0.083rads. This is due to the additional ligament lost as the crack transitions from semi-elliptical to through-thickness for the same depth to crack length ratio.

## 4.9 Conclusion and Future work

This paper presents an assessment of the fitness for purpose of an offshore wind turbine monopile with a known semi-elliptical surface flaw in accordance with the procedure outlined in the industry standard, BS 7910 and comparison with results obtained from finite element analysis.

The results presented in this paper highlight the issues with the calculation of the load ratio, $L_r$ using the methodology outlined in BS 7910 for cracks with depths greater than 80% of the monopile thickness. $L_r$ values for deep cracks calculated from BS 7910 exhibit an asymptotic behaviour as the crack depth nears through-thickness.

The load ratio values obtained from detailed 3D FE limit analysis using elastic-perfectly-plastic material behaviour show that the asymptotic behaviour predicted by BS 7910 as the flaw transitions from deep crack to through-thickness crack is not present. Furthermore, the fracture ratio, $K_r$, predicted by BS 7910 deviates from values obtained from FEA of large diameter pipes typically used for offshore monopiles. This confirms the findings by other researchers such as Bocher et al. [77].

Taken together, the findings suggest that a surface breaking defect may be identified as unacceptable based on BS 7910 when there may still be a non-trivial amount of structural residual life. There are additional issues with the use of BS 7910 for offshore monopiles, such as the lack of sufficient library of shape function (Y) solutions for cylinders with large radius to thickness ratios. There is also a lack of information on the evolution of crack shape for cylinders under bending. It is assumed that initially elliptical flaws remain elliptical as they grow and that the crack aspect ratio remains the same. However, it may be important to account for different growth rates at different points along the crack. Further research is required to address these issues to allow BS 7910 to be used confidently to assess the acceptability of flaws in offshore wind turbine monopiles.

# 5 $L_R$ METHODOLOGY

*Fajuyigbe, A., and F. Brennan (2022), "A simplified formula for calculating the limit load of cracked offshore wind turbine monopile under bending" Marine Structures 83 (2022): 103164.*

*Sections of the content presented below are reproduced from the published peer-reviewed paper.*

## 5.1 Paper Synopsis and Additional Notes

In section 4, the FAD is identified as a suitable tool for assessing the acceptability of a cracked monopile. However, the issues identified in paper 1 indicated that a more appropriate and accurate methodology is required for determining the limit load (used in calculation of $L_r$). A simplified methodology for calculating the plastic collapse (limit) bending moment load of a pipe with a circumferential flaw is presented in this paper. The approach is based on the theory of net section collapse and allows for near instantaneous calculation of limit load for any arbitrary crack configuration and loading direction.

In this paper, novel equations for estimating the limit load of OWT monopiles under bending are derived thus achieving the second research objective of this thesis.

## 5.2 Introduction

An aged structure is likely to already contain a flaw either due to manufacturing defects or through system loading. It is therefore necessary to assess its fitness for service to ascertain if the cracked structure will fail under applied load. One widely accepted method for assessing the acceptability of a flaw in a metallic structure is to plot its position on the failure assessment diagram (FAD) as prescribed in the industry standards such as BS 7910 - Guide to methods for assessing the acceptability of flaws in metallic structures [68].

The FAD delineates regions of safe operation based on data for different materials. The ordinate plots the fracture ratio, $K_r$; a measure of the susceptibility of the structure's unstable brittle fracture calculated using linear elastic fracture mechanics. The abscissa plots the load ratio, $L_r$; a measure of the susceptibility of the structure to plastic collapse as is typical of less brittle or ductile materials where the microstructure allows for deformation/flow of the material.

The load ratio, $L_r$ is the ratio of the applied load to the limit load for a particular cracked component. Therefore, the accurate calculation of plastic limit loads is a cornerstone for assessing the acceptability of a cracked structure.

The limit load of a cracked structure may be determined from elastic-perfectly-plastic 3D finite element (FE) analyses. To do this, an elastic-perfectly-plastic material curve is assumed with the onset of plasticity set as the flow strength. Incremental load is applied to the structure until the magnitude of the applied load that causes global plastic collapse is achieved. This is signalled by the loss of static structural equilibrium due to excessive plasticity. The load applied at the final converged increment is the limit load [78]. The limit

load analysis must be repeated if there is any change in the configuration. It is computationally expensive to set up and run these FE models. Thus, finite element analysis is not practical in situations where the crack geometry is constantly changing under the action of fatigue loads. Some other methodologies for determining the limit load were discussed in section 4.7.4 along with their challenges in implementation.

Thus, another approach is proposed for the estimation of limit load for real time/pseudo-real time assessment of a cracked offshore wind turbine monopile subjected to cyclic loading. The proposed methodology is based on the theory of net section collapse. It is noted that the limit load obtained using the proposed methodology is intended for use in the determination of load ratio, $L_r$ for FAD. The FAD approach is established and enshrined within international standards and design guidance such as BS 7910 [68]. The contribution made in this paper is in a better understanding and calculation of $L_r$ for large diameter tubulars for use within the FAD framework and does not attempt to distinguish between ductile-brittle behaviour which is dealt with elsewhere.

## 5.3 Net Section Collapse

Net section collapse (NSC) is a simple method originally developed in the Electric Power Research Institute (EPRI) project RP585 [138] for determining the collapse load of a cracked pipe containing circumferential cracks. This approach is adopted by a wide range of industrial standards such as R6/Fitnet[74].

NSC analysis of cracked pipes in accordance with industrial standards typically involves idealisations of the crack geometry. For most applications, a crack is often idealised as either a semi-elliptical or constant depth. Rahman and Wilkowski [139] extended the NSC methodology to symmetrical flaws with complex shapes. Iwamatsu et al. [140] extended the methodology to allow non-symmetric flaws to be assessed by adding continuous shift angle. The shift angle allows the position of the coordinate axes which produce the minimum failure bending moment to be established. Several researchers such as Hasegawa et al. [141] and Iwamatsu et al. [142] have validated the use of NSC to determine the limit load of small diameter cracked pipes. This includes experimental validation against 304 stainless steel pipe with various number of circumferential cracks.

To the best of the of the author's knowledge, most research to validate NSC equations such as Hasegawa et al. [141], Iwamatsu et al. [142], Li et al. [143], and Li et al. [144] have focused on small pipes (circa 114.3mm in diameter). There is little work validating the use of the NSC equations for use with large diameter cylinders. The NSC equations derived in this paper are intended for use with offshore wind turbine (OWT) monopile support structures which according to Brennan [4] represent approximately 90% of commissioned offshore wind structures and can be 6m in diameter as stated in Arany et al. [23].

Literature review indicates that net section collapse equations are typically generated for two conditions: either the entire crack is subjected to tension, or the crack is partially subjected to compression. The case where part of the crack is in compression is further divided into cases with crack closure and non-crack closure corresponding to geometries with tight and blunt cracks, respectively. The user must first categorise the crack to allow the selection of the appropriate set of equations.

In this section a generalised equation is formulated that is considered suitable for the limit load analysis of any crack located in either the tensile or compressive zones as long as the crack is capable of crack closure. For monopiles under compressive loads, the crack faces come into contact to transmit loads. This is a primary reason why the cracks do not grow when the stress is compressive. Thus, for these structures, behaviour under crack non-closure is not relevant.

### 5.3.1 NSC Equation Formulation

The internal stress distribution (σ) in the wall of a pipe with external surface cracks is presented in Figure 5.1. The cracks are assessed for Mode I loading which is typical for most fractures. For a crack, subject to Mode I loading, the principal load is applied normal to the crack and tends to open the crack. Although the offshore wind turbine monopile is subject to various types of loads (compressive loads, shear forces, and torsion), only bending moment loads are applicable to Mode I crack opening.

The cracks shown in Figure 5.1 are not symmetrical about the bending plane. The lack of symmetry means that the internal bending moment will have components in both x and y axes. Thus, when the moments are integrated, they may not equate to the externally applied uniaxial bending moment. However, work by multiple researchers such as Iwamatsu et al. [140] show that the minimum collapse load occurs when the axis of the applied bending moment is symmetric with respect to the crack. Therefore, to obtain the minimum collapse capacity, the NSC assessment should consider load applied at the symmetric axis regardless of the actual bending axis.

Two key parameters are noted in Figure 5.1: the location of the neutral axis (N.A) which denote the line of zero stress due to applied bending load, and the associated stress inversion angle β.

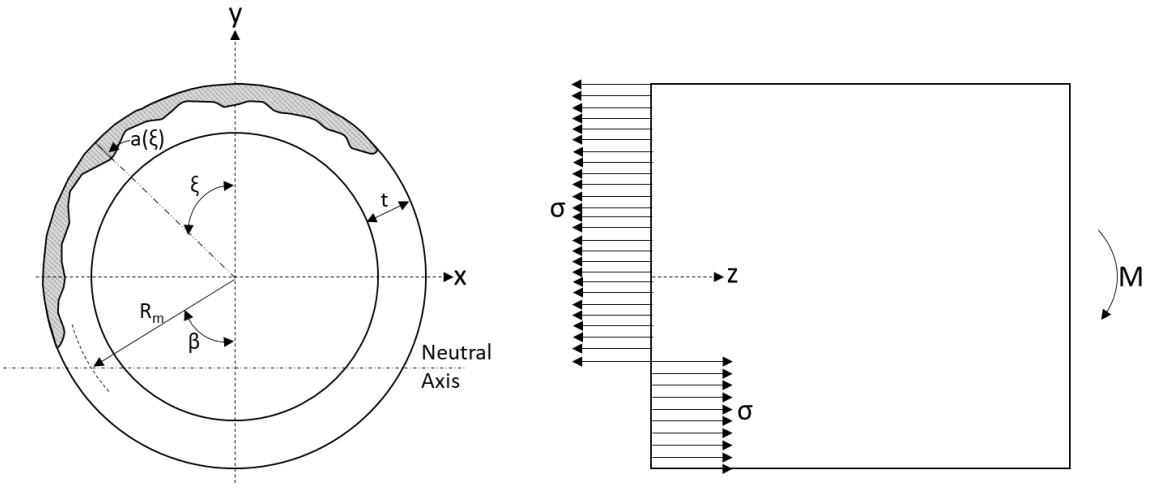


**Figure 5.1 – Crack Geometry and Stress Distribution**

A couple of simplifications are adopted for the purpose of generating the NSC equations. They are as follows:

- It is assumed that the pipe can be classified as thin-walled. For practical engineering applications, thin-walled assumption is adopted for pipes with ratio of diameter to thickness (D/t) greater than twenty. D/t for monopiles used in commercial OWT are in excess of this value [23].

- For a monopile containing multiple co-planer cracks, the cracks are treated as a single crack spanning the entire circumference of the pipe. The crack depth is simply set to zero for the uncracked regions. The manipulation of the crack geometry in this manner removes the need to define the integration limit for each individual crack.

For application of bending moment about an axis that is symmetric with respect to the crack profile, the internal stress system must satisfy equilibrium with the applied loads.

The monopile is only subjected to compressive load due to the weight of the tower, nacelle, and rotors. Thus, the equation for tensile force equilibrium is as follows:

$$\sigma R_m t\left[\int_0^{\pi-\beta}\left(1-\frac{a(\xi)}{t}\right)d\xi+\int_{\pi+\beta}^{2\pi}\left(1-\frac{a(\xi)}{t}\right)d\xi-2\beta\right]=0 \qquad 5.1$$

Re-arranging gives:

$$\beta=\frac{\pi}{2}-\frac{1}{4t}\left[\int_0^{\pi-\beta}a(\xi)d\xi+\int_{\pi+\beta}^{2\pi}a(\xi)d\xi\right] \qquad 5.2$$

The monopile is subjected to a moment load due to wind loads on the tower and the nacelle. Thus, to satisfy moment equilibrium:

$$\sigma {R_m}^2 t \left[ 4sin\beta - \frac{1}{t}\left[ \int_0^{\pi-\beta} a(\xi)cos\xi d\xi + \int_{\pi+\beta}^{2\pi} a(\xi)cos\xi d\xi \right] \right] = M \qquad 5.3$$

For a crack with a complex shape, it is not possible to define a closed function for the crack depth "a", and thus obtain an analytic solution for the integral in equation (1) and (2). However, obtaining a solution by numerical analysis is trivial.

Setting the internal stress (σ) to the flow stress of the material ($\sigma_f$) allows the calculation of the maximum moment that the structure can withstand before plastic collapse. The collapse bending moment is obtained by solving equation 5.2 to obtain the value of $\beta$ for the cracked geometry. $\beta$ is then used in equation 5.3 to obtain the collapse moment.

## 5.4 Validation of Proposed Methodology

### 5.4.1 Literature

Limit load values obtained using the methodology presented above are compared to values found in literature. Hasegawa et al. [141] performed theoretical calculations and also obtained experimental values for geometries containing constant depth, internal circumferential flaws with a material flow strength of 425Mpa. The geometry considered in the research work is summarized in Table 5.1.

**Table 5.1 – Pipe Specimen Geometries [141]**

| Specimen No. | D (mm) | t (mm) | Flaw Depths a1 (mm) | Flaw Depths a2 (mm) | Angle θ (deg) | Angle α (deg) |
|---|---|---|---|---|---|---|
| DP 01 | 114.3 | 8.6 | 6.3 | 6.3 | 60 | 0 |
| DP 02 | | | 6.4 | 6.4 | 60 | 10 |
| DP 03 | | | 6.3 | 6.2 | 60 | 20 |
| DP 04 | | | 6.4 | 6.2 | 60 | 30 |
| DP 05 | | | 6.3 | 6.2 | 45 | 30 |
| DP 06 | | | 6.3 | 6.3 | 45 | 40 |

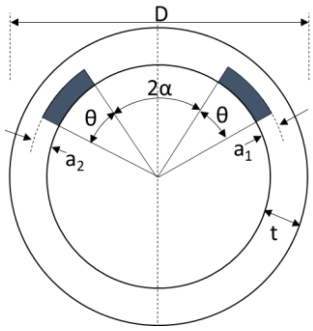


Figure 5.2 shows that the proposed methodology agrees with the calculated values from Hasegawa et al [141]. Both calculated values are correlated well (<10% difference) with the experimental results thus validating the NSC approach for limit load calculation.

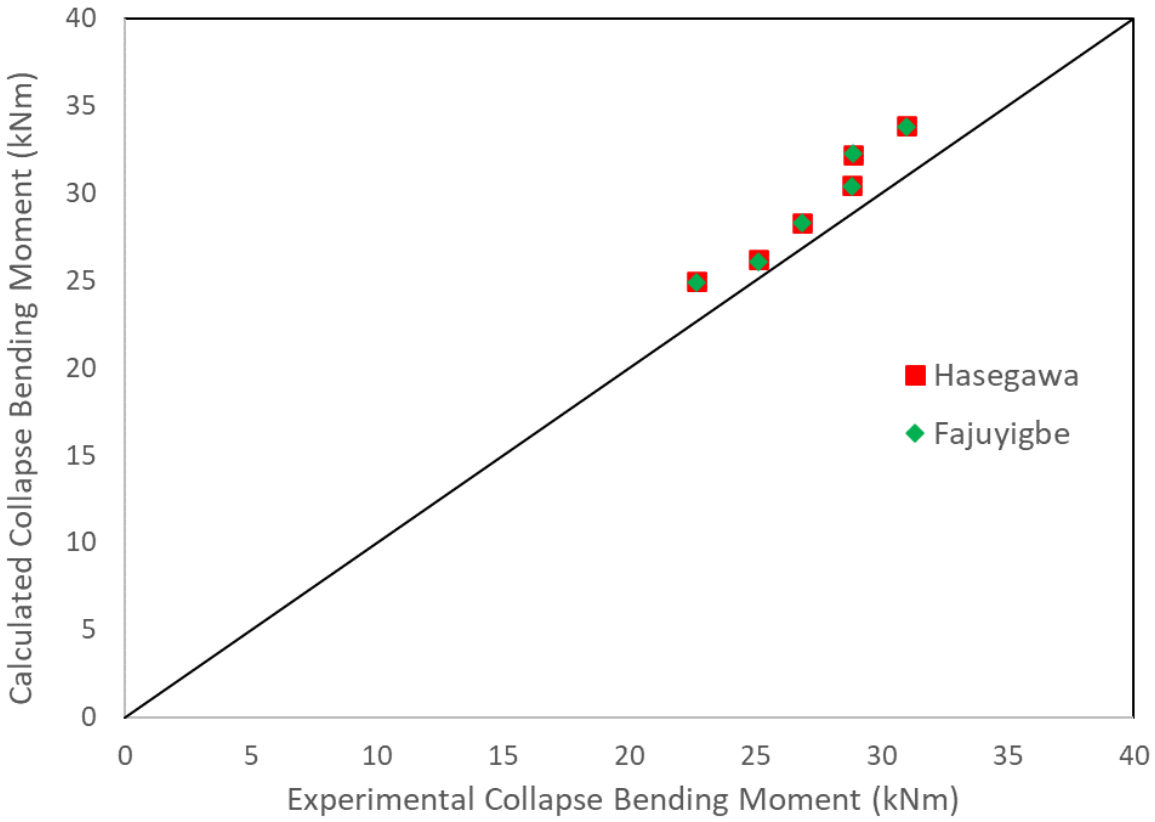


**Figure 5.2 – Comparison of Collapse Moment using Proposed Methodology and Hasegawa Data [141]**

### 5.4.2 Finite Element Analysis

The validation case presented in section 5.4.1 is based on a small diameter pipe. There is a valid question concerning the applicability of Net Section Collapse to large diameter cracked pipe. Due to the scale of the geometry, it is not practical to perform physical testing to obtain limit loads of cracked monopiles. An alternative method for systematic validation is to use finite element (FE) analysis.

FE limit load analysis is a well-established method for predicting plastic collapse. The process involves the application of an elastic-perfectly-plastic material curve to the structure with the onset of plasticity set as the material flow strength. Incremental load is applied to the structure until the structure cannot carry more load. This is signalled by the loss of static structural equilibrium. The load applied at the final converged increment is the limit load [132]. Confidence in the FE limit analysis is gained by comparing results obtained against the idealised plastic limit load solutions for uncracked pipe.

The monopile used for validation has an outer radius,($r_o$) of 3m, inner radius, ($r_i$) of 2.9m and wall thickness, ($t$) of 100mm in line with typical sizes of existing monopiles in various wind farms across Europe as reported in [23]. The length of the monopile is set as 40m which is the typical water depth of monopile foundation installations [77]. S355 steel is the most common material used in the fabrication of monopile support structure [121]. The material properties for S355 steel are as follows; the minimum yield strength, $\sigma_Y$ is taken as 335MPa, the tensile strength, ($\sigma_u$) is taken as 470MPa, the modulus of elasticity, E is

210GPa [122]. The flow strength is taken as 402.5MPa which is the average of the yield and ultimate tensile strength.

The monopile is modelled in the finite element software package, ABAQUS [127]. The FE model is pinned at one end. The moment load is applied to a reference point coupled to the free surface generating a pure bending load in the monopile. The crack is located at the longitudinal midspan of the monopile. To avoid problems associated with incompressibility, quadratic reduced integration elements within ABAQUS (element type: C3D20R) are used [133]. A schematic FE model is presented Figure 5.3. The implementation of the boundary condition and reference point for moment load application is shown in Figure 5.4a. The variation of element size around the crack region is shown in Figure 5.3b and in Figure 5.3c.

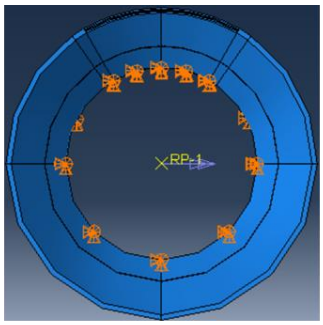


(a) Reference point and boundary condition

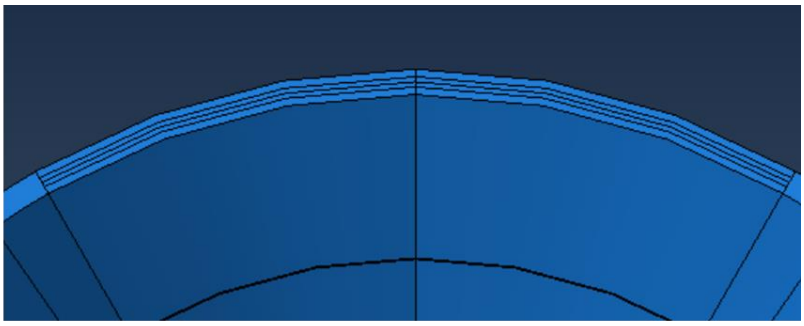

(b) Constant depth crack partitioning (detailed view)

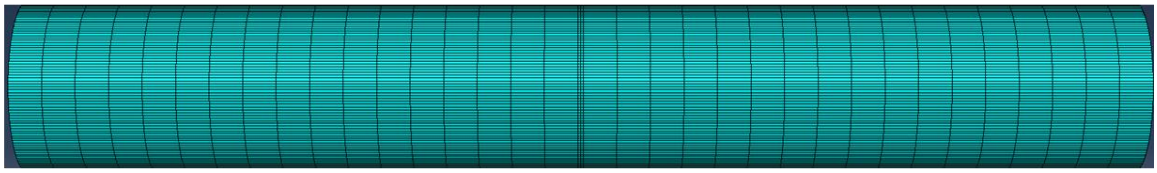

(c) Mesh side view and mid-length partitioning

**Figure 5.3 – Finite Element Model & Crack Depth Distribution vs angle**

## 5.5 Results and Discussion

The results of the FE analysis validation for various crack cross-sections using the pipe geometry is presented below. Firstly, the proposed methodology is validated against cracks of various depth/pipe thickness (a/t) ratios, and half angle, θ. Each crack is a constant depth external surface crack and symmetrical about the applied moment axis.

Figure 5.4 shows that the proposed methodology gives the same outcome as results obtained from limit load analysis for external surface flaw in thin-walled cylinder oriented circumferentially following the procedure set out in clause B.6.4 of the widely accepted R6/Fitnet procedures [74]. The limit load solution in R6/Fitnet for this case is based on solutions proposed by Lei and Budden [145] where the limit load for a perfectly plastic material is obtained according to the von Mises yield criterion.

The results using the proposed methodology are also similar to the values obtained from the bespoke FE analysis performed for this study with a maximum deviation below 10% for crack half angles below 60°. The deviation increases as the crack becomes very large relative to the pipe. This points to some limiting condition for the applicability of Net Section

Collapse theory to obtain limit loads for cases where the crack is very large relative to the monopile section. However, for cracks of these sizes there may be other pertinent failure mechanisms such as brittle fracture such that the limit load value is of lower importance.

Furthermore, the limiting loads from FE analysis are consistently larger, indicating that results obtained from the proposed methodology are conservative. This is consistent with literature [133] [146] as well as limit loads obtained from the industry code R6 [74]. It is known that these analytical solutions derived from simple equilibrium stress fields and yield criterion, such as Tresca or Von Mises, tend to under-predict actual limit loads, but the degree of conservatism is difficult to quantify. The conservatism in predicting plastic collapse loads using these methods may be one reason for their adoption as they should inherently lead to a safe design. For all cases, the plastic limit load defaults to the uncracked pipe value when θ or a/t =0 granting confidence in the methodology.

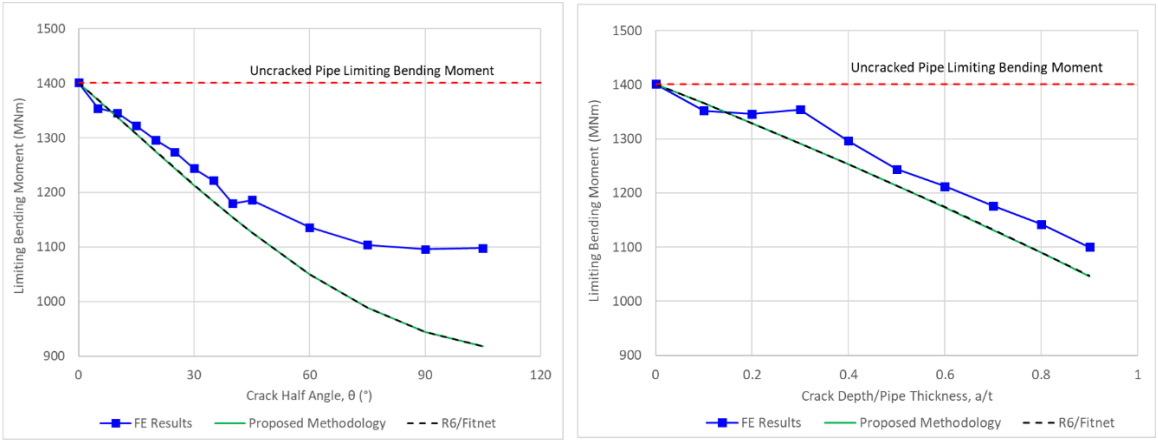


(a) Varying crack half angle (θ) for fixed crack depth/pipe thickness (a/t = 0.5)

(b) Varying crack depth/pipe thickness (a/t) for a fixed crack half angle (θ=30°)

**Figure 5.4 – Limiting Bending Moment for Various Crack Geometry**

One advantage of the proposed methodology over the existing approaches is that there is no need to categorise cracks into those entirely in the tension zone, and those straddling the compression zone. In existing approaches, the categorisation is then used to select the appropriate equations to determine the limit load of the cracked geometry. Mathematically, the categorisation is implemented by checking if $\theta+\beta \leq \pi$ or $\theta+\beta \geq \pi$. This is problematic as β is in itself an outcome of the net section collapse calculations. The proposed methodology is valid for cracks located in both the tension and compression zone as is shown in Figure 5.5(a). The plot shows that the limit load plateaus as $\theta+\beta > \pi$. This is because part of the crack is now in the compression zone and is able to transmit load in the same manner as an uncracked pipe.

Another advantage of the proposed methodology is the ability to determine the limiting bending moment applied at an axis that is not symmetrical to the crack profile. The practical implication is that limiting load can be determined for loading applied to the pipe in any arbitrary direction. This is particularly useful for offshore wind turbine monopile where environmental loads affect the structure from various directions. As shown in Figure 5.5(b), the limiting bending moment increases as more of the crack profile moves into the compression zone relative to the axis of the applied moment. The limiting moment reaches

the value for uncracked pipe when the axis of the applied moment is oriented such that the applied moment tends to close the crack (γ=180°).

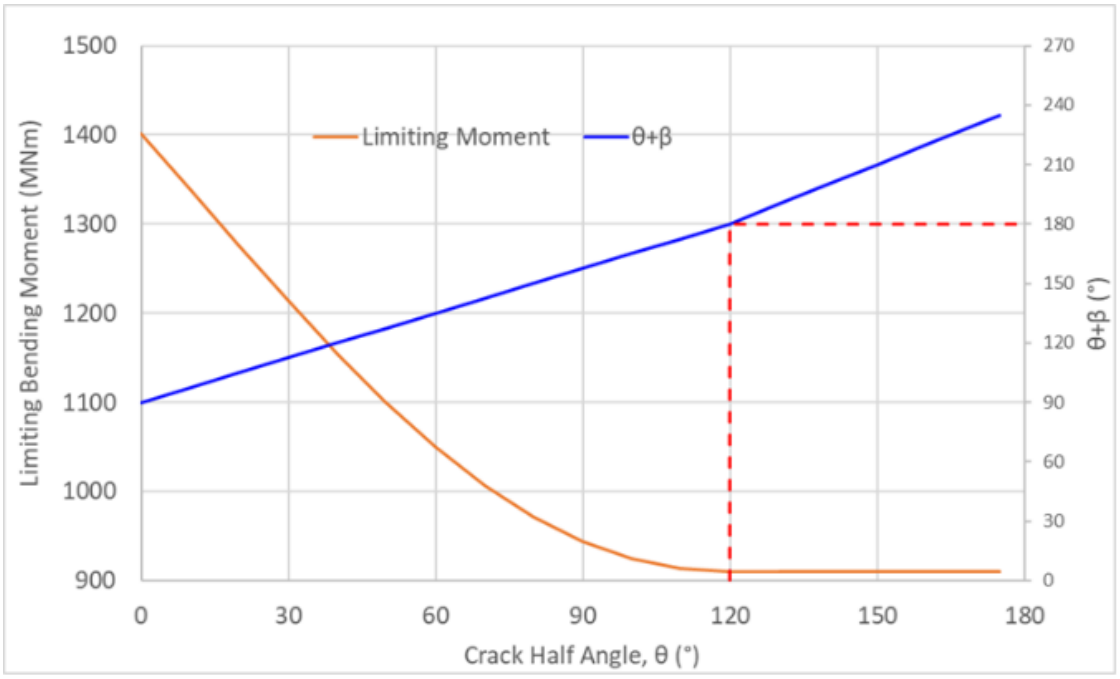


(a) Analysis of cracks in tension and compression zone

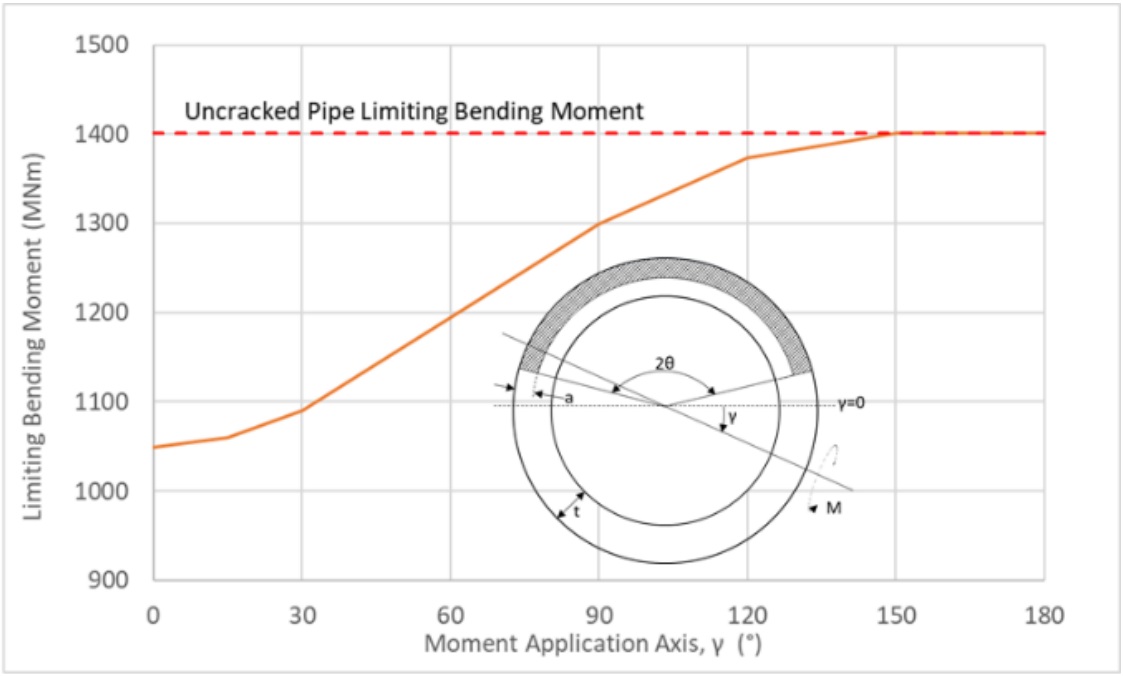


(b) Limiting bending moment for various load axis

**Figure 5.5 – Capability of New Methodology**

## 5.6 Variable Crack Analysis

Current NSC design guidelines such as R6/Fitnet [74] require a crack to be categorised as either semi-elliptical or constant depth for the estimation of plastic limit load. Real cracks can have an arbitrary profile. Crack shape idealisations such as semi-elliptical or constant depth can lead to under-estimation of the plastic collapse load. Cracks with arbitrary shaped profile can be assessed using the methodology proposed in this paper.

A crack with a variable depth is modelled in the monopile geometry presented above. The crack depth/pipe thickness ratio (a/t) varies between a/t of 0.4 - 0.6. The crack's half-angle (θ) is 60°. The crack profile is illustrated in Figure 5.6. The discretised values of the crack depth around the circumference of the pipe is presented in Appendix B. It is noted that zero degree crack angle is the position (0,3) and the orientation is positive in the anti-clockwise direction

The limit bending moment obtained from calculations and finite element analysis are presented in the Figure 5.7. Results are presented for constant cracks with a/t of 0.4, 0.5, 0.6 and the variable crack in Figure 5.7. All cracks have a half-angle (θ) of 60°. The results show that limit load for a crack with variable depth is between the bounding limits of results for a/t=0.4 and a/t=0.6. The results for the variable crack are also similar to the results for a constant crack with a/t=0.5. This is also expected as the area of loss ligament for the variable is equivalent to a constant crack depth with a/t=0.495. From the comparison, it is clear that the plastic collapse bending moment load for a variable crack is well predicted by the methodology proposed in this paper.

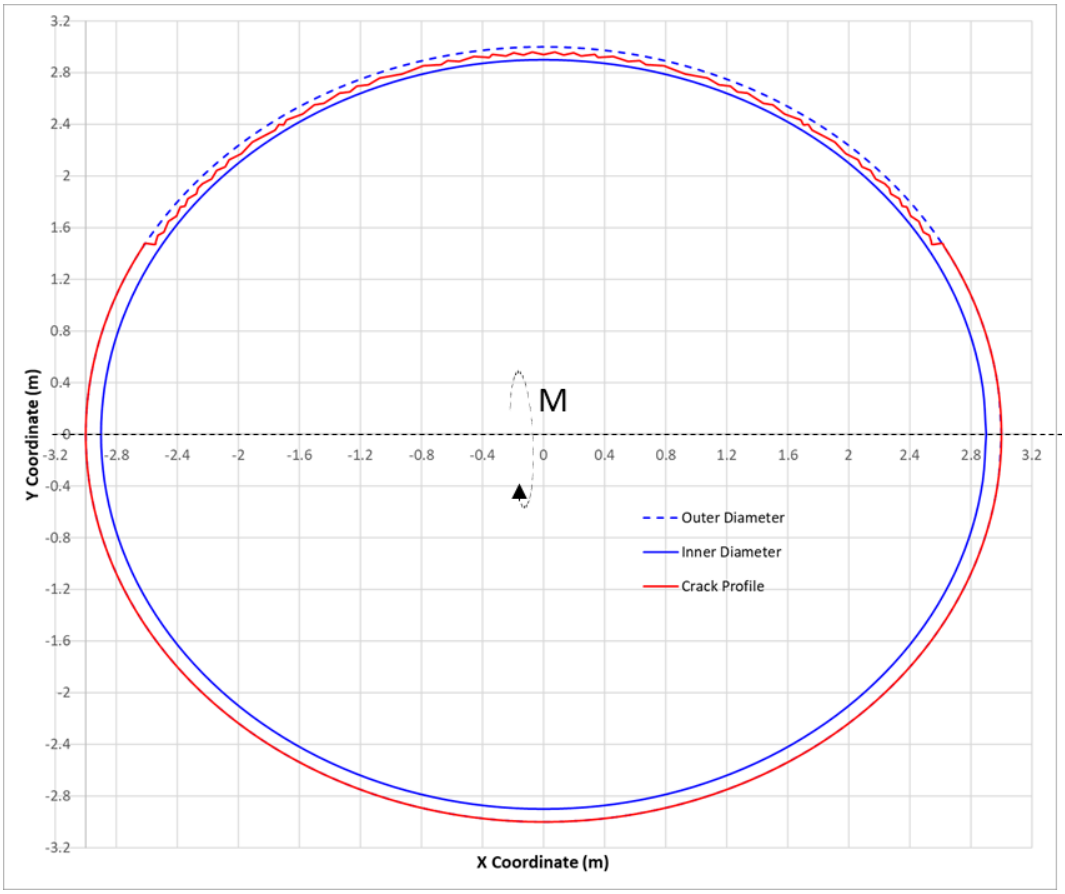

**Figure 5.6 - Variable Crack Profile**

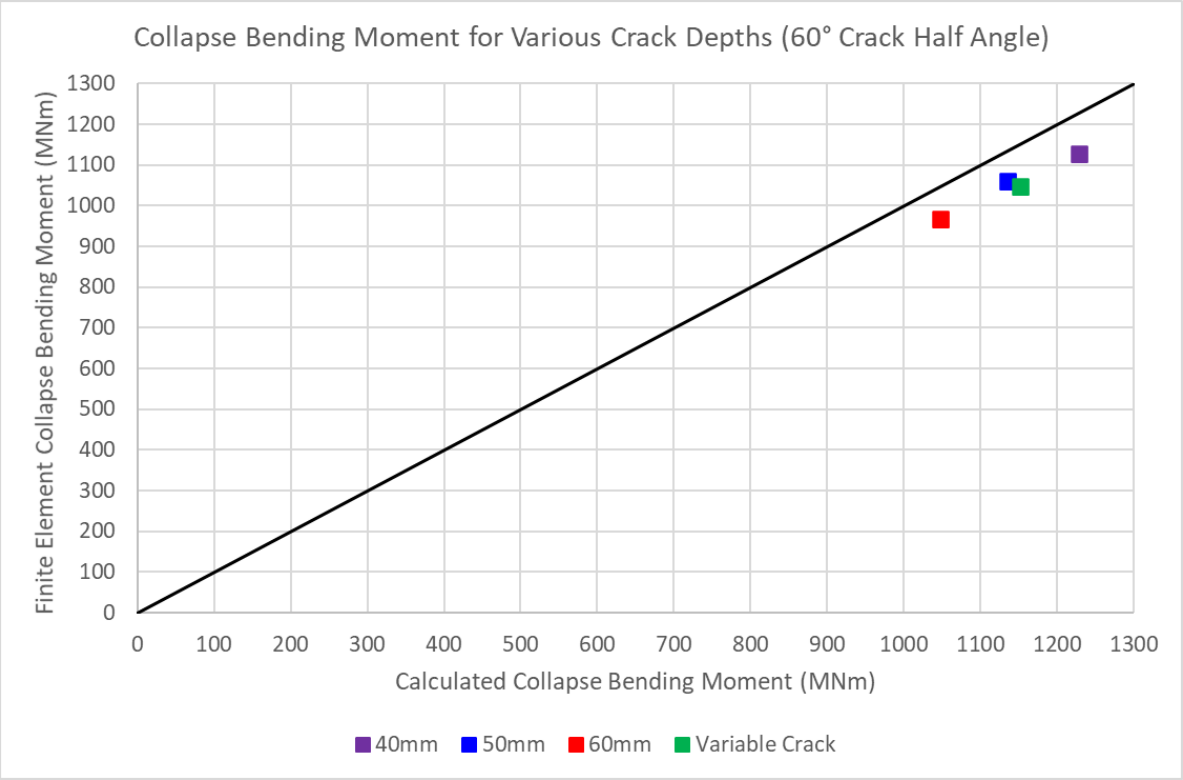


**Figure 5.7 – Variable Crack Results**

## 5.7 Conclusions

This paper presents a methodology for calculating the plastic collapse (limit) bending moment load of a pipe with a circumferential flaw with an emphasis on its application in the assessment of cracked offshore wind turbine monopiles. The limit load is a key component of the calculation of the load ratio which is used in the assessment of the fitness for purpose of a cracked structure. The methodology proposed in this paper is based on the theory of net section collapse (NSC) but differs from existing approaches in the following ways:

- The crack does not need to be categorised as occupying the tensile or compression zone.
- For multiple cracks, there is no need to define the span limits of each individual crack in the pipe geometry.
- The crack shape does not need to be idealised as either semi-elliptical or constant depth.
- The crack does not need to be symmetrical about the axis of the applied bending moment.

The proposed methodology is validated against results presented in literature and also finite element analysis results. Although it is possible to obtain limit loads using FE analysis, this is computationally expensive and time consuming. The proposed approach allows for near-instantaneous calculation of limit load for any arbitrary crack configuration and loading direction. This is a significant development for the analysis of offshore wind turbine monopiles as it allows the suitability of the cracked structure to be assessed in pseudo-real time.

# 6 $K_R$ METHODOLOGY

*Fajuyigbe, A. and Brennan, F. (2022). "Estimating stress intensity factor for semi elliptical circumferential cracks in offshore wind turbine monopiles using weight functions". In Ageing and Life Extension of Offshore Facilities (pp. 158-164).*

*Sections of the content presented below are reproduced from the published peer-reviewed paper.*

## 6.1 Paper Synopsis and Additional Notes

In addition to $L_r$ (addressed in section 5), Brittle ratio, $K_r$, is the other parameter required for plotting the position of a cracked monopile of the FAD. Calculating $K_r$ requires the SIF, which is a function of the stress acting on a crack and geometry of the cracked body. SIF may be obtained from FEA, but this is not practical for the large load cases associated with fatigue analysis of OWT monopiles. Literature review indicates that handbook solutions are not precise for OWT monopiles.

Given these issues, another methodology for estimating the stress intensity factor of OWT monopiles is proposed. The approach is based on the theory of weight functions. The ability to obtain fast and accurate SIF for OWT monopile cracks addresses the third of the thesis research objectives.

## 6.2 Introduction

The FAD delineates regions of safe operation based on empirical data for different materials. The ordinate plots the fracture ratio, $K_r$; a measure of the susceptibility of the structure to unstable brittle fracture failure in the presence of a crack calculated using linear elastic fracture mechanics. The fracture ratio, $K_r$, is the ratio of the stress intensity factor (SIF) at the current crack size due to applied loads to the fracture toughness, $K_{mat}$, of the structure material. This is defined mathematically as:

$$K_r = \frac{K_I^p + VK_I^s}{K_{mat}} \text{ or } \frac{K_I^p + K_I^s}{K_{mat}} + \rho \qquad 6.1$$

Where $K_I^p$ and $K_I^s$ are SIFs obtained from linear elastic fracture mechanics (LEFM), that is, only elastic methods, under the actions of relevant primary and secondary loads respectively. $V$ and ρ are functions of both the primary and secondary loads and account for plasticity interaction effects. Thus, calculating $K_r$ requires the stress intensity factor, $K_I$ which is a function of the stress acting on a crack and geometry of the cracked body. There are handbook solutions available for simple geometries, idealised crack shapes and orientations. For many real-life flaws and geometries that are not readily idealised, SIFs are typically generated from finite element analysis.

$K_I$ derived from finite element analysis is applicable only to the specific component and crack geometry and loading condition meaning that analysis must be repeated for any change in the configuration. It is computationally and temporally expensive to set up and run these FE models. Thus, the use of SIF generated from finite element analyses is not

practical in situations where the crack geometry is constantly changing such as under the action of fatigue loads. Hence, a more computationally efficient approach for estimating $K_I$ is required for use in assessing cracked structures in real or pseudo-real time.

The objective of this paper is to introduce a suitable methodology for estimating the stress intensity factor of cracked offshore wind turbine (OWT) monopiles. The remainder of this paper is organised as follows: Section 6.3 presents the formulation of the proposed approach. The generation of the reference solutions is presented in section 6.4. The shape function results, and validation are discussed in section 6.5. The validation of the weight function solutions are presented in section 6.6. The conclusions and outlook are presented in section 6.7.

## 6.3 Weight Function Formulation

Bueckner [147] and Rice [148] showed that the stress intensity factors for a variety of loading conditions can be calculated by simple integration of the parameter called the weight function and the stress distribution along the potential crack plane. The local stress field $\sigma(x)$ in the prospective crack plane is due to the external load S and it is determined for uncracked body by ignoring the presence of the crack. For a one-dimensional crack with depth, a:

$$K = \int_0^a \sigma(x) m(x,a) dx \tag{6.2}$$

Equation 6.2 states that if the weight function is known for a given cracked body, the stress intensity factor due to any load system applied to the body can be determined by using the same weight function. Bueckner [147] and Rice [148] further showed that the weight function is only dependent on geometry, that is, the weight function is a unique geometrical property of a cracked body for any given geometry and is independent of stress system. For a two-dimensional cracked body, the weight function $m(x,a)$ is defined in [147, 148] as:

$$m(x,a) = \frac{H}{2K_{ref}} \frac{\partial u_r(x,a)}{\partial a} \tag{6.3}$$

Where $K_{ref}$ is reference stress intensity factor, $u_r(x,a)$ is the corresponding crack opening displacement (COD) field, and $H$ is a function of Young's modulus ($E$): for an isotropic material it is $E/1-\nu^2$ for plane strain and $E$ for plane stress. Simply put, equation 6.3 suggests that the SIF solution subjected to one set of boundary conditions has sufficient information to obtain SIFs for any boundary conditions on the same geometry.

The expression presented in equation 6.3 was not immediately useful due to the difficulty in obtaining suitable pairs of reference SIF and corresponding COD. This was overcome when Petroski and Achenbach [149] proposed an approximate function for $u_r(x,a)$. The resulting three term expression was shown to sufficiently approximate a range of crack configurations but could not accurately describe some weight functions [150, 151]. Fett [152] proposed a five-term expression for $u_r(x,a)$ which performed better but with added complexity of extra terms.

Finally, Shen and Glinka [153] analysed the performance of several expressions for multiple known weight functions for edge and through cracks in plates and cylinders finding that a variety of existing weight functions have the same singular term and they can be accurately approximated by a general expression:

$$m(x,a) = \frac{2}{\sqrt{2\pi(a-x)}}\left[1 + M_1\left(1-\frac{x}{a}\right)^{1/2} + M_2\left(1-\frac{x}{a}\right) + M_3\left(1-\frac{x}{a}\right)^{3/2}\right] \quad 6.4$$

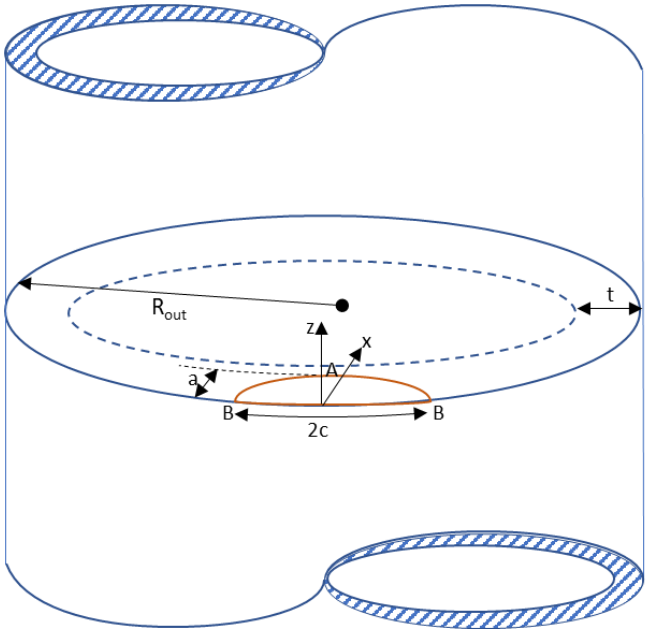


**Figure 6.1 - Semi-Elliptical External Surface Crack**

Equation 6.4 is considered as a universal form of a weight function for solving Mode I crack problems. For three known independent reference SIF and corresponding stress states, the three unknown coefficients $M_1$, $M_2$ and $M_3$ can be determined for any cracked body using equation 6.5. Furthermore, Fett [152] noted the slope of the crack surface under symmetrical loading should be zero at x=0, thus:

$$\frac{\partial m(x,a)}{\partial x}\Big|_{x=0} = 0 \quad 6.5$$

Fett [152] also notes that for deeper cracks the curvature of the crack surface is zero, thus the second derivative of the weight function should also be zero:

$$\frac{\partial^2 m(x,a)}{\partial x^2}\Big|_{x=0} = 0 \quad 6.6$$

These observations mean that the parameters $M_1$, $M_2$ and $M_3$ can be determined for any cracked body if there are two known independent reference stress intensity factors and corresponding stress states. $M_1$, $M_2$ and $M_3$ are obtained by solving the following 4 simultaneous equations:

$$K_{ref1} = \int_0^a \frac{2\sigma_{ref1}(x)}{\sqrt{2\pi(a-x)}}\left[1 + M_1\left(1-\frac{x}{a}\right)^{1/2} + M_2\left(1-\frac{x}{a}\right) + M_3\left(1-\frac{x}{a}\right)^{3/2}\right]dx \quad 6.7$$

$$K_{ref2} = \int_0^a \frac{2\sigma_{ref2}(x)}{\sqrt{2\pi(a-x)}}\left[1 + M_1\left(1-\frac{x}{a}\right)^{1/2} + M_2\left(1-\frac{x}{a}\right) + M_3\left(1-\frac{x}{a}\right)^{3/2}\right]dx \quad 6.8$$

$$\frac{\partial}{\partial x}\left\{\frac{2}{\sqrt{2\pi(a-x)}}\left[1 + M_1\left(1-\frac{x}{a}\right)^{1/2} + M_2\left(1-\frac{x}{a}\right) + M_3\left(1-\frac{x}{a}\right)^{3/2}\right]\right\}\Bigg|_{x=0} = 0 \quad 6.9$$

Or

$$\frac{\partial^2}{\partial x^2}\left\{\frac{2}{\sqrt{2\pi(a-x)}}\left[1 + M_1\left(1-\frac{x}{a}\right)^{1/2} + M_2\left(1-\frac{x}{a}\right) + M_3\left(1-\frac{x}{a}\right)^{3/2}\right]\right\}\Bigg|_{x=0} = 0 \quad 6.10$$

Where $K_{refn}$ and $\sigma_{refn}(x)$ are reference SIF solutions and corresponding stress states respectively.

### 6.3.1 2D Cracks

The equations presented above are for one-dimensional crack problems. An OWT monopile typically has a 2-dimensional semi-elliptical crack originating from the internal or external surface of the cylinder as illustrated in Figure 6.1. For a semi-elliptical crack, the stress intensity factor changes along the crack front. However, for most configurations, the highest and lowest values of SIF occur at the deepest point (A) or the surface point (B). Therefore, it is possible to transform the 2-D problem into a 1-D problem by replacing the semi-elliptical crack with appropriate 1-D cracks. One crack approximates the deepest point A on the crack front. Shen and Glinka [154] show that the equations presented in equation 6.7 to 6.10 for an edge crack are valid for this condition.

Shen and Glinka [154] also show that for the surface point (B), equations 6.7 and 6.8 may be written as:

$$K_{ref1} = \int_0^a \frac{2\sigma_{r1}(x)}{\sqrt{\pi x}}\left[1 + M_1\left(\frac{x}{a}\right)^{1/2} + M_2\left(\frac{x}{a}\right) + M_3\left(\frac{x}{a}\right)^{3/2}\right]dx \quad 6.11$$

$$K_{ref2} = \int_0^a \frac{2\sigma_{r2}(x)}{\sqrt{\pi x}}\left[1 + M_1\left(\frac{x}{a}\right)^{1/2} + M_2\left(\frac{x}{a}\right) + M_3\left(\frac{x}{a}\right)^{3/2}\right]dx \quad 6.12$$

Given that the weight function must be zero at x=a, the third condition is:

$$1 + M_1 + M_2 + M_3 = 0 \quad 6.13$$

## 6.4 Reference Solution

SIF for an arbitrary stress field is based on superposition of the behaviour of structure under the reference stress files, thus it is advantageous for the stress fields $\sigma_{r1}$ and $\sigma_{r2}$ used to generate $K_{r1}$ and $K_{r2}$ respectively to linearly independent of each other. A crack can experience three types of loading termed Mode I (opening mode), Mode II (shearing mode) and Mode III (tearing mode). The focus of this paper is on cracks subject to Mode I loading which is typical for most fractures. For a crack subject to Mode I loading, the principal load is applied normal to the crack and tends to open the crack. Thus, stress distribution from uniform uniaxial tension and from pure bending are used to generate reference SIF.

It is noted that a thin pipe subjected to bending moment about it central axis has a dominant mean stress field in its thickness that is similar to stress field generated under uniaxial tension. However, the presence of the additional linear bending stress profile from the outer to inner fibre should provide a distinction in the computation of the weight function. Furthermore, combinations of axial force and bending moment are the dominant loads for Mode I fracture of OWT monopiles, thus it is expected that the weight function produced in this work will provide an accurate estimation for OWT turbines loaded in this manner. There is a question of the accuracy of this weight function for the estimation of SIF under very complex stress fields such as in welding residual stresses which has not been tested in this work. In future, accuracy of the weight function for complex residual stress may be improved in the future by the addition of a third independent reference loadcase which can be used with equations 6.7 and 6.8 to generate three simultaneous equations sufficient for the determination of the three unknown parameters $M_1$, $M_2$ and $M_3$.

Reference solutions suitable for offshore wind turbine (OWT) monopiles are generated in this work. BS 7910 [117] contains reference solutions for cylinders with internal and external surface flaws oriented circumferentially. These solutions are mostly based on the work of Newman and Raju [75, 76]. The Newman and Raju solutions are generated for pipes with relatively small ratios of radius to thickness ($R_{out}/t$). It is shown in recent work by Bocher et al. [77] and Fajuyigbe [78] that for pipes with large $R_{out}/t$ as is common in OWT monopiles, these solutions provide an inaccurate estimation of the stress intensity factor. However, the new solutions generated by Bocher et al. [77] are only for pipes subjected to pure bending and are limited to crack aspect ratios (a/c) greater than 0.4. In this work, reference solutions are generated for monopiles with $R_{out}/t$ ranging from 10 to 60 and for cracks with depth/thickness ratio ranging from 0.2 to 0.8 and crack aspect ratio (a/c) ranging from 0.1 to 0.8. Four sampling points shown in Table 6.1 are selected within each range leading to a permutation of 64 crack and geometry configurations.

**Table 6.1 – Sampling points**

| Crack Depth / Pipe Thickness (a/t) | Crack Depth / Half Length (a/c) | Outer Radius / Pipe Thickness $R_{out}/t$ |
|---|---|---|
| 0.2 | 0.1 | 10 |
| 0.4 | 0.2 | 25 |
| 0.6 | 0.5 | 40 |
| 0.8 | 0.8 | 60 |

Notes

1) c is arc length at the outer surface of monopile.

Each cracked monopile has a wall thickness of 100mm in line with typical sizes of existing monopiles in various wind farms across Europe as reported in [23]. Consequently, the monopile diameters analysed range from 2 – 12m covering the range of diameter of current and expected next generation wind turbine monopiles. For finite element modelling, the length of the monopile is set as 40 m which is the typical water depth of monopile foundation installations [78].

### 6.4.1 Finite Element Modelling

Each monopile is modelled in the finite element (FE) software package, Abaqus [127]. The monopile model is pinned at one end (Figure 6.2a). Only one half of the cylinder is modelled for computational efficiency. Instead, a symmetry boundary condition is applied on the free surfaces along the longitudinal axis of the monopile to account for the unmodelled half of the cylinder (Figure 6.2b). For load cases with uniform tension, uniform pressure is applied to the free surface of the monopile. For pure bending, the moment load is applied to a reference point coupled to free surface of the monopile. The moment axis is oriented to cause crack opening under the applied load.

The model is then partitioned at mid length to create a surface to locate the crack. Two further partitions above and below the partition at mid-length are created to form a region. Where only half the monopile is modelled, a quarter-elliptical partition is extruded through the length of the monopile (Figure 6.3a). The edge created at the intersection of this extrusion and the mid-length partition is the crack line. Two additional quarter-elliptical partitions are created, one towards the centre of the monopile, and the other towards the surface. These form the bounding region of the crack front in the thickness direction.

The quarter-ellipticals are seeded with 150 elements. The gap between the quarter-ellipticals are seeded with 10 elements. Bias seeding with a minimum size of 0.1m and a maximum size of 2m is applied along the length of the monopile with the bias towards the crack region. Away from the cracked region, the rest of the monopile is seeded with an element size of approximately 0.2m in the circumferential direction and the thickness of the pipe is split into four elements.

The finite element model is meshed with linear hexagonal elements with reduced integration; C3D8R. The crack is modelled using the ABAQUS interaction module. A discussion of the analysis of SIF using Abaqus [127] was provided in section 4.7.1.

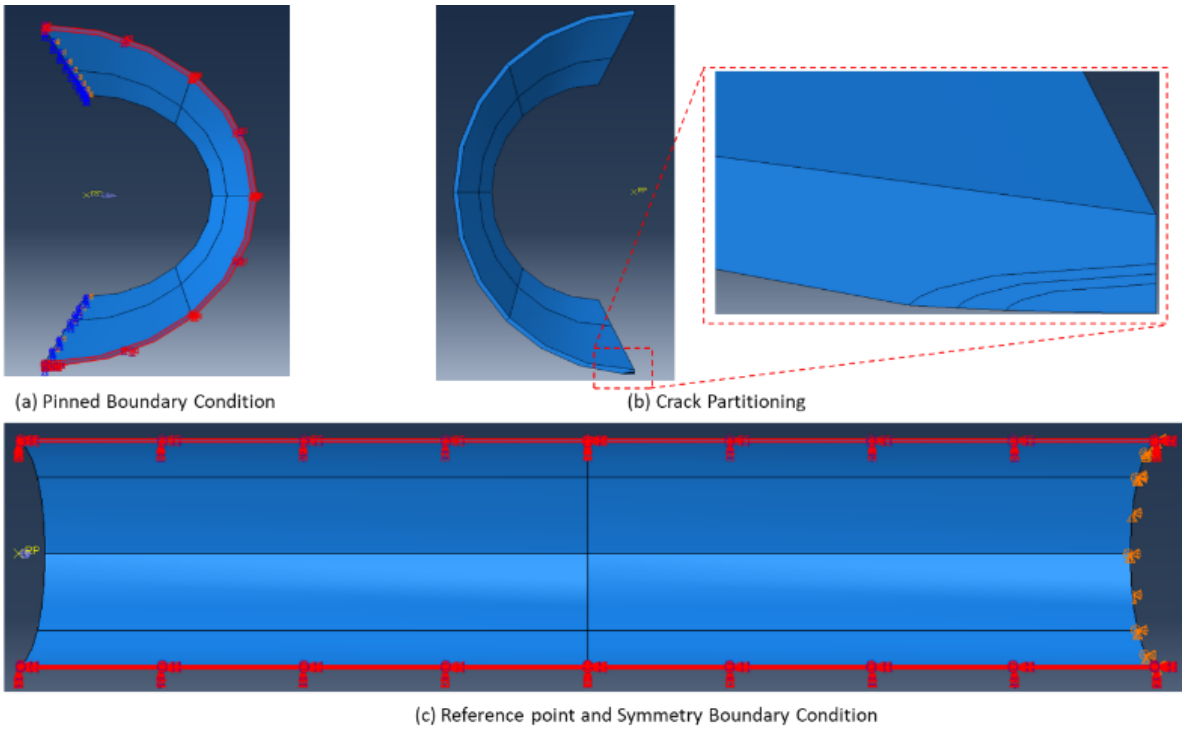


**Figure 6.2 – Finite Element Model**

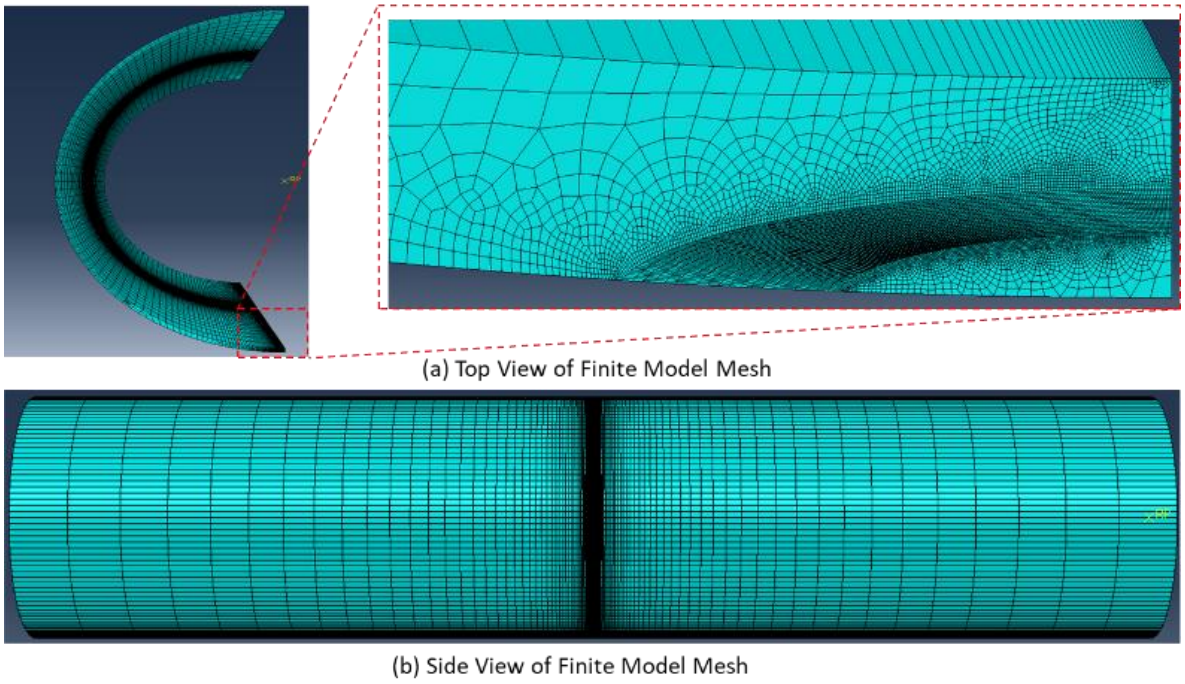


**Figure 6.3 – Finite Model Mesh**

## 6.5 Results

The SIF for each crack at the surface and deepest points are obtained from the Abaqus runs and collated. The SIF is converted into shape function (Y) to remove the dependency on the magnitude of the applied load. The shape function Y is calculated as follows:

$$Y = \frac{K}{\sigma\sqrt{\pi a}} \tag{6.14}$$

Where $\sigma$ is the global applied stress. For pure tension load cases, $\sigma$ is equal to the uniform surface tension applied in Abaqus. For pure bending load cases, the applied bending moment (M) is converted to bending stress as follows:

$$\sigma = \frac{4MR_{out}}{\pi(R_{out}^4 - R_{in}^4)} \tag{6.15}$$

This process produces a value for shape function at the crack surface and deepest point or the combination of the three inputs analysed: $R_{out}/t$, a/c, a/t. The task is to define the relationship between the three inputs and single output which would allow for predictions of shape function to be made given any arbitrary values for the three inputs.

The regression analysis to define this relationship is performed with SciPy [156]. SciPy is a collection of mathematical algorithms and convenience functions built on the NumPy extension of Python. It adds significant power to the interactive Python session by providing the user with high-level commands and classes for manipulating and visualizing data. SciPy's curve fit function uses non-linear least squares to fit a function, f, to data.

The work done by Bocher et al. [77] indicated that a second order polynomial is sufficient to capture the relationship between $R_{out}/t$, a/c, a/t and Y. Therefore, the following basis function incorporating all of the permutations of the inputs is assumed.

$$\begin{aligned} Y = A + B\left(\frac{a}{t}\right) + C\left(\frac{a}{t}\right)^2 + D\left(\frac{a}{c}\right) + E\left(\frac{a}{c}\right)^2 + F\left(\frac{R_{out}}{t}\right) + G\left(\frac{R_{out}}{t}\right)^2 \\ +H\left(\frac{a}{t}\right)\left(\frac{a}{c}\right) + I\left(\frac{a}{t}\right)\left(\frac{R_{out}}{t}\right) + J\left(\frac{a}{c}\right)\left(\frac{R_{out}}{t}\right) + K\left(\frac{a}{t}\right)\left(\frac{a}{c}\right)\left(\frac{R_{out}}{t}\right) \end{aligned} \tag{6.16}$$

The best fit values for the coefficients A to K obtained from SciPy are presented in Table 6.2.

**Table 6.2 – Curve Fit Coefficients and Coefficient of Determination**

| Coefficient | Y – Surface Point | | Y – Deepest Point | |
|---|---|---|---|---|
| | Uniform Tension | Pure Bending | Uniform Tension | Pure Bending |
| A | 2.176E-01 | 1.283E-01 | 1.199E+00 | 1.189E+00 |
| B | -6.837E-01 | -5.183E-01 | 9.446E-01 | 8.938E-01 |
| C | 4.640E-01 | 4.392E-01 | -4.052E-02 | -6.385E-02 |
| D | 1.946E+00 | 2.085E+00 | -1.545E+00 | -1.525E+00 |
| E | -1.833E+00 | -1.849E+00 | 1.160E+00 | 1.134E+00 |
| F | 4.586E-03 | 6.561E-03 | -1.405E-03 | -9.236E-04 |
| G | -4.045E-05 | -4.599E-05 | -4.242E-05 | -5.343E-05 |
| H | 9.448E-01 | 7.151E-01 | -9.757E-01 | -9.494E-01 |
| I | 6.534E-03 | 3.551E-03 | 1.673E-02 | 1.821E-02 |
| J | -2.557E-03 | -5.142E-03 | 6.263E-03 | 6.792E-03 |
| K | -7.511E-03 | -2.538E-03 | -2.569E-02 | -2.706E-02 |
| $R^2$ | 0.85 | 0.86 | 0.97 | 0.97 |

### 6.5.1 Results Validation

The R-squared values presented in Table 6.2 show that the regression lines provide good fit to the data. The quality of the fit is poorer for the shape function at the surface point. This highlights the difficulty in obtaining good quality SIF results at the free surface. One reason is that the $r^{-1/2}$ singularity of the near crack tip stress field vanishes at the intersection of three free surfaces such as the crack surface point [157, 158].

The proposed equations are validated against results presented in literature. For uniform tension, the solutions are compared against Y for cylinders containing external surface flaws oriented circumferentially presented in clause M.7.3.4 of BS 7910 [68]. BS 7910 uses the same solution as flat plates (Clause M.4.1) for cylinders. The comparison of SIF obtained from the proposed equations and for flat plates subjected to membrane loading is presented in Figure 6.4.

It must be noted that this is not a direct comparison. Shape function obtained for BS 7910 are for flat plates. The BS 7910 equations for SIF contain a width correction factor, $f_w$ which is dependent on the width of the plate containing the crack. For a monopile, there is no equivalent width. $F_w$ tends to 1 as the width of the plate increases, as such, for the monopiles considered, $f_w$ is set to a value of 1 in line with the recommendation for cylinders containing internal surface flaws oriented circumferential (Clause M.7.3.2 of BS 7910). This means that the value of Y obtained from BS 7910 does not have any sensitivity to the change in diameter of the monopile.

Figure 6.4 shows the deviation between the new equations and BS 7910. For simplicity, the difference between the largest value of shape function for either the surface or deepest point is reported, that is, only the critical SIF location is shown. Some further plots are presented in Figure 6.5 and Figure 6.6 showing the deviation for fixed Rout/t for further clarity. The results show that the majority of the predictions from the new equations are within 10% of the values from BS 7910. The main outliers are for load cases with low Rout/t such as Figure 6.6. This is likely due to the effect of the lack of suitable width correction

factor to allow a like-for-like comparison with the values SIF obtained for flat plate approximation used in BS 7910.

For pure bending, the proposed equations are compared against values presented in work by Bocher et al. [77]. Figure 6.7 shows the deviation between the new equations and [77]. For simplicity, the difference between the largest value of shape function for either the surface or deepest point is reported, that is, only the critical SIF location is shown. Some further plots are presented in Figure 6.8 and Figure 6.9 showing the deviation for fixed a/c for further clarity. The results show that the majority of the predictions from the new equations are within 5% of the values presented in [77]. There are some outliers, particularly for cracks which are 80% of the pipe thickness. This is the limiting value considered in the analysis and it is likely that the regression line has a poorer goodness-of-fit at the extreme of the dataset. This may be improved by running further analysis beyond a/t of 0.8.

Taken together, these results suggest that the proposed equations are suitable for predicting the shape function, and hence the SIF for a cylinder with an external semi-elliptical crack oriented circumferentially with arbitrary values of $R_{out}/t$, a/t and a/c subjected to either uniform tension or pure bending loads.

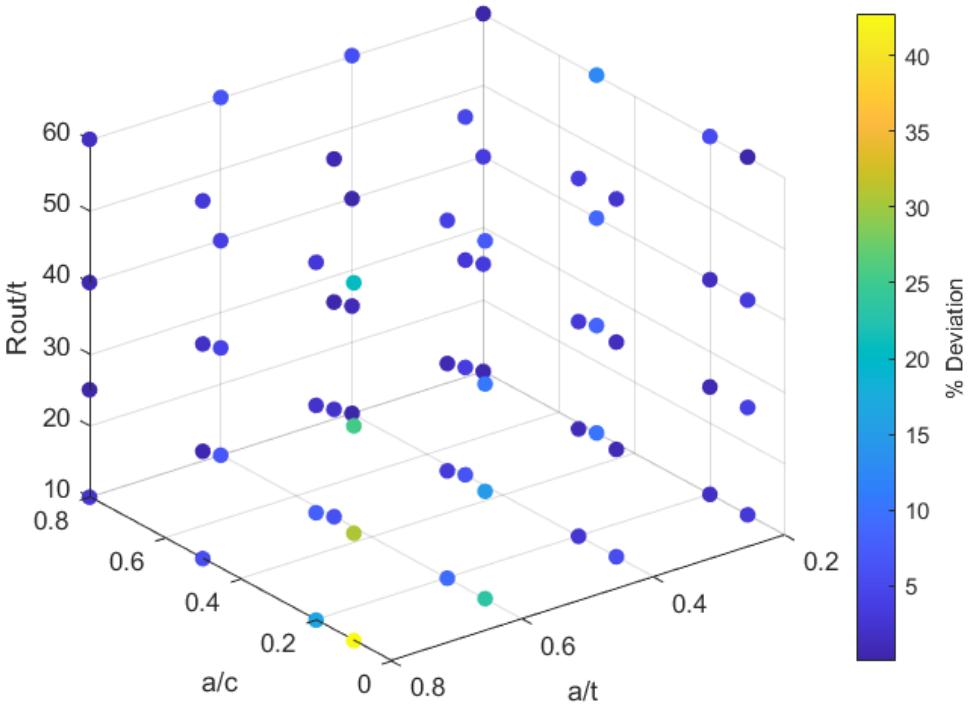


**Figure 6.4 – % Deviation between Shape Function from New equations and BS 7910 (Uniform Tension Load cases) – All Results**

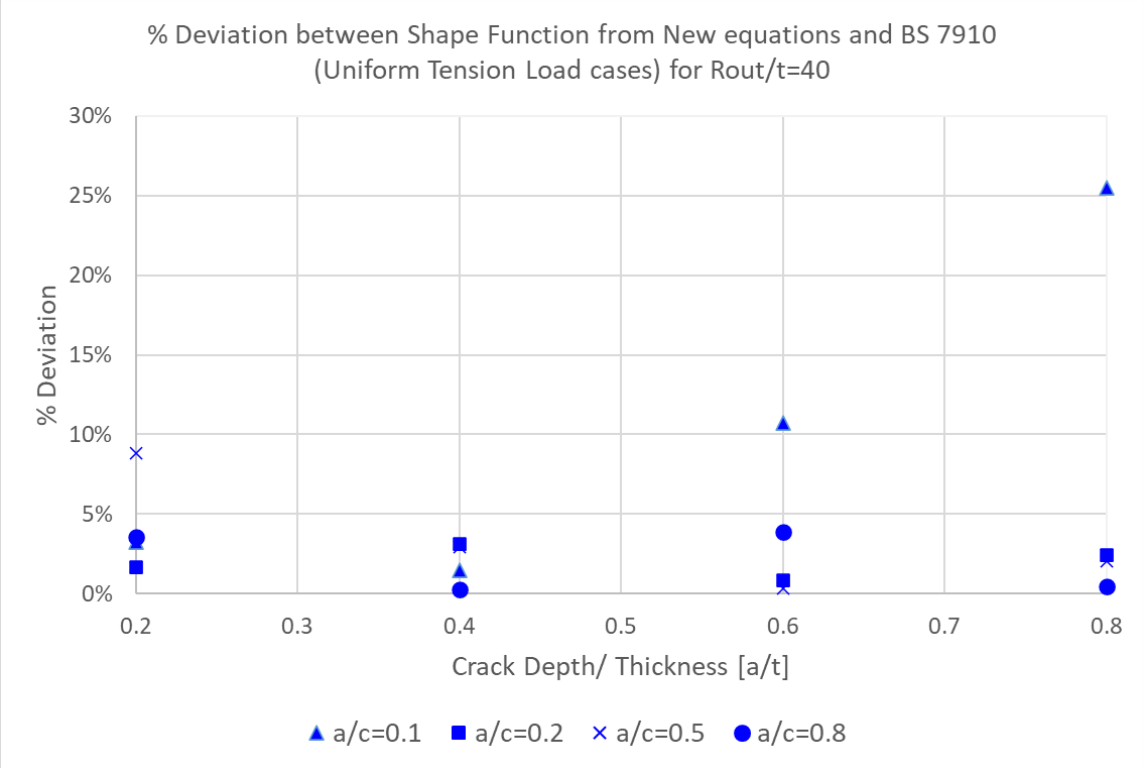


**Figure 6.5 – % Deviation between Shape Function from New equations and BS 7910 (Uniform Tension Load cases) – Rout/t =40**

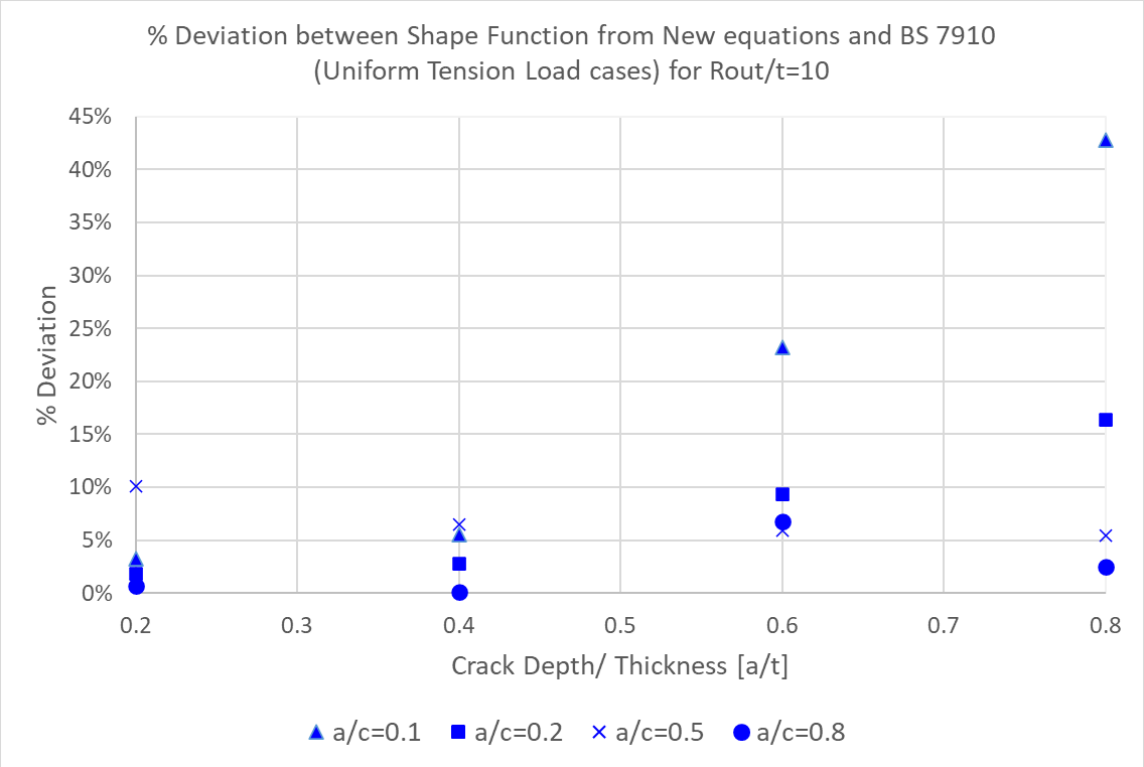


**Figure 6.6 – % Deviation between Shape Function from New equations and BS 7910 (Uniform Tension Load cases) – Rout/t =10**

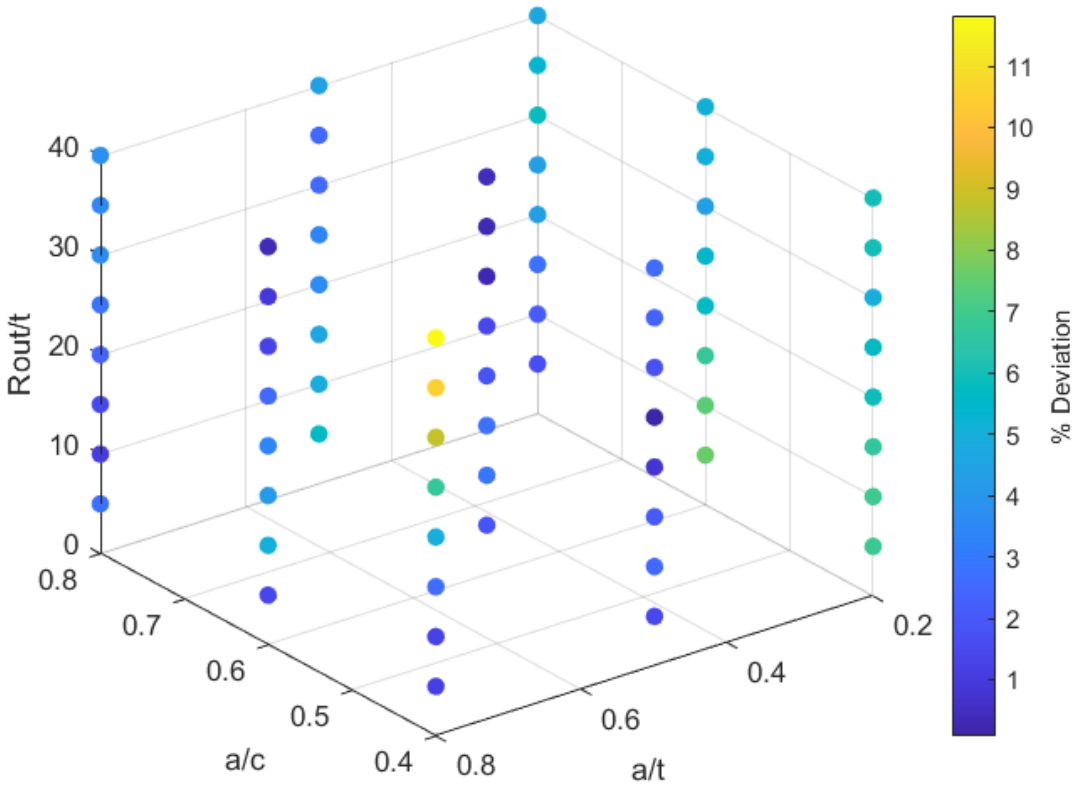


**Figure 6.7 - % Deviation between Shape Function from New equations and Bocher et al. [77] (Pure Bending Load cases) – All Results**

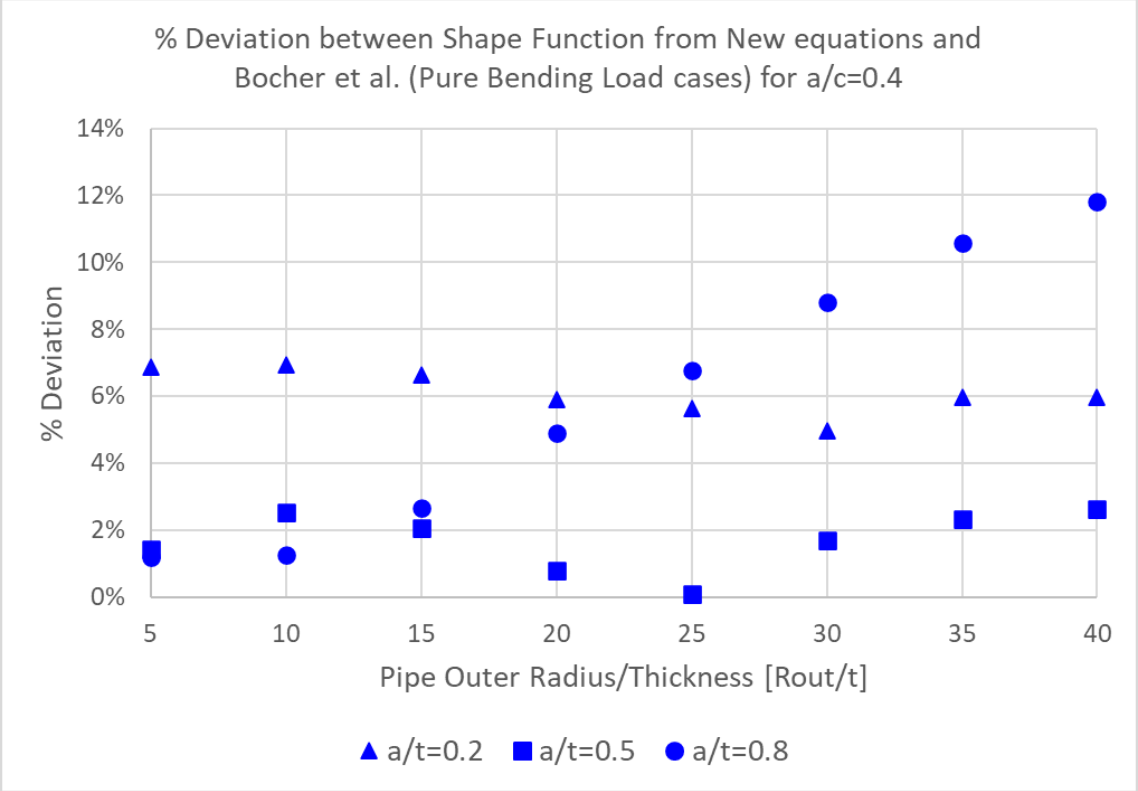


**Figure 6.8 – % Deviation between Shape Function from New equations and Bocher et al. [77] (Pure Bending Load cases) – for a/c=0.4**

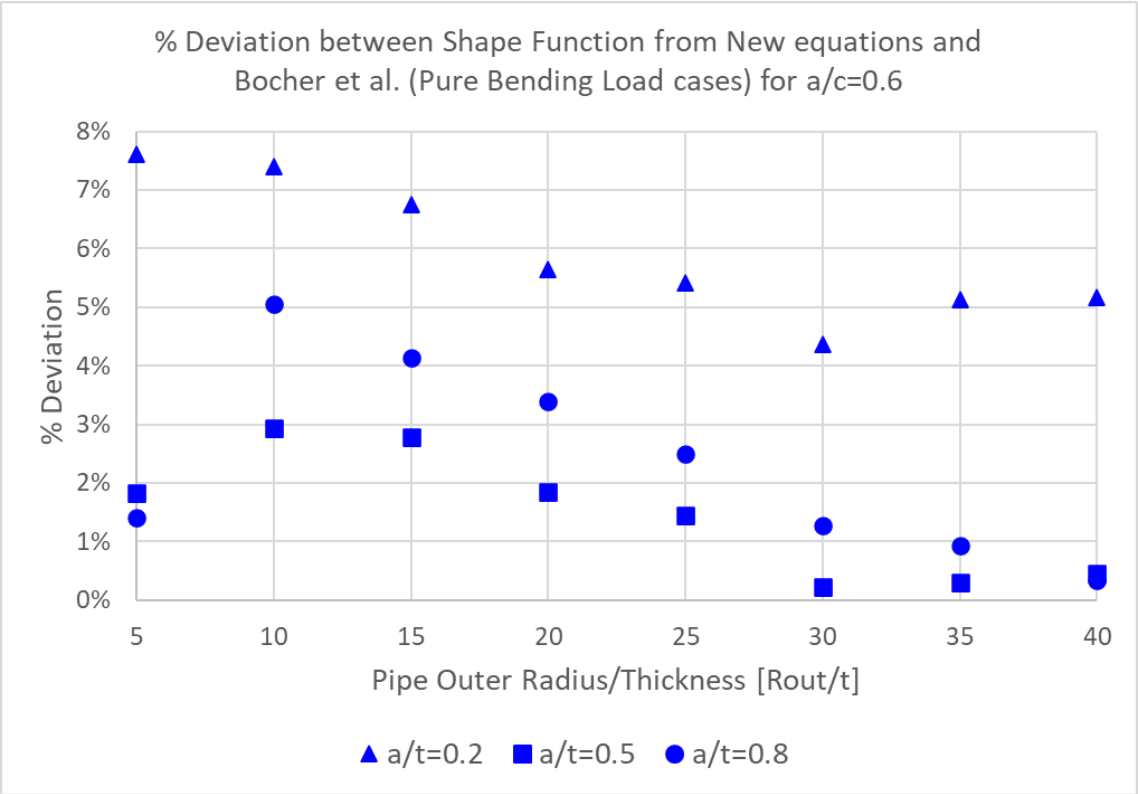


**Figure 6.9 – % Deviation between Shape Function from New equations and Bocher et al. [77] (Pure Bending Load cases) – for a/c=0.6**

## 6.6 Weight Function Validation

The shape function presented in section 6.5 and Table 6.2 is incorporated into the wider system to predict SIF for any complex distribution applied to a cracked monopile as illustrated in Figure 6.10. $M_1$, $M_2$ and $M_3$ are obtained by solving equations 6.7 to 6.10 and equations 6.11 to 6.13 respectively. The SIF for any generic complex stress is then obtained by solving equation 6.2.

The SIF predictor is mainly for use in predicting the SIF at the deepest point of the crack which is the critical value for the majority of cases. The prediction of SIF for the surface point of the semi-elliptical crack is only included for completeness. Care must be taken when using the SIF predicted for the surface point for two main reasons. Firstly, as stated by Shen and Glinka [154], the weight function for the surface point is derived by analogy to the weight function at the deepest point of the crack and for the penny shape crack entirely embedded in the material. The stress field singularity condition at the surface point deviates from that of the deepest point/penny shape cracks and, as such, the weight function is only a crude approximation. Secondly, there are issues with the obtaining of accurate reference SIF values for use in the solution of $M_1$, $M_2$ and $M_3$ as previously discussed.

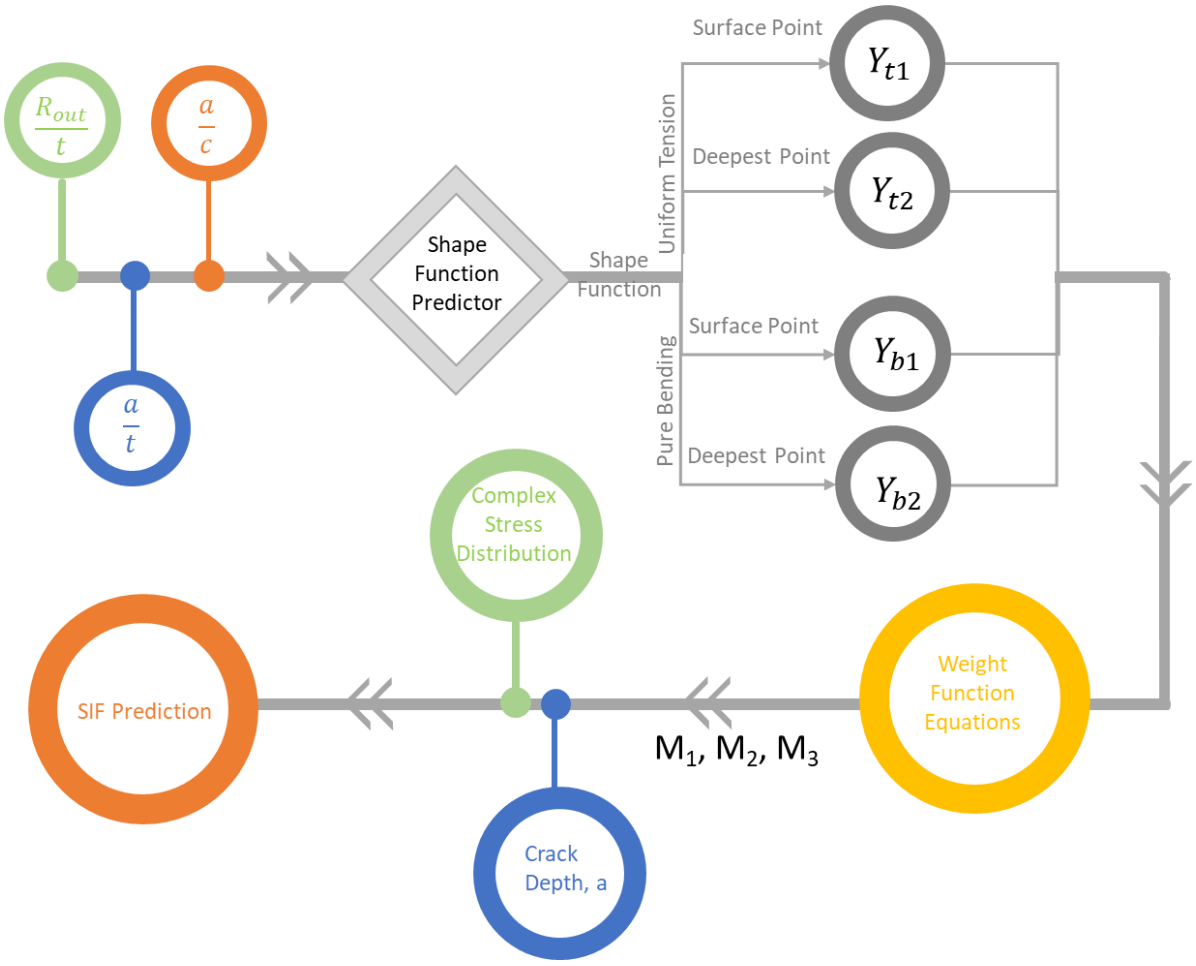


**Figure 6.10 – SIF Prediction Schematic**

An additional 17 load cases are modelled and analysed in Abaqus following the steps outlined in section 6.4.1. The combination of a/t , a/c and $R_{out}$/t were chosen to avoid any combinations previously analysed during the generation of the reference solutions. Each cracked monopile is subjected to a combination of pure bending and uniform tension load such that the stress developed along the crack x-axis (Figure 6.1) is of the form:

$$\sigma(x) = 100 + 2000 * \frac{R_{out} - x}{I} \qquad 6.17$$

Where $I$ is the second moment of area of the monopile. A comparison of the results predicted by weight function and obtained from FE analysis is presented in Table 6.3. For clarity, the difference between the largest value of shape function for either the surface or deepest point is reported, that is, only the critical SIF location is shown. The results show good agreement between the two approaches with the highest deviation less than 10%. The highest deviation is for load cases with a/t of 0.8 which is at the limit of the dataset used to generate the reference solutions. 76% of the validation load cases have a maximum SIF within 5% of the value predicted from FEA.

**Table 6.3 – SIF Prediction Validation**

| Case Number | a/t | a/c | $R_{out}/t$ | Maximum SIF | | Location of Max SIF | % Deviation |
|---|---|---|---|---|---|---|---|
| | | | | Predicted | FEA | | |
| 1 | 0.5 | 0.4 | 32 | 335 | 332 | A | 0.8% |
| 2 | 0.3 | 0.3 | 50 | 121 | 121 | A | 0.3% |
| 3 | 0.7 | 0.7 | 47 | 183 | 182 | B | 0.4% |
| 4 | 0.2 | 0.2 | 27 | 285 | 284 | A | 0.2% |
| 5 | 0.8 | 0.4 | 39 | 363 | 330 | A | 9.9% |
| 6 | 0.6 | 0.6 | 41 | 202 | 202 | A | 0.1% |
| 7 | 0.6 | 0.5 | 22 | 674 | 684 | A | 1.4% |
| 8 | 0.4 | 0.7 | 31 | 230 | 233 | A | 1.1% |
| 9 | 0.4 | 0.3 | 52 | 145 | 142 | A | 1.8% |
| 10 | 0.3 | 0.6 | 52 | 87 | 92 | A | 5.9% |
| 11 | 0.2 | 0.6 | 51 | 69 | 74 | A | 6.3% |
| 12 | 0.4 | 0.3 | 50 | 153 | 151 | A | 1.4% |
| 13 | 0.2 | 0.4 | 11 | 1369 | 1436 | A | 4.6% |
| 14 | 0.6 | 0.4 | 28 | 490 | 487 | A | 0.6% |
| 15 | 0.4 | 0.3 | 14 | 1488 | 1520 | A | 2.1% |
| 16 | 0.2 | 0.2 | 19 | 557 | 560 | A | 0.6% |
| 17 | 0.3 | 0.6 | 15 | 811 | 856 | A | 5.3% |

Notes

1) A is the crack deepest point.
2) B is the crack surface point.

## 6.7 Conclusions and Future Work

This paper presents an analytical methodology for obtaining the Mode I stress intensity factor (SIF) of a semi-elliptical external surface crack in an offshore wind turbine (OWT) monopile subjected to non-pure bending or uniform tension stress distribution. The SIF is a key component of the calculation of fracture ratio used in the assessment of the fitness-for-purpose of a cracked structure. The approach is based on the theory of weight functions and has the following advantages over existing methodologies:

- It is significantly faster than performing finite element fracture mechanics simulation. The methodology allows near instantaneous determination of SIF.
- The proposed weight function solution is generated from FEA SIF analysis of typical monopile sizes; thus, it should provide a more appropriate estimation of SIF than industry standards such as BS 7910. The SIF solution in BS 7910 is based on a flat plate solution and does not precisely capture the SIF for monopiles which are cylinders with large radius/thickness ratios.

The proposed methodology is validated against results presented in literature and also bespoke finite element analysis. The near-instantaneous calculation of SIF for any cracked monopile is a significant development in certifying the integrity of aged offshore wind turbine monopiles as it allows the fitness for purpose of the cracked structure to be assessed in pseudo real time. Future research should use the framework provided to propose similar methodologies for internal surface and embedded cracks.

# 7 CRACK INTERACTION

Paper 4: Fajuyigbe A. and Brennan F. (2022), "Interaction of Stress Intensity Factor of Cracks in Offshore Wind Turbine Monopile" (in review)

*Sections of the content presented below are reproduced as submitted for peer-review*

## 7.1 Paper Synopsis and Additional Notes

An area of interest in this research work is to explore the impact of multiple cracks on the structural integrity of the monopile. In this work, it is proposed that structural integrity be assessed using the failure assessment diagram which requires the calculation of collapse ratio ($L_r$) and fracture ratio ($K_r$). The treatment of multiple cracks in inherent in the methodology proposed in section 5 for determining the collapse ratio. Methodology for estimating the SIF of a crack used in the calculation of the fracture ratio was presented in section 6. However, this pertains to a single crack located in the monopile. The inclusion of the effect of multiple cracks in the determination of fracture ratio still requires exploration.

There are two considerations for the analysis of multiple cracks: the first is to determine the influence of the cracks on each other (interaction), the second is to determine if the cracks may join together (coalescence). After coalescence, the cracks once again behave as a single crack, thus the methodology proposed in section 6 should hold after crack coalescence. The question remains on the behaviour of the cracks in the period where they are interacting before coalescence. It is widely accepted that flaws in close proximity will interact with the degree of interaction decreasing as the flaws become further apart. Various international design standards offer guidance on the definition of the interaction cut-off point. The interaction criteria provided in these assessment procedures are designed to be simple, easy to use, and conservative.

One of the most detailed is the criteria provided in BS 7910 [68] which provides a geometric limit at which two co-planar semi-elliptical surface flaws are said to interact significantly such that both cracks can be re-characterised and drawn as a single crack encompassing the original two cracks. The aim of this work is to test the interaction criteria provided in BS 7910 to explore if cracks in monopiles may still experience interaction outside of the cut-off distance specified in the guideline. A possible methodology for incorporating the effect of interaction (pre-coalescence) is briefly discussed. However, detailed treatment of the interacting cracks with respect to fracture or fatigue analysis is not in the scope of this work. Furthermore, the contribution made in this paper is in a better understanding and calculation of SIF for large diameter tubulars for use within the failure assessment diagram (FA) framework and does not attempt to distinguish between ductile-brittle or plastic behaviour which is dealt with elsewhere.

## 7.2 INTRODUCTION

Typically, fatigue analysis of OWT monopiles only considers a single dominant crack. The consideration of multiple cracks is a novelty for the fatigue/fracture assessment of OWT monopile. Although a novelty in the analysis of OWT monopiles, the cumulative effect of multiple cracks is well known in other industries such as aerospace and nuclear [97-99].

There was the failure of the Aloha 737 airplane in 1988 due to the linking of numerous small cracks at a number of fastener holes [100]. The failure of the reboiler at the ESSO plant in Longford was also caused by multi-site cracks/flaws in the weld [101] and a similar problem leading to the loss of seven bulk carriers off the coast of Western Australia during the period January 1990 to August 1991 [102].

A large number of studies have attempted to quantify the interaction and coalescence of two co-planar cracks. Soboyejo et al. [159] and Carpinteri et al. [160] further used FEA to determine the stress intensity factor and interaction parameters for a range of semi-elliptical crack geometries. Kishimoto et al. [106] and Lin and Smith [104] further extended the use of FEA to assess coalescence of initially independent semi-elliptical cracks. However, these bodies of work focused on identical defect pairs. This omits a very large set of cracks with differing sizes and aspect ratios. More recently, Coules [161-163] performed finite element analysis on a range of dissimilar crack pairs and subjected to non-uniform stress distributions. To the author's knowledge, there is no research work on the quantification of the interaction effect between dissimilar crack sizes for large diameter cylinders used for OWT monopiles.

In the various studies into crack interaction and coalescence, it is clear that one of the most important findings is the concept of a critical distance, that is, a set distance between two cracks at which the interaction effect between them becomes negligible [164]. There is a wide body of work ([165-171]) devoted to examining what this critical distance should be and the behaviour of the cracks when they are separated by a distance less than the critical distance.

One of the most detailed is the criteria provided in BS 7910 [68] which provides guidance on the critical distance after which both cracks can be re-characterised and drawn as a single crack encompassing the original two cracks. Bezensek et al. [172] provided a brief history of the BS 7910 flaw interaction criteria. The interaction criteria in BS 7910 is illustrated using the cylindrical geometry presented in Figure 7.1. The cylinder contains a pair of external surface circumferential cracks. According to BS 7910 , cracks are said to interact when:

$$\begin{cases} s \leq max\{0.5a_1, 0.5a_2\}\, for\ \ a_1/c_1 < 1\ and\ \ a_2/c_2 < 1 \\ \qquad\qquad or \\ s \leq \min\{2c_1, 2c_2\}\, for\ \ a_1/c_1 > 1\ or\ \ a_2/c_2 > 1 \end{cases} \tag{7.1}$$

If either of the inequalities is satisfied, then the two flaws are redrawn as a single flaw with:

$$a = max\{a_1, a_2\}\ \ and\ \ 2c = 2c_1, + 2c_2 + s \tag{7.2}$$

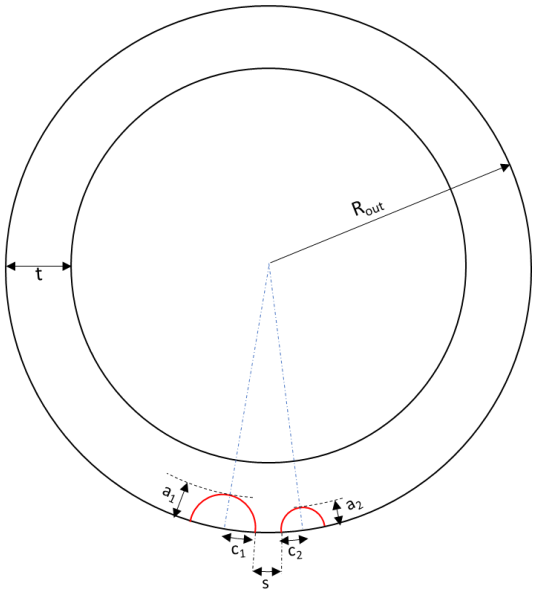


**Figure 7.1 – Crack Interaction Nomenclature**

The accuracy of the recharacterisation of interacting flaws as a single flaw is not the scope of this paper. The reader is directed to literature such as Zeng et al. [173] who used the line-spring analysis technique by Rice and Levy [174] to compare results for identical surface cracks recharacterised as a single crack. In this paper, it is assumed that the recharacterisation of the flaws in accordance with BS 7910 [68] is valid up to the cut-off separation distance.

The focus of this work is on the interaction when the separation distance is greater than the value for which BS 7910 deems a pair of cracks to be non-interacting. It is likely that integrity assessment based on interaction criteria such as equation 7.1, may miss some level of interaction given the abrupt termination of the zone of interaction. For instance, cracks separated by a distance slightly greater than the threshold would not consider any interaction effects. The aim of this paper is to assess the interaction effect of two cracks in an OWT monopile when outside of the interaction criteria specified in BS 7910 [68]. If significant interaction is found outside of the criteria provided in BS 7910 [68], then a methodology is required for the estimation additional interaction between the cracks.

It is noted that FEA can be used to directly obtain the interaction effects of multiple flaws if all of the flaws are included in the FE model. However, FE techniques have a greater computational cost that is not practical in the analysis of structure with changing crack geometry such as structures subjected to fatigue loading. Therefore, the aim of this research work is to propose a methodology to determine the suitable modifier of the SIF of single flaws quickly and accurately in OWT monopiles to include the effects of flaw interaction.

This paper considers semi-elliptical circumferential external surface flaws. Offshore wind turbine (OWT) monopiles are fabricated by rolling and then welding thick structural steel plates longitudinally to produce “cans” which are then welded together circumferentially to achieve the desired length. OWT monopiles are subject to bending loads so cracks typically start from a surface flaw situated at the weld/parent metal interface. The crack grows gradually as a semi-elliptical flaw until it penetrates the wall thickness.

## 7.3 Interaction Model

Fracture analysis relies on the computation of the crack SIF. Therefore, it is convenient to define an interaction factor to describe the impact of the presence of a neighbouring crack on a crack's SIF. The interaction factor $\mu$ is defined as:

$$\mu = \frac{K_I^{int}}{K_I^{\infty}} \tag{7.3}$$

Where $K_I^{\infty}$ is the SIF of the crack in the absence of any other cracks and $K_I^{int}$ is the SIF of the crack in the presence of another crack. For a semi-elliptical crack both $K_I^{\infty}$ and $K_I^{int}$ vary along the crack front. However, the largest SIF is typically at the deepest point of crack, so the interaction factor is defined for this point. $K_I^{\infty}$ and $K_I^{int}$ are obtained for a range of crack geometry applicable for OWT monopiles using FE analysis. The SIFs are obtained from linear elastic fracture mechanics (LEFM) analyses. For simplicity and conservatism, rules for considering the interaction between adjacent defects are normally based on LEFM.

## 7.4 Finite Element Modelling

FE analysis is used to examine the interaction of various combinations of dissimilar semi-elliptical circumferential surface cracks in an OWT monopile. Each cracked monopile has an outer radius, ($r_o$) of 4m, inner radius, ($r_i$) of 3.9m and wall thickness, ($t$) of 100mm in line with typical sizes of existing monopiles in various wind farms across Europe as reported in [23]. S355 steel is the most common material used in the fabrication of monopile support structure [121]. The material properties for S355 steel are as follows; the minimum yield strength, $\sigma_Y$ is taken as 335MPa, the tensile strength, $\sigma_u$ is taken as 470MPa, the modulus of elasticity, E is 210GPa [122].

The monopile is modelled in the FE software package, ABAQUS [127]. The FE model is pinned at one end. For load cases with uniform tension, uniform pressure is applied normal to the free surface of the monopile. For pure bending, the moment load is applied to a reference point that is coupled to free surface of the monopile to generate a pure bending load in the pipe. The moment axis is oriented to cause crack opening under the applied load.

The model is partitioned for ease of meshing and locating the crack. The monopile is partitioned longitudinally to facilitate a swept mesh. The model is partitioned at mid length to create a surface to locate the two cracks. For each crack, a semi-elliptical partition is extruded through the length of the monopile. The edge created at the intersection of this extrusion and the mid-length partition is the crack line. Two additional semi-elliptical partitions are created, one towards the centre of the cylinder and the other towards the surface. These form the bounding region of the crack front in the thickness direction. Two further partitions above and below the partition at mid-length are created to form a region surrounding the crack for finer meshing. The remainder of the model is then coarsely meshed for computational efficiency (Figure 7.2c).

The semi-ellipticals are seeded with 200 elements. The gap between the semi-ellipticals are seeded with 10 elements. Bias seeding with a minimum size of 0.1m and a maximum size of 1m is applied along the length of the monopile with the bias towards the crack region. The

transitional regions around the cracks are bias-seeded with element size ranging from 1mm to 70mm with the bias towards the crack. Away from the cracked region, the rest of the monopile is seeded with an element size of approximately 0.2m in the circumferential direction and the thickness of the pipe is split into four elements. The finite element model is meshed with linear hexagonal elements with reduced integration: C3D8R. The crack is modelled using the ABAQUS interaction module. SIF estimation using Abaqus [127] was discussed in section 4.7.1.

Each structure/crack geometry is analysed thrice. Two analyses with just either the left or right crack active and a final run with both cracks modelled. A schematic FE model is presented in Figure 7.2. The implementation of the boundary condition and reference point for moment load application is shown in Figure 7.2a. The variation of element size around the crack region is shown in Figure 7.2d and in Figure 7.2e.

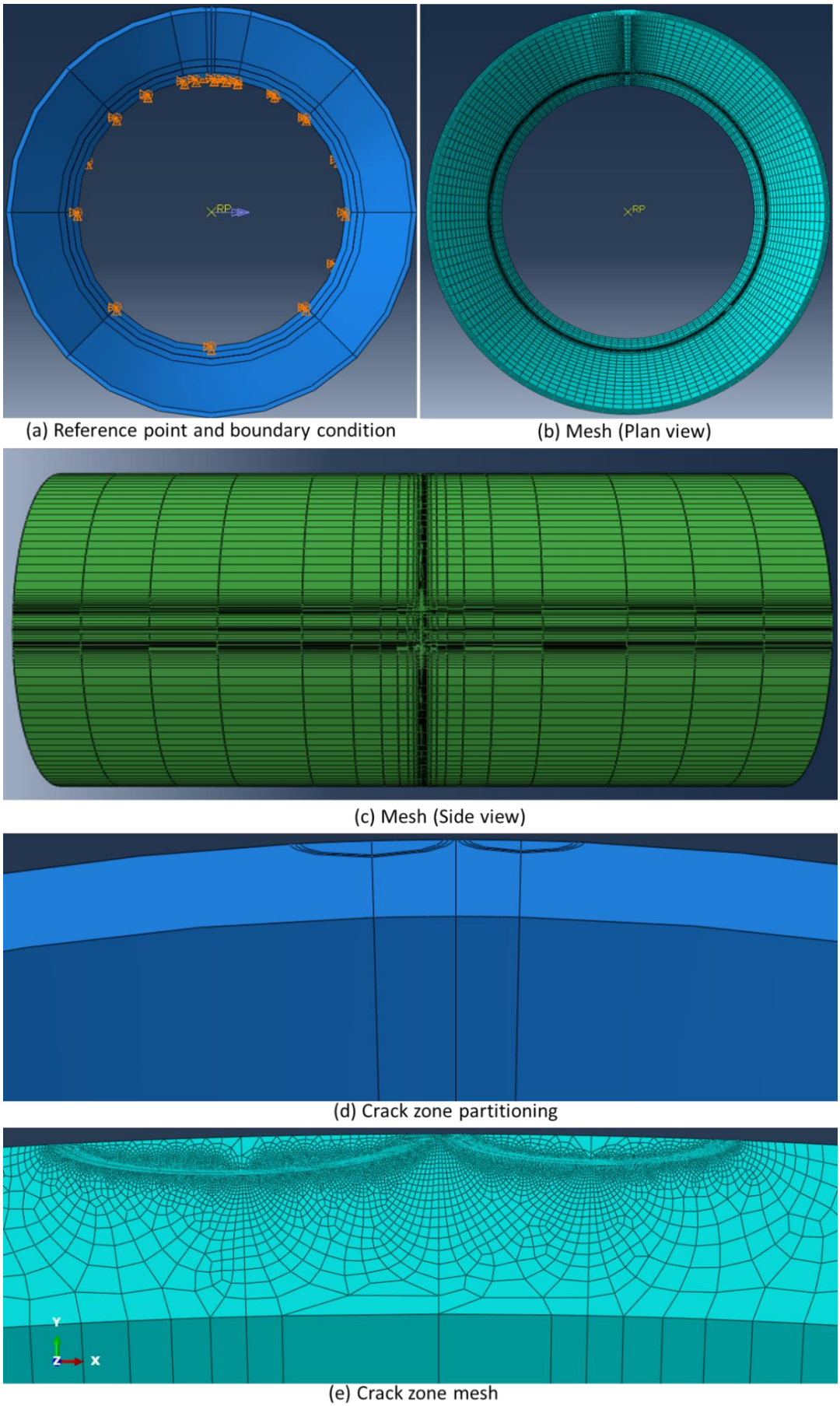


(a) Reference point and boundary condition (b) Mesh (Plan view)

(c) Mesh (Side view)

(d) Crack zone partitioning

(e) Crack zone mesh

**Figure 7.2 – Finite Element Model**

### 7.4.1 Crack Geometry Parametrisation

A pair of dissimilar circumferential external surface cracks are shown in Figure 7.1. For either crack it is convenient to parameterise the geometry by defining the following non-dimensional terms. The subscript "c" are parameters of the cracks for which we are assessing $K_I^{int}$ and $K_I^{\infty}$. The subscript "nc" are parameters of the neighbouring crack that is influencing the crack denoted with subscript "c". As an example, using Figure 7.1, if interested in the right crack, then subscript "c" is 1 and subscript "nc" is 2. If interested in the left crack, then subscript "c" is 2 and subscript "nc" is 1:

- $\alpha = \frac{a_{nc}}{t}$ is the ratio of the neighbouring crack depth to the thickness of the pipe,
- $\beta = \frac{a_c}{a_{nc}}$ is the ratio of the depth of the crack under consideration to the neighbouring crack depth,
- $\gamma = \frac{s}{a_{nc}}$ is the ratio of the crack separation to the depth of the neighbouring crack,
- $\delta_c = \frac{a_c}{c_c}$ is the aspect ratio of the crack under consideration,
- $\delta_{nc} = \frac{a_{nc}}{c_{nc}}$ is the aspect ratio of the neighbouring crack,

The interaction criteria provided in BS 7910 (equation 7.1) does not depend on the crack aspect ratio beyond the choice of equation for a/c greater than or less than 1. This was examined in a preliminary series of finite element analyses. Monopiles with single circumferential external surface cracks of various depths and aspect ratios are analysed in ABAQUS [127]. The schematic of the monopile analysed is shown in Figure 7.3. The pipes are subjected alternately to pure bending load and pure tensile loads. The distribution of normal stress around the outer circumference for the cracked pipe is compared to the theoretical distribution for an uncracked pipe as illustrated in Figure 7.4.

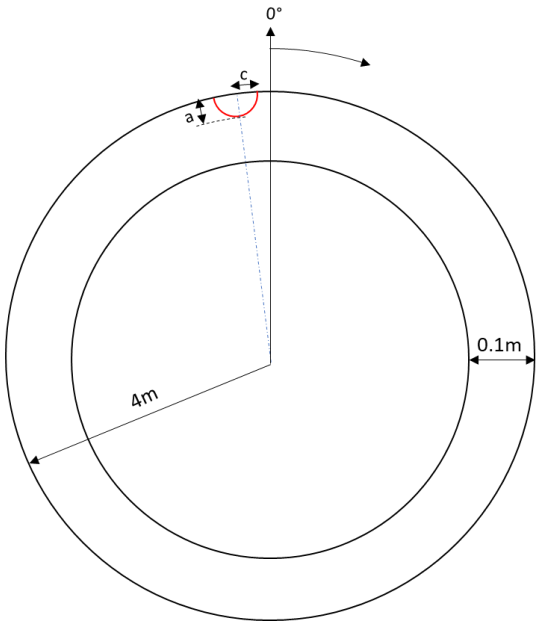


**Figure 7.3 – Bending Stress Analysis**

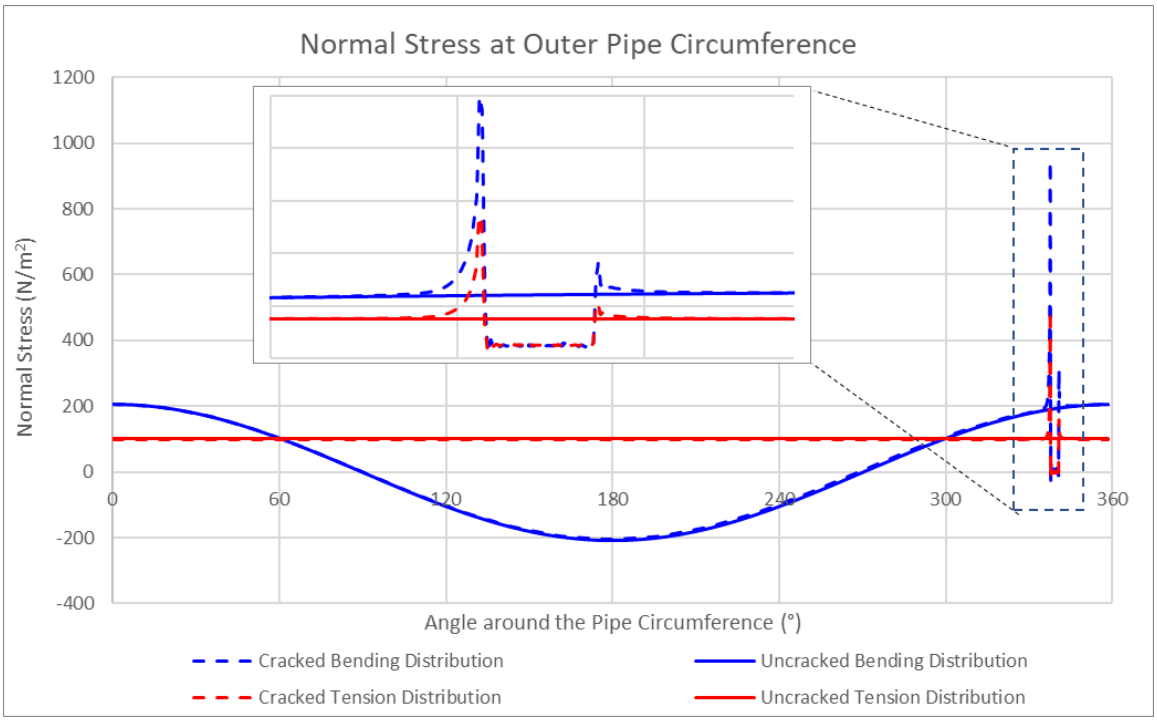


**Figure 7.4 – Normal Stress at Outer Pipe Circumference**

The crack influence zone is defined as the region away from the crack zone for which the normal stress remains elevated compared to the normal stress for an uncracked pipe. The angle of the influence zone for various sizes is presented in Table 7.1 and Table 7.2. The results show that for most cases the cracks depth has a much stronger influence on the extent of the influence zone than the aspect ratio. Hence, to reduce the size of the sample space for this paper, variations in $\delta_1$ and $\delta_2$ are eliminated from the parameter space. A crack aspect ratio of $\frac{a_c}{c_c} = \frac{a_{nc}}{c_{nc}} = 0.2$ is considered in this paper.

**Table 7.1 – Angle of Influence Zone in Degrees for Bending Load**

| Crack Depth / Pipe Thickness (a/t) | Crack Aspect Ratio (a/c) | | | |
|---|---|---|---|---|
| | **0.2** | **0.3** | **0.4** | **0.5** |
| 0.3 | 1.63 | 1.80 | 1.70 | 1.59 |
| 0.4 | 2.29 | 2.50 | 2.37 | 2.30 |
| 0.5 | 2.86 | 3.00 | 2.88 | 2.89 |
| 0.6 | 4.70 | 3.71 | 3.73 | 3.58 |
| 0.7 | 6.93 | 5.10 | 4.48 | 4.48 |
| 0.8 | 7.42 | 6.02 | 5.49 | 4.76 |

**Table 7.2 – Angle of Influence Zone in Degrees for Tensile Load**

| Crack Depth / Pipe Thickness (a/t) | Crack Aspect Ratio (a/c) | | | |
|---|---|---|---|---|
| | 0.2 | 0.3 | 0.4 | 0.5 |
| 0.3 | 1.63 | 1.64 | 1.55 | 1.37 |
| 0.4 | 2.29 | 2.50 | 2.25 | 2.13 |
| 0.5 | 3.01 | 3.00 | 3.02 | 2.89 |
| 0.6 | 4.82 | 3.88 | 3.90 | 3.58 |
| 0.7 | 5.90 | 4.74 | 4.48 | 4.48 |
| 0.8 | 7.84 | 6.42 | 5.69 | 4.76 |

### 7.4.2 Parameter Space

All cracks are co-planar, circumferential, semi-elliptical, external surface flaws. The following range for the parameters presented in section 7.4.1 are considered in this paper

- $\alpha$ ranges from 0.2 to 0.8 in increments of 0.1. This covers the range of usable crack depths likely in OWT monopiles. Cracks with $\alpha$ greater than 0.8 are nearing through-thickness.

- β ranging from 0.25 to 1 in increments of 0.25. In this paper, crack 1 is always deeper than crack 2 such that β ≤ 1. This creates a range of ratio of the neighbouring crack depth to the thickness of the pipe ( $\frac{a_{nc}}{t}$ ) spanning between 0.05 and 0.8

- $\gamma$ ranges from $max\{0.5a_1, 0.5a_2\}$ to the limit determined from the preliminary influence zone analysis presented in section 7.4.1. Six levels of separation are analysed within these limits. Below the lower limit, the two cracks are recharacterised as a single crack in accordance with BS 7910.

## 7.5 Results and Discussion

### 7.5.1 Pure Bending Results

There is very little data available on the interaction of circumferential, semi-elliptical surface cracks in large diameter cylinders. The SIF obtained for single cracks in this work is compared against values presented for large cylinders subjected to pure bending in work by Fajuyigbe [175]. The SIFs for single cracks obtained in this paper are within 5% of the values presented in Fajuyigbe [175]. It is noted that the work in Fajuyigbe [175] is validated against Bocher et al. [77]. There is no directly comparable data in literature for the interaction ratios. However, results presented for dissimilar co-planar, surface flaws in flat plates by Coules [163] show a maximum global interaction factor of 1.3. This is in line with results obtained in this study.

A total of 582 analytical runs; 194 runs each for left (larger) or right (smaller) crack active and 194 runs for both cracks active, are performed for cracked monopiles subjected to pure bending. The impact of crack interaction is presented as percentage increase/decrease in the SIF of the crack under consideration due to the presence of another crack ($\mu$-1) and is plotted for various ratios of crack depths, β in Figure 7.5 to Figure 7.8. Each plot shows $\mu$-1

against the normalised crack separation distance, $\gamma$ for the various normalised crack depths ($\alpha$) analysed. Some key findings from the results are as follows:

- The largest interaction effect ($\mu - 1$) occurs when a relatively small crack (small β) is in close proximity (small $\gamma$) to a large crack (large $\alpha$).

- The separation between the crack has the largest influence on the interaction factor. The interaction factor falls quickly for increasing $\gamma$. Changes in value of $\mu$ is more gradual for changes in $\alpha$ and β.

- Interaction factor is in general lowest when the cracks are same sized (β = 1).

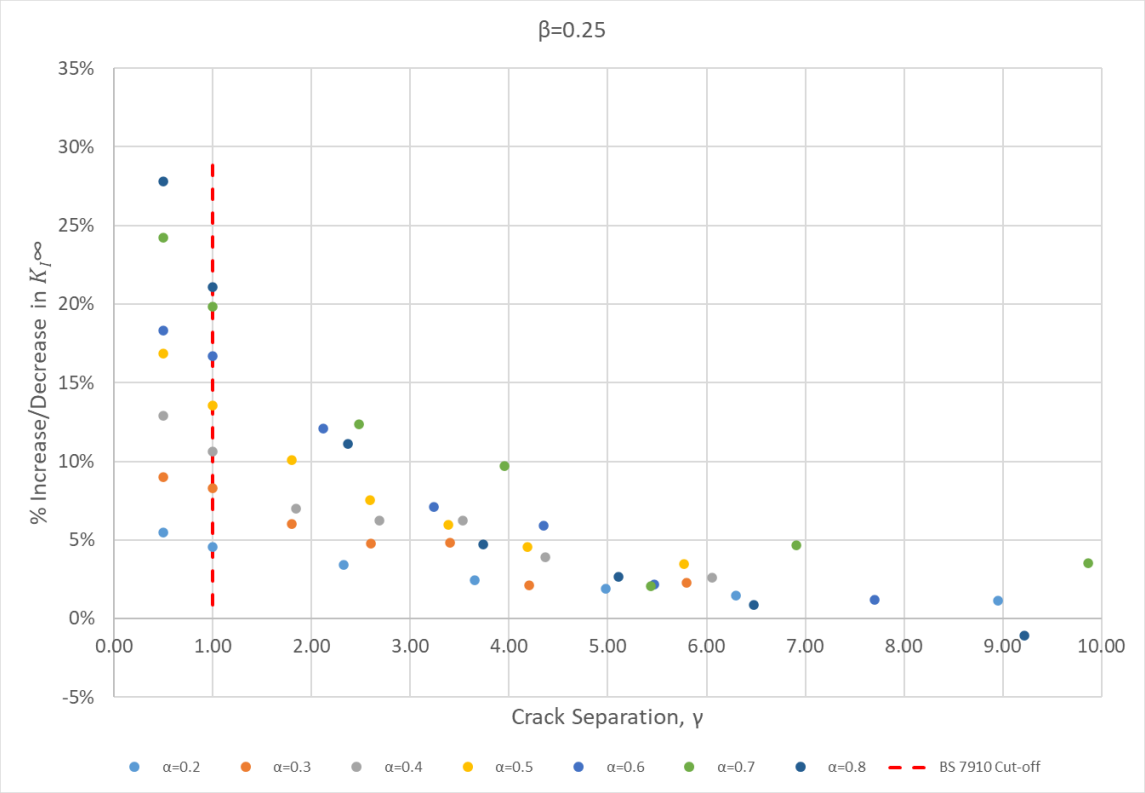


**Figure 7.5 – Interaction Effect under Pure Bending Loads (β=0.25)**

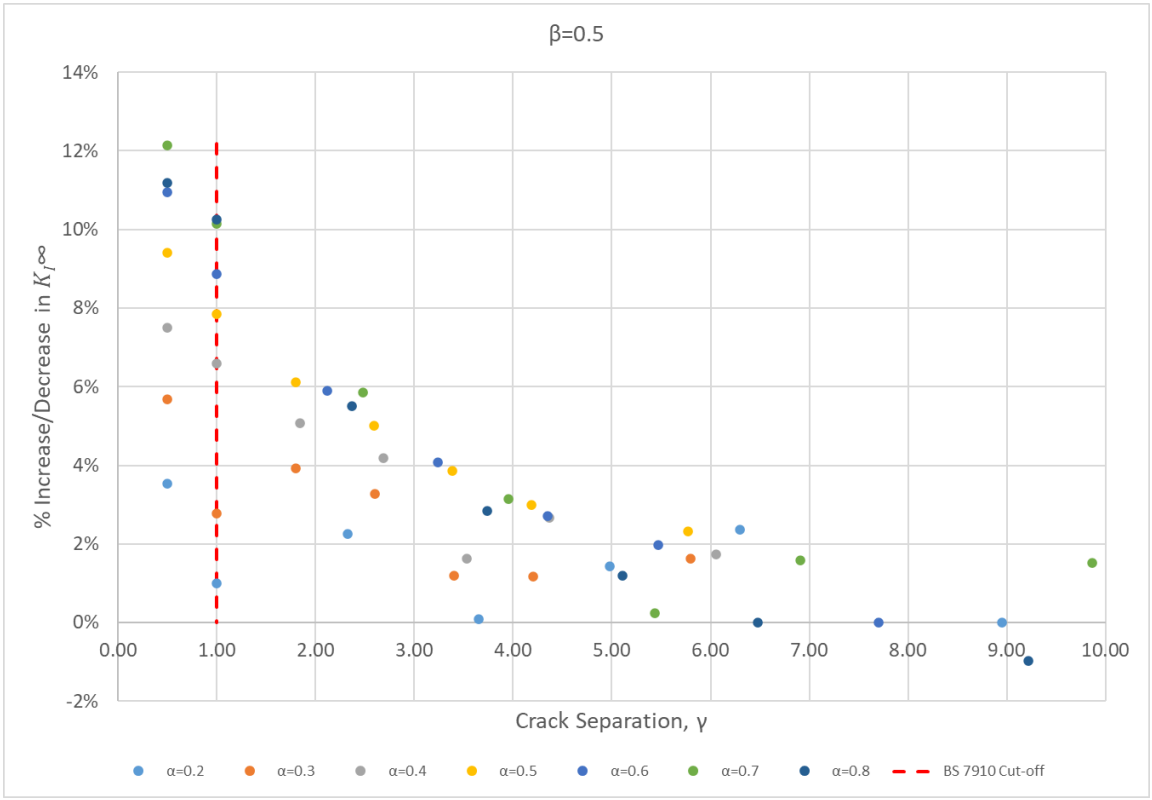


**Figure 7.6 – Interaction Effect under Pure Bending Loads (β=0.5)**

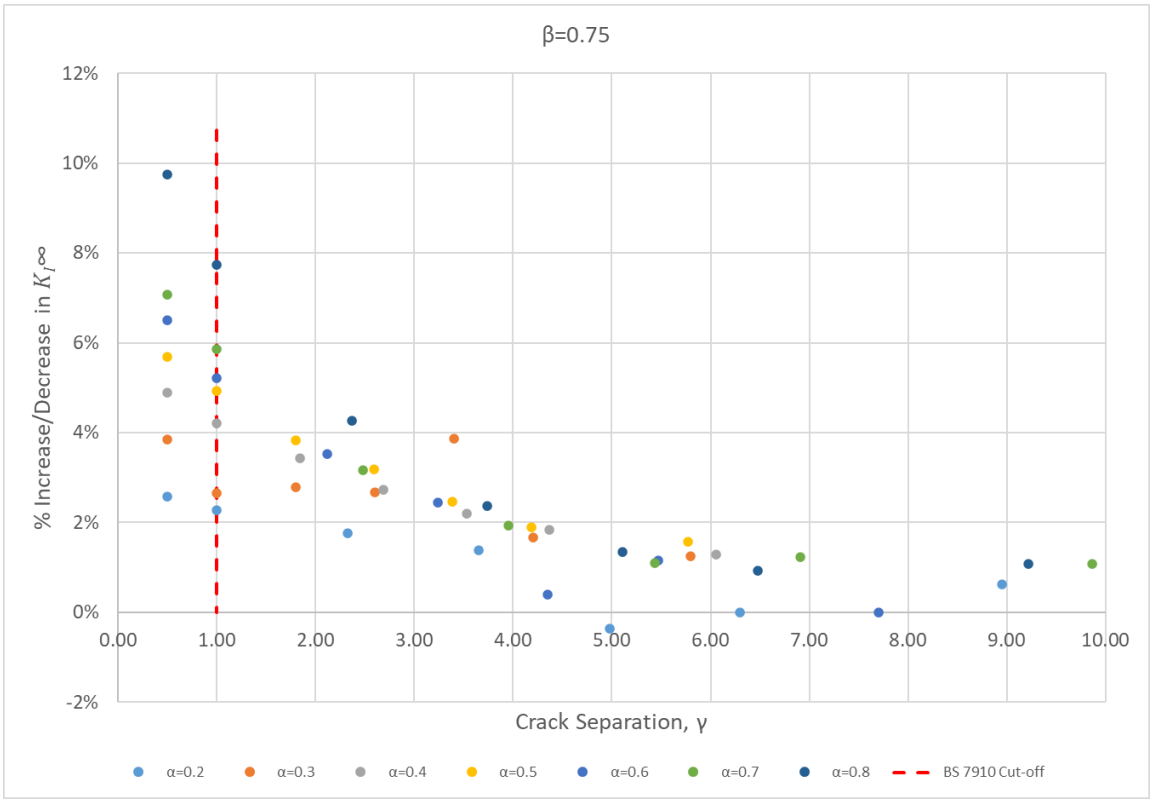


**Figure 7.7 – Interaction Effect under Pure Bending Loads (β=0.75)**

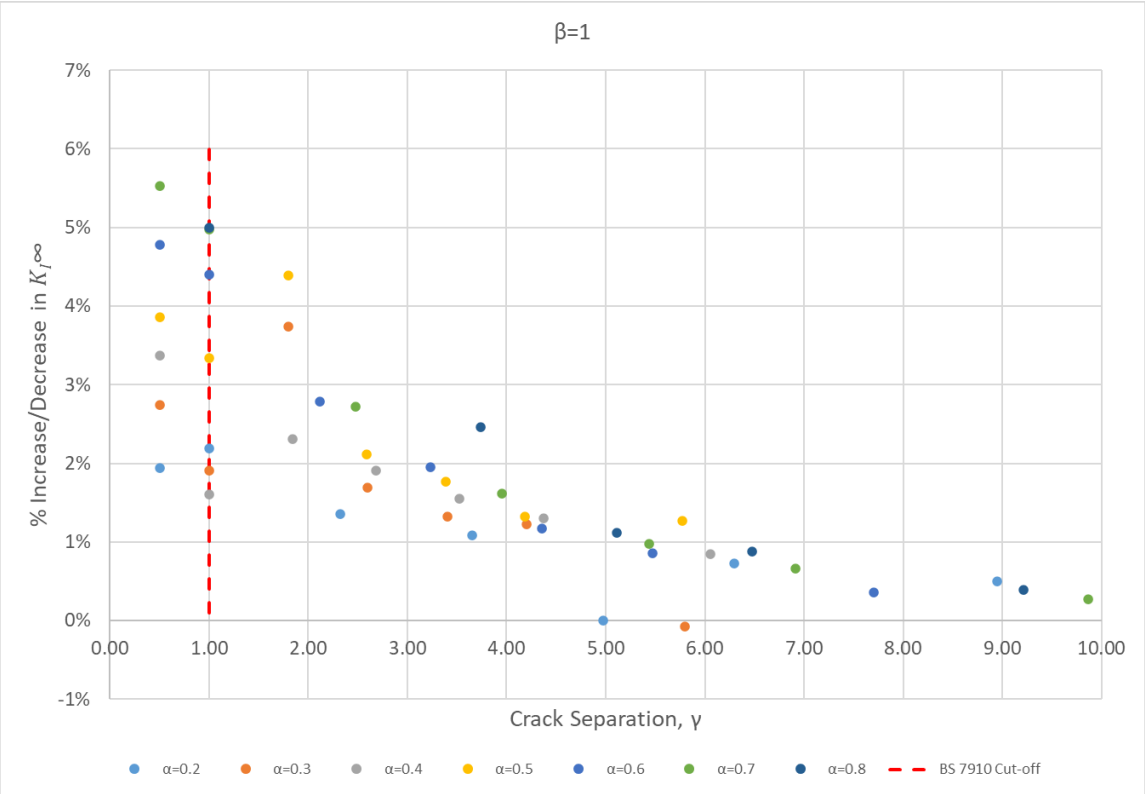


**Figure 7.8 – Interaction Effect under Pure Bending Loads (β=1)**

The next task is to define a mathematical relationship between the interaction effect on SIF; $(\mu - 1)$ and the three input parameters: $\alpha$, $\beta$, and $\gamma$. The regression analysis to define this relationship is performed with SciPy [156]. SciPy is a collection of mathematical algorithms and convenience functions built on the NumPy extension of Python. It adds significant power to the interactive Python session by providing the user with high-level commands and classes for manipulating and visualizing data. SciPy's curve fit function uses non-linear least squares to fit an objective function, f, to data.

The objective function may take any form. Various candidate objective functions were assessed for goodness of it and the general form of a polynomial fit was the best fit for the data. The general form of the objective function is shown in equation 7.4. The optimum values for coefficients A to O are determined using SciPy [156].

$$A + B\alpha^C + D\beta^E + F\gamma^G + H(\alpha\beta)^I + J(\alpha\gamma)^K + L(\beta\gamma)^M + N(\alpha\beta\gamma)^O \qquad 7.4$$

The optimum values for coefficients for equation 7.4 for these results obtained using SciPy [156] are presented in Table 7.3. The coefficient of determination (R-squared) is also presented and shows that the regression analysis provides a good fit to the data. The residuals are also examined to ensure that there is no bias.

**Table 7.3 – Curve Fit Coefficients and Coefficient of Determination (Pure Bending)**

| Coefficient | Value |
|---|---|
| A | -3.416319749 |
| B | 7.010546742 |
| C | 0.164954764 |
| D | 4.144373259 |
| E | 0.199298068 |
| F | 0.039667301 |
| G | 0.990842872 |
| H | -7.758988238 |
| I | 0.147271158 |
| J | -0.638595105 |
| K | 0.435930035 |
| L | -0.082169998 |
| M | 0.777488276 |
| N | 0.754251213 |
| O | 0.392760197 |
| $R^2$ | 0.953 |

These coefficients presented in Table 7.3 are for β ranging from 0.25 to 1, that is, only considering the impact of the larger crack on the smaller crack. Results for β greater than 1 are also available by considering the changes in SIF for the larger crack for single and dual crack analysis runs. Results are available for beta value of 1.33 (corresponds to 1/0.75), 2 (corresponds to 1/0.5) and 4 (corresponds to 1/0.25).

The results show that for β greater than 1.33, there isn't a noticeable impact on the SIF of the large crack by the small crack. Even for a β value of 1.33, the increase in SIF is ~1% at the closest separation distance. Therefore, a small crack may be assumed to have negligible impact on the SIF of a larger crack.

### 7.5.2 Tensile Loading

An OWT monopile is subject to various types of loads: compressive loads, shear forces and torsion, and bending moment loads. However, for an OWT monopile bending moment loads are the only primary loads applicable to Mode I crack opening. For a crack subject to Mode I loading which is typical for most fractures, the principal load is applied normal to the crack and tends to open the crack.

There are no direct causes of uniform tensile loads on an OWT monopile. However, it is possible that the monopile may be subject to complex stresses due to the combination of primary and secondary loads. It is known that through the application of weight functions [147] [148] [175], SIF for complex stress distribution can be derived from the combinatory knowledge of SIF of a cracked structure under various simplified stress conditions which can

include pure bending and uniform tension stress distributions. Thus, effect of tensile loading on the interaction factor should be defined. A subset of the parameter space presented in section 7.4.2 is analysed under the action of uniform tensile loads. The selected parameters are as follows:

- $\alpha$ values of 0.2, 0.4 and 0.6
- β ranging from 0.25 to 1 in increments of 0.25.
- $\gamma$ ranges from $max\{0.5a_1, 0.5a_2\}$ to the limit determined from the preliminary influence zone analysis presented in section 7.4.1.

Figure 7.9 to Figure 7.11 show the difference between the interaction factor obtained for pure bending loads ($\mu_{bending}$) and those obtained for uniform tensile loads ($\mu_{tension}$). Note that a positive value indicates that the interaction factor is greater for tensile loading and vice versa. A larger dataset may be required to establish the exact numerical relationship but generally, the results show that the interaction factors are increased under uniform tension compared to bending loads.

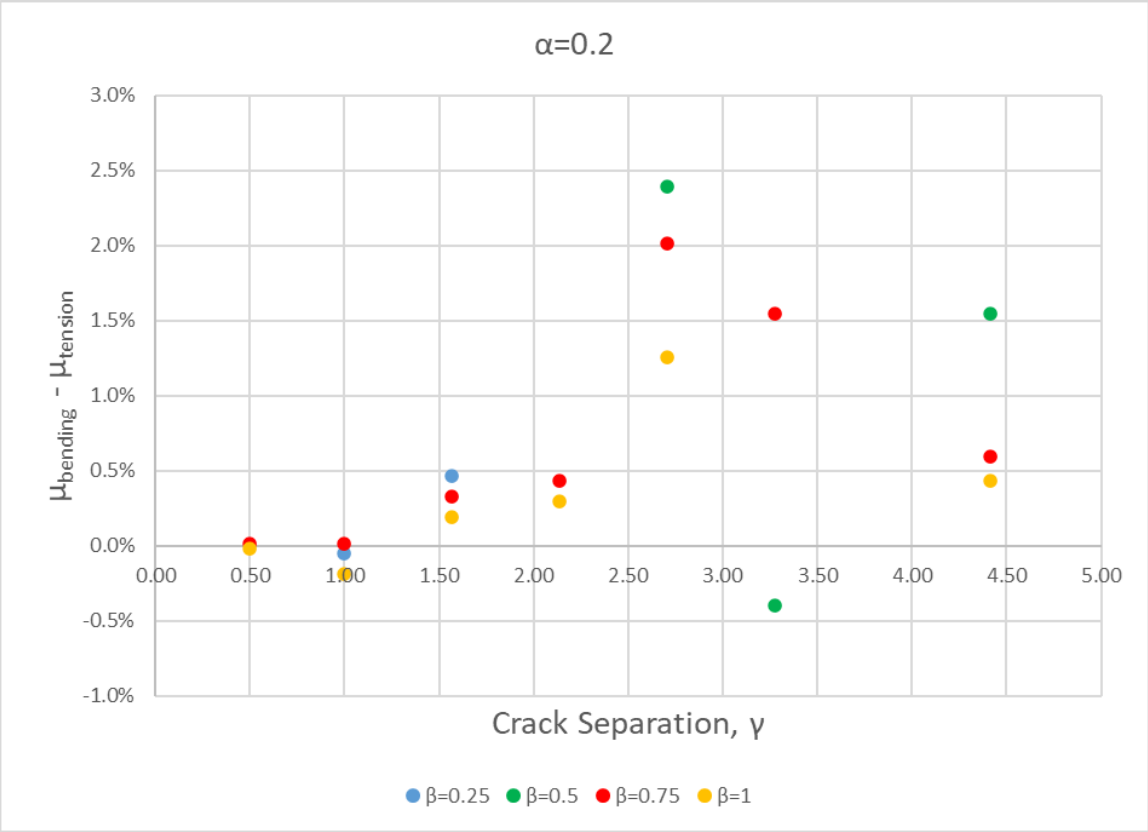


**Figure 7.9 – Comparison of Interaction Factor for Tensile and Pure Bending Loads (α=0.2)**

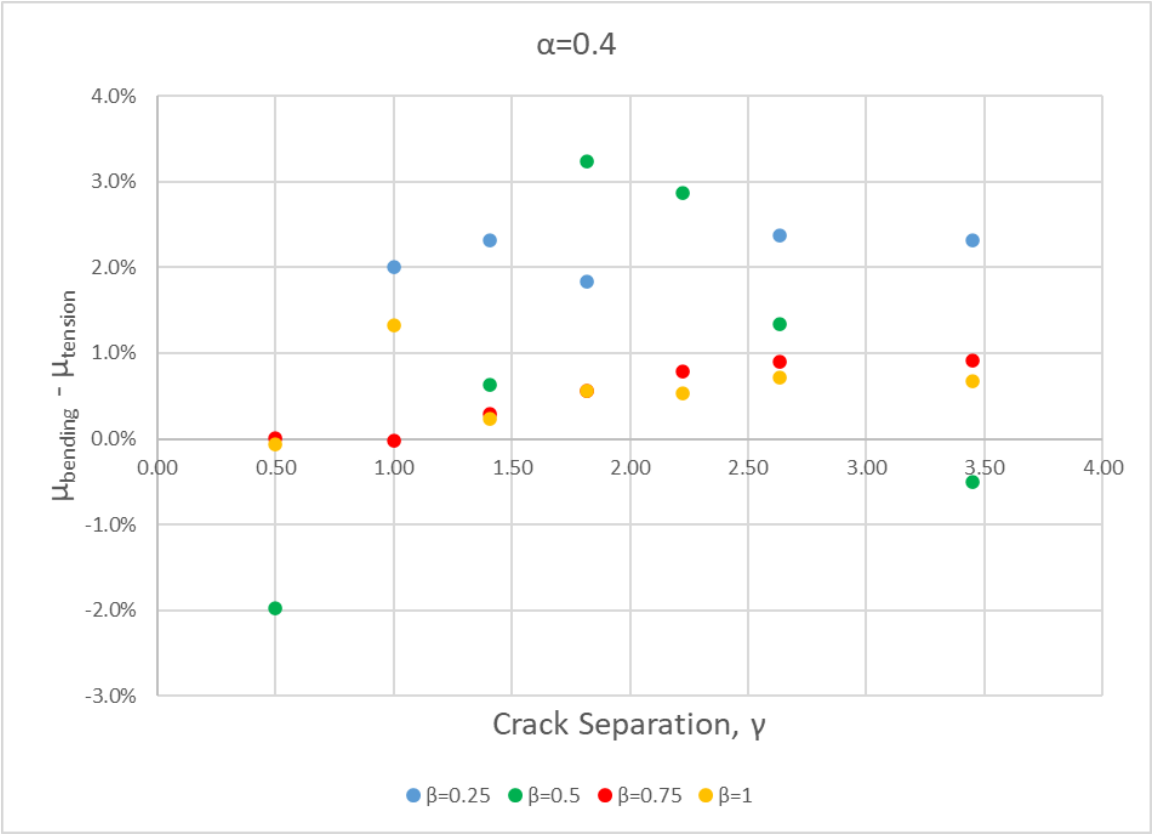


**Figure 7.10 - Comparison of Interaction Factor for Tensile and Pure Bending Loads (α=0.4)**

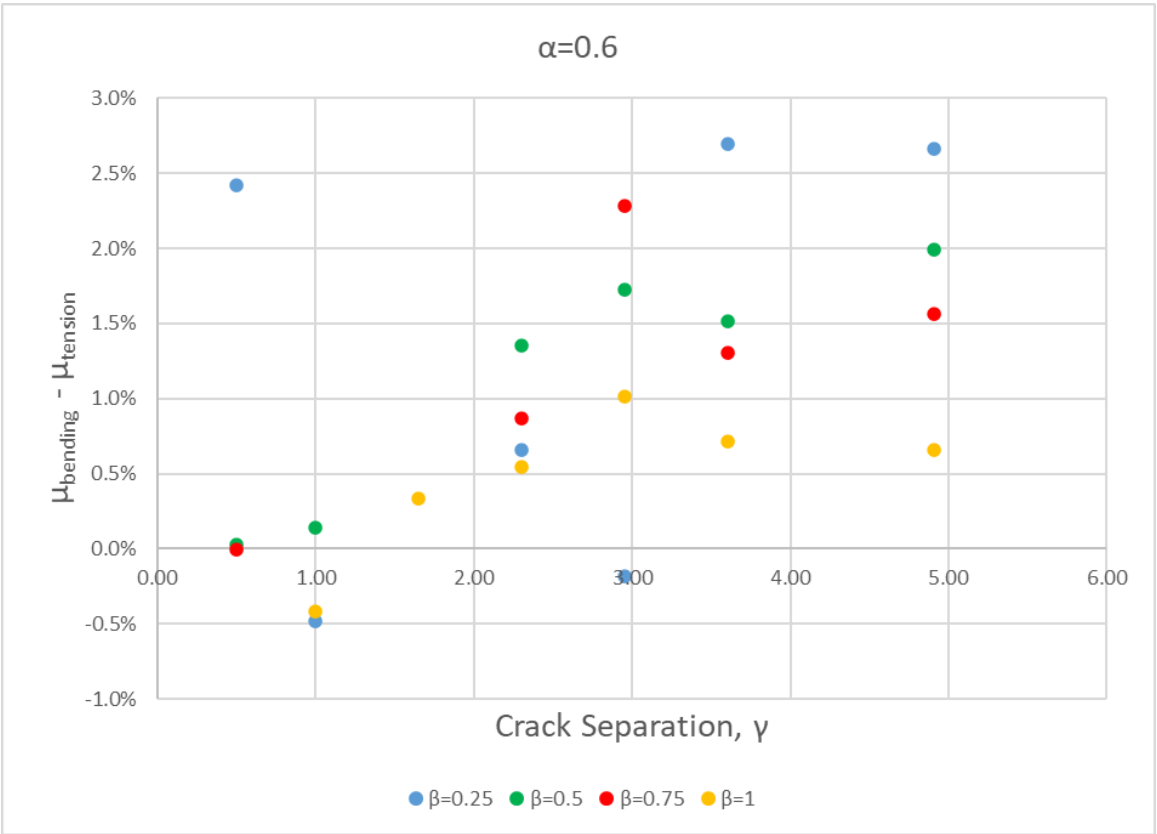


**Figure 7.11 – Comparison of Interaction Factor for Tensile and Pure Bending Loads (α=0.6)**

### 7.5.3 Crack Aspect Ratio

The results of the preliminary analysis (section 7.4.1) and the flaw interaction criteria provided in BS 7910 indicate that the interaction of cracks is independent of the crack aspect ratio. This is examined by performing analysis for a subset of the baseline parameter space for two additional crack aspect ratio of $\frac{a_c}{c_c} = \frac{a_{nc}}{c_{nc}} = 0.5\ and\ 0.7$. The other crack parameters are as follows:

- A single $\alpha$ value of 0.5
- β ranging from 0.25 to 1 in increments of 0.25.
- $\gamma$ ranges from $max\{0.5a_1, 0.5a_2\}$ to the limit determined from the preliminary influence zone analysis presented in section 7.4.1.

Figure 7.12 and Figure 7.13 show the difference between the global interaction factor for the new crack aspect ratios compared to the baseline results presented in section 7.5.1. The results show that there is no significant change in the value of the interaction ratios. There are marginal changes in values of the interaction ratio but there is no clear trend. A larger data set may allow a more meaningful relationship to be extracted.

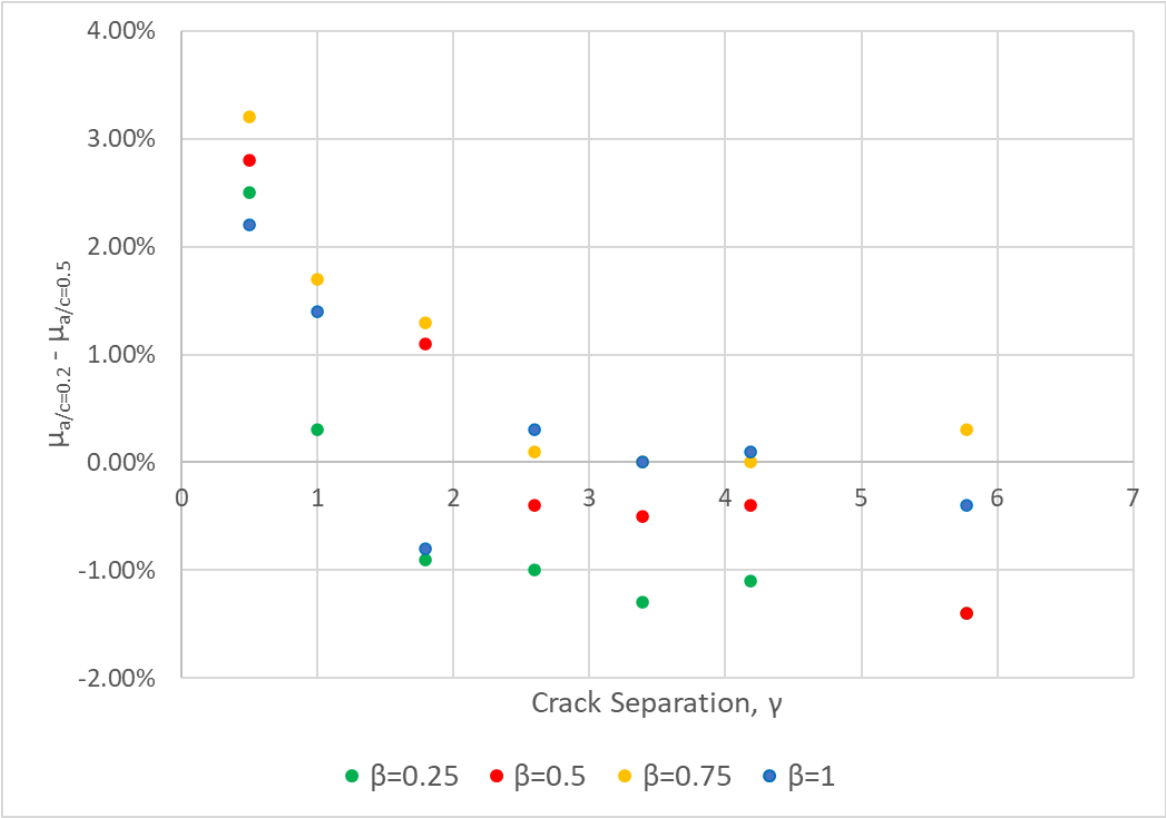


**Figure 7.12 – Sensitivity to Crack Aspect Ratio (a/c=0.5)**

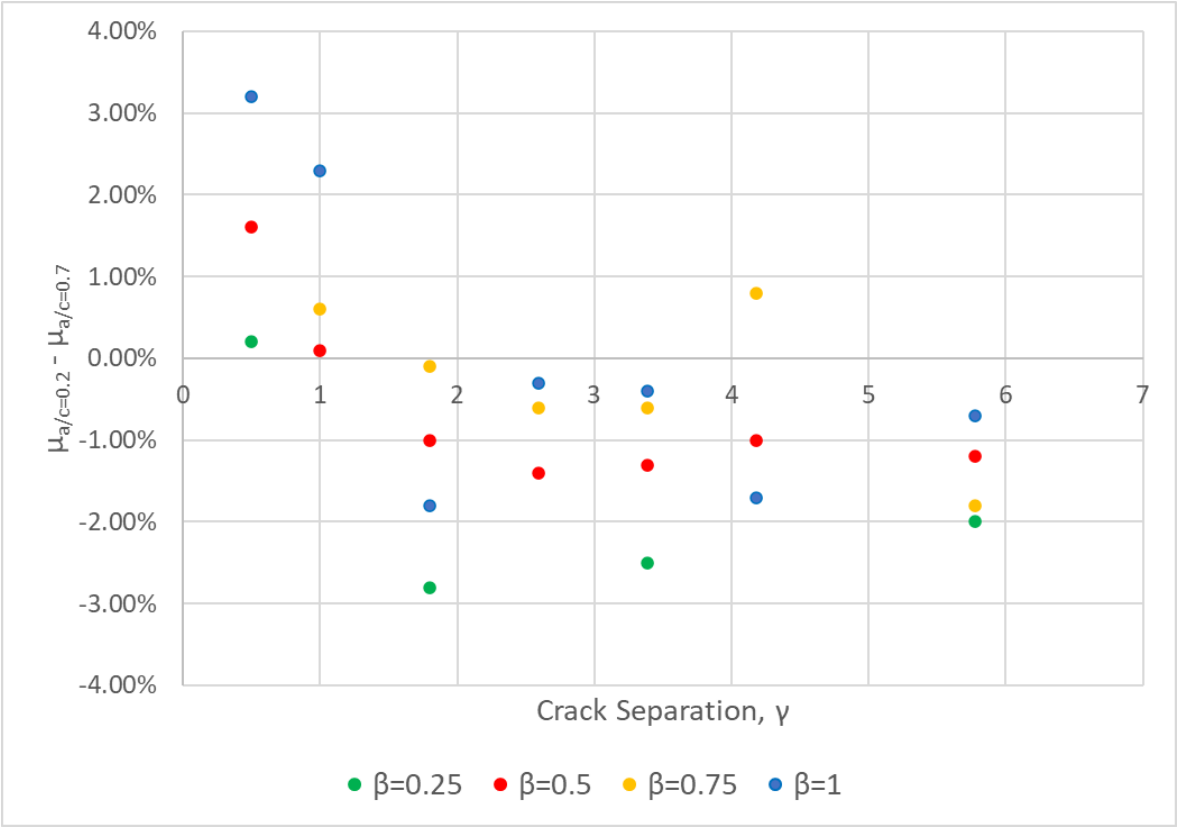


**Figure 7.13 – Sensitivity to Crack Aspect Ratio (a/c=0.7)**

## 7.6 Conclusions and Future Work

This paper investigates the interaction between co-planar, circumferential, semi-elliptical, external surface flaws located in OWT monopiles. The interaction is characterised through its influence on the stress intensity factor (SIF) obtained from linear elastic fracture mechanics (LEFM). SIF is a key parameter in assessing crack growth under applied cyclic load.

There are interaction criteria presented in industry guidelines such as BS 7910 which define a cut-off distance within which the interacting cracks are redrawn as a single crack. Outside of the cut-off point, the cracks are deemed to be non-interacting. The results from this work show that non-trivial interaction between cracks still exists outside of the cut-off distance. The impact of this increased interaction on fracture/fatigue analysis is still to be assessed, however, it could mean that using the interaction criteria presented in BS 7910 may miss the quicker increase in the size of a small crack in the presence of a larger crack in the region outside the interaction zone defined in BS 7910, and hence, underestimate the time to coalescence.

It is also shown that the load type has an influence on the interaction factor, thus, future work should aim to establish a similar equation for uniform tensile loads. The impact of other parameters such as crack aspect ratio, monopile diameter to thickness ratio could also be investigated

The interaction factors presented are for the deepest points in the crack which has the largest SIF. A semi-elliptical crack in a monopile has an infinite number of points on the semi-ellipse at which SIFs can be obtained. There may be a need to study if the interaction effect are greater at other points along the crack front, for instance at the free surface. Whilst this does not affect the conclusion of the FAD, that is, it is plotted using the largest SIF along the crack line, it may affect the change of the crack shape (aspect ratio) if the crack growth differs significantly in the circumferential direction relative to the radial direction.

For this work it is assumed that the recharacterisation of interacting flaws as a single flaw based on BS 7910 criteria is acceptable. Further research to assess if the recharacterisation of two flaws as per BS 7910 is either conservative or unconservative for OWT monopiles should be conducted.

# 8 DEVELOPED APPLICATION

As part of this thesis, an application was written using the Visual Basic .Net object-oriented programming language incorporating the various proposed methodologies. The application is intended to demonstrate the framework for continual assessment of the integrity of cracked monopiles.

The application consists of 3 pages as shown in Figure 8.1 to Figure 8.3. Pipe geometry, mechanical properties, crack geometry and load data are input in page 1. The failure assessment diagram is presented in page 2. The failure assessment line, and file control settings are controlled in page 3.

The process flow diagram of the application is presented in Figure 2.1. The system comprises of several interlinked sub-assemblies (dashed boundaries). The key characteristics of each sub-assembly are discussed subsequently.

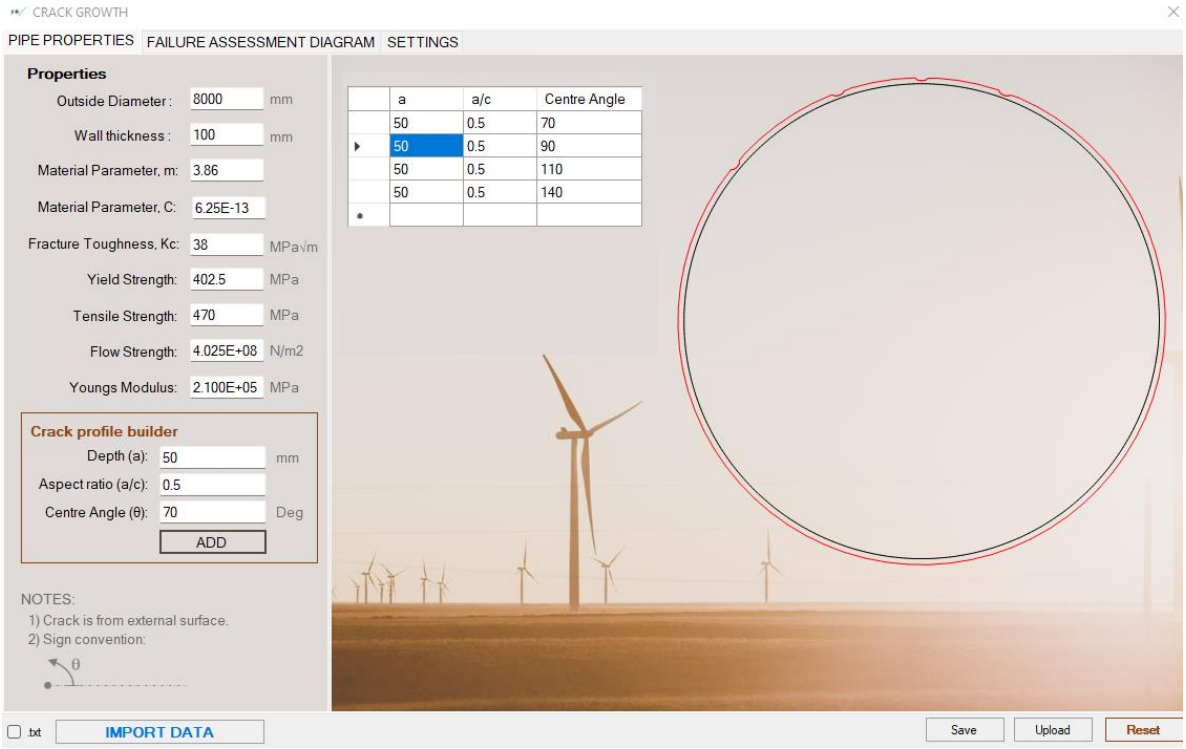


**Figure 8.1 – Developed Application (Page 1)**

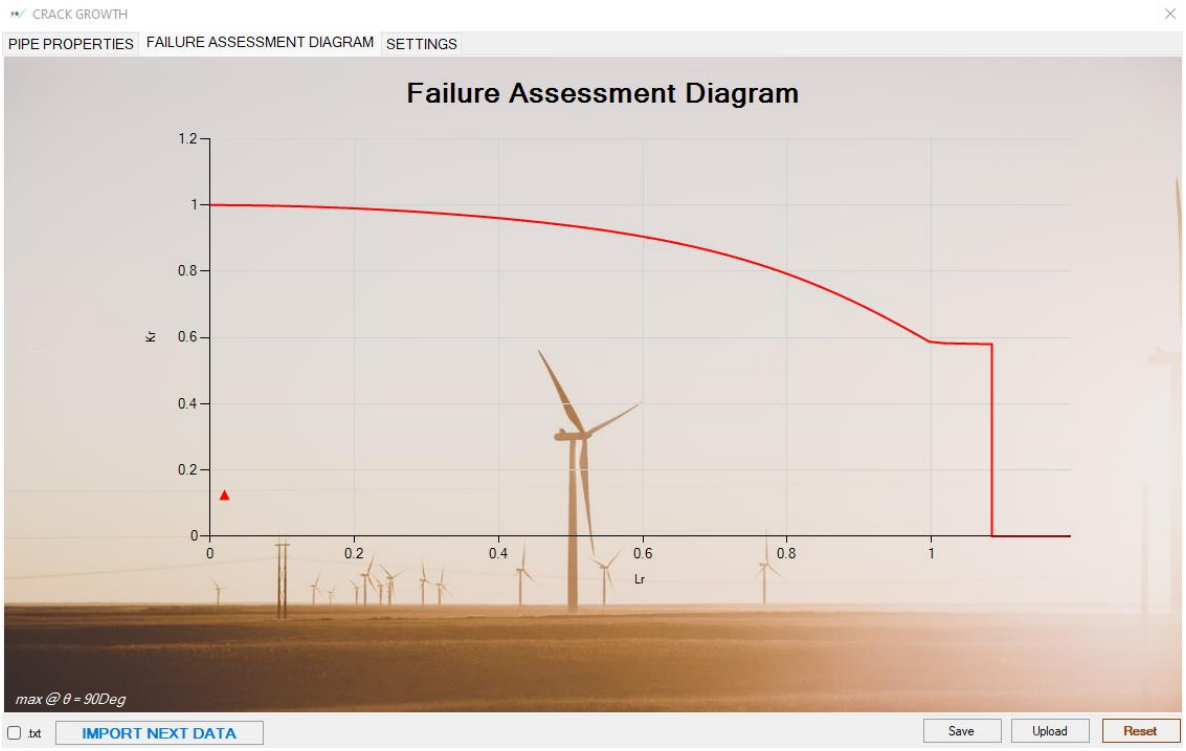


**Figure 8.2 – Developed Application (Page 2)**

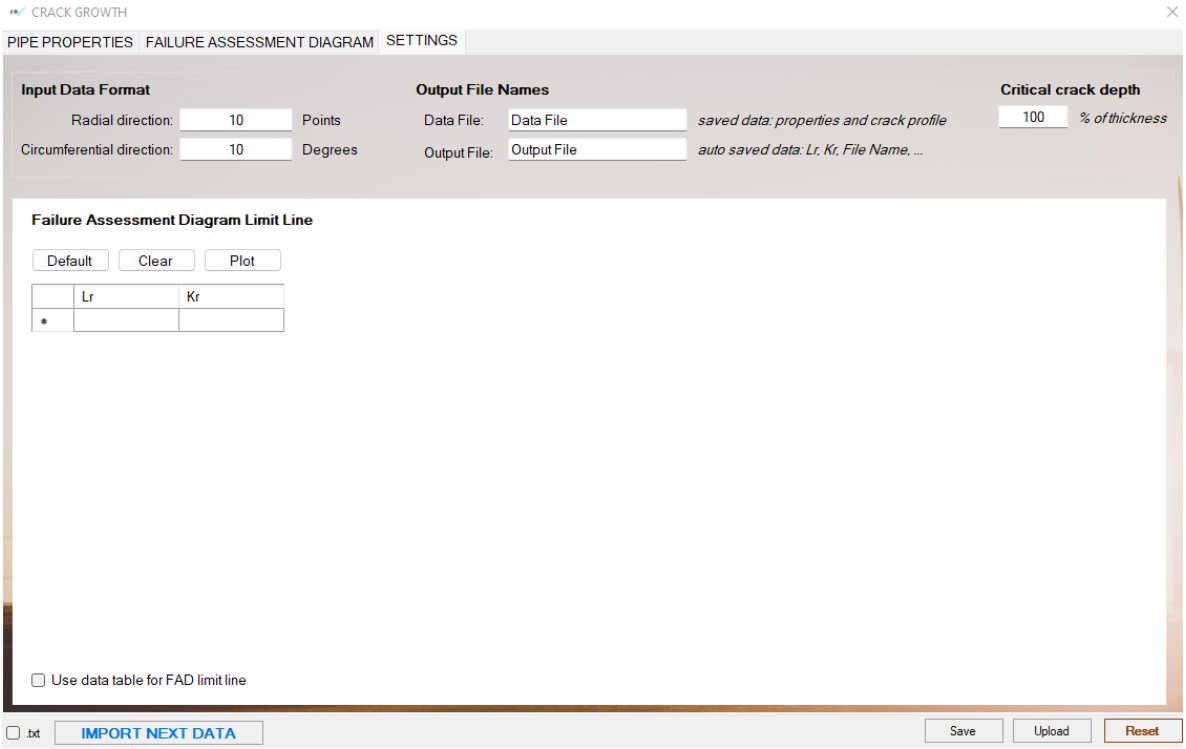


**Figure 8.3 – Developed Application (Page 3)**

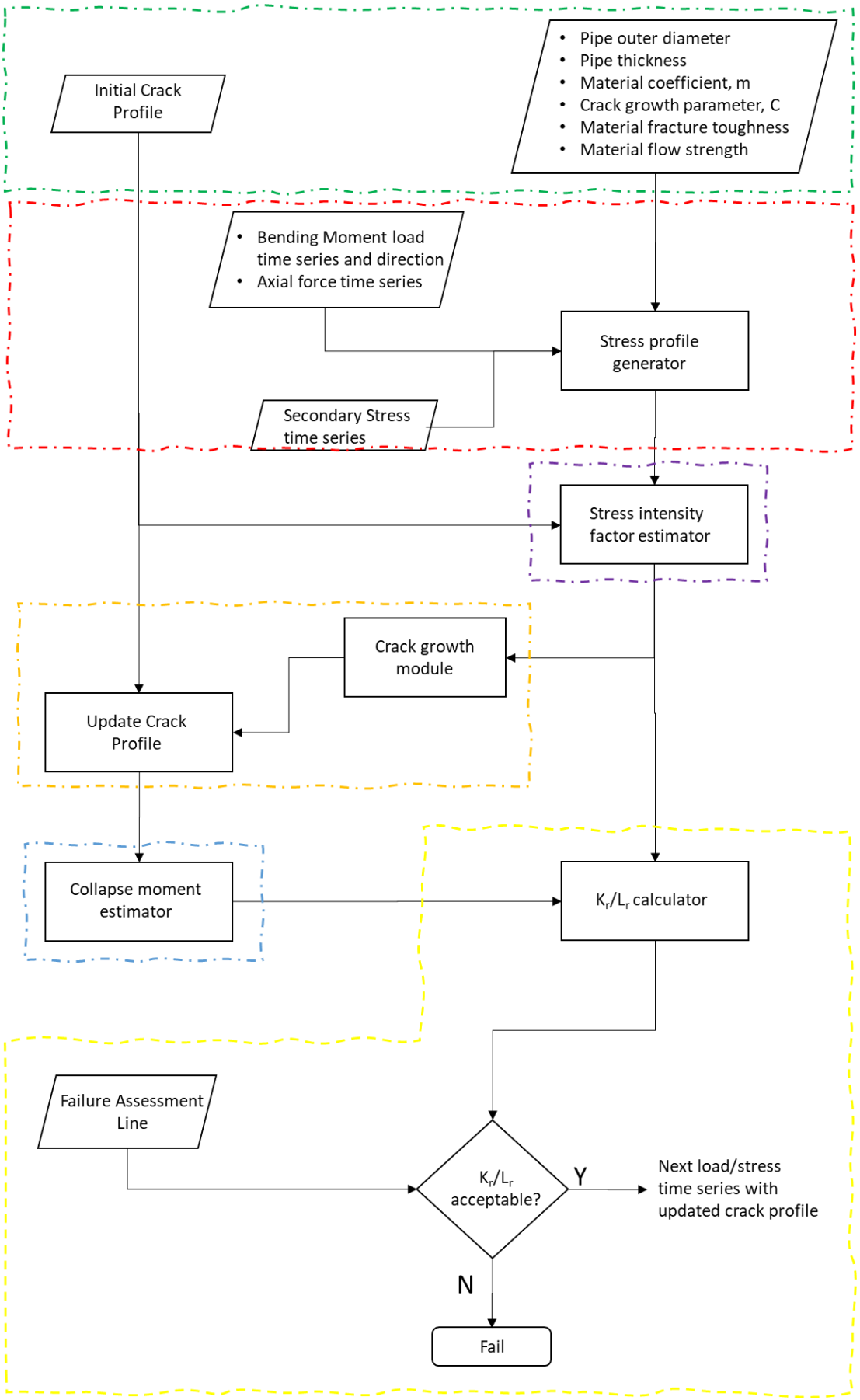


**Figure 8.4 – Proposed Methodology**

## 8.1 Pipe Geometry and Material sub assembly

The key properties of the monopile and cracks are defined in this sub assembly. They are:

- Outside diameter of the monopile ($R_{out}$) and Wall thickness of the monopile (t).
- Material coefficient (m) and Crack growth parameter (C).
- Material fracture toughness ($K_{mat}$).
- Flow strengths, $\sigma_f$ is the stress at which a material experiences plastic deformation as discussed by Altan and Boulger [176]. Rahman and Wilkowski [139] state that it is typically assumed as the average of the yield and ultimate tensile strength.
- Crack profile - the crack profile obtained using appropriate NDT techniques as illustrated in Figure 8.5. The crack profile is defined in terms of crack depth (a) and angle (ξ), where ξ is in the range of 0 to 360°. The crack depth equal to zero at uncracked locations. The cracks are characterised to extract the appropriate crack depth as aspect ratio (a/c). Any crack pairs that fulfil the interaction criteria as specified in BS 7910 [68] are recharacterised as a single flaw.

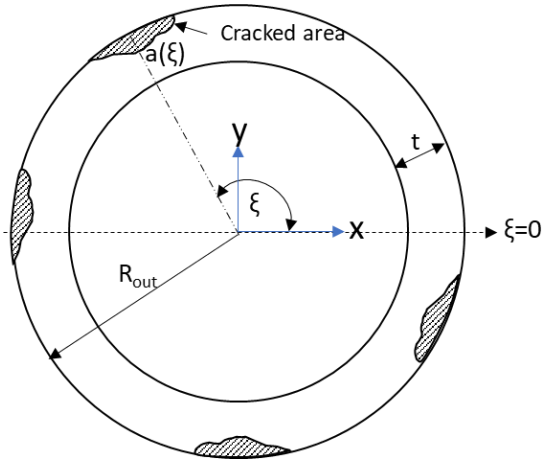


**Figure 8.5 – Definition of Crack Profile**

## 8.2 Stress profile Sub-Assembly

The stress time series to be applied to the monopile is created in this sub assembly. Although the OWT monopile is subject to various types of loads (axial, shear, bending and torsional moments), for the critical Mode I crack opening the applied stress is normal to the plane of the crack. Thus, for circumferential cracks, the applicable loads are bending and axial stresses.

By default, it is assumed time series of bending moments and axial loads are available. However, the system can also use any arbitrary stress profile. Provided that the stress distribution along the potential crack plane can be obtained. For semi-elliptical, circumferential external flaws, the potential crack plane runs from the external surface to the centre of the pipe through the deepest point of the crack. For supplied moment and axial loads, the crack opening stress at any location in the pipe cross-section is.

$$Stress(\sigma) = \frac{M_{Res} * y * \sin(\beta - \alpha)}{I} + \frac{F}{A} \quad 8.1$$

Where:

$M_{Res}$ is the resultant of the orthogonal bending moments $M_x$ and $M_y$
$y$ is the distance of the location from the neutral axis $R_{in} \leq y \leq R_{out}$
$\beta$ is the angular orientation of the location relative to the x-axis
$\alpha$ is the angle of the resultant moment axis relative to the x-axis
$I$ is the second moment of area of the monopile
$F$ is the axial force (along z axis)
$A$ is the cross-sectional area of the monopile

Bending moment and axial loads are classed as primary loads. However, secondary stresses may impact on the integrity of cracked structures as they may contribute to SIF. BS 7910 [68] provides guidance on secondary stresses stating that the direct stress component perpendicular to the plane of the flaw should be used in the calculation of the SIF.

For OWT monopiles, longitudinal and circumferential welding of the "cans" are a source of residual stresses. There are various studies such as [177-179] exploring the impact of residual stresses on fracture behaviour. However, work by Oyeniran and Asiaka [180] using FEA to investigate the impact of residual stresses on fatigue damage of OWT monopiles concluded that even residual stresses as high as the yield stress of the monopile material had a negligible contribution to the fatigue damage. SIF due to residual stresses is not included in this iteration of the application.

## 8.3 SIF Sub-Assembly

Using weight function methodology, the SIF at the deepest point of a crack with depth a, subject to a stress distribution $\sigma(x)$ is calculated as:

$$K_I = \int_0^a \frac{2\sigma(x)}{\sqrt{2\pi(a-x)}}\left[1 + M_1\left(1-\frac{x}{a}\right)^{1/2} + M_2\left(1-\frac{x}{a}\right) + M_3\left(1-\frac{x}{a}\right)^{3/2}\right]dx \qquad 8.2$$

Fajuyigbe [175] provides a methodology for estimating the coefficients $M_1$, $M_2$ and $M_3$. For a linear stress distribution, it is possible to integrate equation 8.2 analytically. Accurate numerical integration is difficult due to the singularity as $x$ approaches $a$. However, for non-linear or complex stresses, analytical integration is not possible. The solution is to divide any stress distribution into a series of intervals where the stress distribution within each interval may be approximated as a linear function such that:

$$\sigma_i(x) = A_i x + B_i \qquad 8.3$$

Where:

$$A_i = \frac{\sigma_i(x) - \sigma_{i-1}(x)}{x_i - x_{i-1}} \qquad B_i = \sigma_i(x) - A_i x_i \qquad 8.4$$

The stress intensity factor becomes:

$$K_I = \sum_{i=1}^{i=n} \int_{x_{i-1}}^{x_i} \frac{2(A_i x + B_i)}{\sqrt{2\pi(a-x)}} \left[1 + M_1\left(1-\frac{x}{a}\right)^{1/2} + M_2\left(1-\frac{x}{a}\right) + M_3\left(1-\frac{x}{a}\right)^{3/2}\right] dx \quad 8.5$$

The general solution for the integration between x=0 and x=a may be expressed as:

$$K_I = \sum_{i=1}^{i=n} \sqrt{\frac{2}{\pi a}} [\alpha_i(C_{1i} + M_1 C_{2i} + M_2 C_{3i} + M_3 C_{4i}) + \beta_i(C_{3i} + M_1 C_{4i} + M_2 C_{5i} + M_3 C_{6i})] \quad 8.6$$

Where:

$$\alpha_i = B_i + aA_i \qquad \beta_i = -aA_i$$

$$C_{1i} = 2a\left[\left(1-\frac{x_{i-1}}{a}\right)^{\frac{1}{2}} - \left(1-\frac{x_i}{a}\right)^{\frac{1}{2}}\right] \qquad C_{2i} = a\left[\left(1-\frac{x_{i-1}}{a}\right) - \left(1-\frac{x_i}{a}\right)\right]$$

$$C_{3i} = \frac{2a}{3}\left[\left(1-\frac{x_{i-1}}{a}\right)^{\frac{3}{2}} - \left(1-\frac{x_i}{a}\right)^{\frac{3}{2}}\right] \qquad C_{4i} = \frac{a}{2}\left[\left(1-\frac{x_{i-1}}{a}\right)^{2} - \left(1-\frac{x_i}{a}\right)^{2}\right]$$

$$C_{5i} = \frac{2a}{5}\left[\left(1-\frac{x_{i-1}}{a}\right)^{\frac{5}{2}} - \left(1-\frac{x_i}{a}\right)^{\frac{5}{2}}\right] \qquad C_{6i} = \frac{a}{3}\left[\left(1-\frac{x_{i-1}}{a}\right)^{3} - \left(1-\frac{x_i}{a}\right)^{3}\right]$$

## 8.4 Crack Growth Sub-Assembly

The output of the SIF sub-assembly is a time series of stress intensity factor. Rainflow cycle counting technique is used to decompose the stochastic time trace into ranges (ΔK) and corresponding number of cycles (N). As stress intensity range (ΔK) applied to a material for some number of cycles (ΔN) will cause a crack to grow by a specific amount (Δa). The overall relationship between da/dN and ΔK is normally observed to be a sigmoidal curve in a log(da/dN) versus log(ΔK) plot as shown in Figure 8.6.

Crack growth determined by Paris Law [67] only covers the central, approximately linear, portion of the curve. This is often reasonable as, at low values of ΔK, the rate of growth falls off rapidly, such that, below a threshold SIF range, $\Delta K_0$, crack growth is insignificant. This has led to the inclusion of a minimum threshold SIF in the calculation of crack growth in design standards such as DNVGL-ST-0126 [22] :

$$\frac{da}{dN} = C(\Delta K^m - \Delta {K_{th}}^m) \quad 8.7$$

Higher mean stress is known to increase the rate of crack growth and is known as the mean stress effect. The mean stress is expressed in terms of a stress ratio (R) which may be defined as the ratio of minimum SIF to the maximum SIF. Both equations 3.4 and 8.7 do not explicitly account for the stress ratio. If these equations are to be used for a non-zero stress

ratio, then appropriate values of the crack growth parameter, C must be chosen for the specific stress ratio. Alternatively, some industrial guidelines such as BS 7910 [68] provide an amendment to Paris' law which accounts for the stress ratio. This is the default equation used in the proposed methodology:

$$\frac{da}{dN} = C\left(\frac{\Delta K - \Delta K_{th}}{1-R}\right)^{m} \tag{8.8}$$

There is a general crack growth equation (NASGRO) which accounts for the stress ratio, the lower growth near the threshold and the increased growth at the upper tail of the sigmoidal curve [181]. However, it requires additional empirical coefficients that determine the curvature of the growth rate curve in the tail regions which is not often practical.

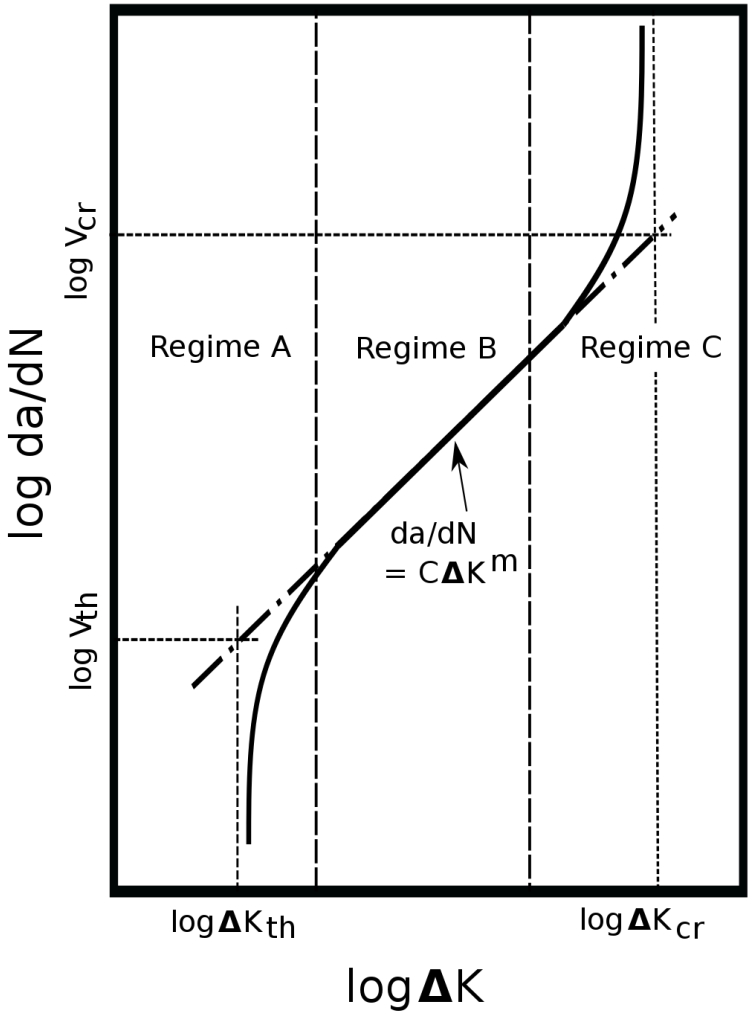


**Figure 8.6 – Crack Growth Regimes**

## 8.5 Collapse Moment Sub-Assembly

Using net section collapse methodology as presented by Fajuyigbe [182] the plastic limit load under axial force and bending moment is calculated in this sub assembly. The plastic limit load is calculated for 8 cardinal directions to ensure that the minimum conservative value may be obtained.

An OWT monopile may also be subjected to torsional loads caused by forces acting on the rotor. Therefore, ignoring the effect of torsion in the derivation of the limit load may lead to an overestimation. There are methods based on defining an equivalent collapse moment which include the effect of torsion in the plastic collapse moment [183-185]. However, these mainly focus on small diameter piping systems. For monopile foundations, torsional moments are usually only a small fraction of the bending moment [186]. Therefore, torsional moments are not expected to be a major contributor to plastic collapse. The proposed methodology does not include torsional moments in the estimation of plastic limit loads by default.

## 8.6 FAD Sub-Assembly

The maximum brittle, and load ratio for the time series of SIF and bending moment are computed in this sub assembly. The maximum value of brittle and load ratios for all cracks considered is plotted on a FAD for comparison against the failure assessment line (FAL). The default FAL is based on option 1 from BS 7910 [68] but user specified FAL is also allowed.

# 9 CASE STUDY 1

## 9.1 Introduction

The capability of the developed application is illustrated though a case study. As discussed previously, SIF may be obtained from FEA of the cracked structure. SIF is obtained from linear elastic fracture mechanics (LEFM), that is, only elastic methods, under the actions of relevant primary and secondary loads respectively. SIF derived from FEA is applicable only to the specific component and crack geometry and loading condition meaning that analysis must be repeated for any change in the configuration. It is computationally and temporally expensive to set up and run these FE models. Thus, the use of SIF generated from finite element analyses is not practical in situations where the crack geometry is constantly changing such as under the action of fatigue loads.

For simple loading, SIF can be obtained from hand-book solutions such as those presented in industry standard BS 7910. SIF provided in handbooks are not specifically for the type of structures used in monopiles (large diameter pipes). It is shown in research that for typical monopile sizes, these solutions provide an inaccurate estimate of the shape function.

A new methodology for rapid and accurate estimation of Mode I SIF of a circumferential semi-elliptical external surface crack in an OWT monopile is developed as part of this thesis and is included in the developed application. The proposed methodology is validated against results presented in literature and also bespoke finite element analysis.

In this case study, the estimation of SIF using the new methodology is compared against BS 7910 through the calculation of the number of cycles for taken for a crack to grow between two depths. The case study considers a monopile with a single planar external surface flaw oriented circumferentially. The monopile has an outer radius ($r_o$) of 3m, inner radius ($r_i$) of 2.9m, and wall thickness ($t$) of 100mm, in line with typical sizes of existing monopiles in various wind farms across Europe as reported in [23]. The flaw has an initial depth ($a_i$) of 30mm (a/t=0.3) and an aspect ratio (a/c) of 0.3. The final crack depth ($a_f$) is 99mm. For simplicity it is assumed that the aspect ratio remains the constant as the crack grows.

The monopile is constantly cycled between peak bending stresses of 10 and 100MPa. These stress range are larger than typical values for OWT monopiles but is chosen for plotting convenience. In any case, the purpose of the case study is to compare the number of cycles obtained from two methodologies. The comparison is independent of the applied stress range as shown below:

$$\frac{da}{dN} = C(\Delta K^m) \tag{9.1}$$

$$\Delta K = Y(\Delta\sigma)\sqrt{\pi a} \tag{9.2}$$

therefore, for constant $\Delta\sigma$

$$N = \frac{1}{C\Delta\sigma^m \pi^{m/2}} \int_{a_i}^{a_f} Y^{-m}\, a^{-m/2} da \tag{9.3}$$

Thus:

$$\frac{N_{app}}{N_{BS7910}} = \frac{\int_{a_i}^{a_f} Y_{app}^{-m} a^{-m/2} da}{\int_{a_i}^{a_f} Y_{BS\,7910}^{-m} a^{-m/2} da} \quad 9.4$$

$Y_{app}$ and $Y_{BS\,7910}$ are the shape factors obtained from the developed app and BS 7910 [68] respectively. The material parameters (C and m) are selected based on the simplified Paris law constants recommended by BS 7910 [68] for steels freely corroding in a marine environment and are provided in Table 9.1. For welded steels unprotected in a marine environment, the threshold SIF ($\Delta K_{th}$) is 0MPa√m.

**Table 9.1 – Crack Growth Parameters (da/dN in m/cycle and ΔK in MPa√m)**

| C | m |
|---|---|
| 7.27 x 10 -11 | 3.0 |

The general procedure for crack growth assessment of planar flaws is provided in clause 8.4 of BS 7910 [68]. The solution for SIF for external surface flaws oriented circumferentially is provided in clause M.7.3.4. For fatigue assessment:

$$Y(\Delta\sigma) = Mf_w\{k_{tm}M_{km}M_m\Delta\sigma_m + k_{tb}M_{kb}M_b[\Delta\sigma_b + (k_m - 1)\Delta\sigma_m]\} \quad 9.5$$

$M$, $M_m$, $M_b$ and $f_w$ (finite width correction) are factors specific to the component geometry, crack geometry and load type and are provided in clause M.7.3.4 . $M_{km}$ and $M_{kb}$ apply when the flaw is in a region of local stress concentration and set to 1 in this case. $k_m$ , $k_{tm}$ , and $k_{tb}$ are magnifiers due to misalignment or local structural discontinuities and are set to 1. $\Delta\sigma_m$ is the change in mean stress through the section thickness and $\Delta\sigma_b$ is the component of stress that varies linearly across the section thickness. The applied bending stress is decomposed into $\Delta\sigma_m$, and $\Delta\sigma_b$ using stressed at the outer ($\sigma_1$) and inner ($\sigma_2$) diameters:

$$\Delta\sigma_m = \frac{\Delta\sigma_1 + \Delta\sigma_2}{2} \qquad \sigma_b = \frac{\Delta\sigma_1 - \Delta\sigma_2}{2} \quad 9.6$$

## 9.2 Results and Discussion

The estimated crack propagation against the number of cycles is presented in Figure 9.1. Crack growth assuming that Y=1 as is used by some researchers [187] is also included in addition to crack growth predicted by the newly developed app and by BS 7910. The plot shows that an assumption of Y=1 significantly overestimates the number of cycles for the crack to grow to through thickness. This shows that even small changes in the shape factor can lead to large deviations in the calculation of fatigue life.

The plot shows that the predicted crack growth from the newly developed application and BS 7910 are similar. However, the predicted number of cycles for the crack to grow from 30mm to 99mm is approximately 9.5% greater than the value from the newly developed application. This margin of difference is in line with the values reported by Bocher et al. [77] for a monopile with outer diameter of 5m, thickness of 90mm, and a circumferential semi-elliptical crack at the outer surface with a fixed aspect ratio of a/c = 0.6.

This is a significant difference. For a monopile with a design life of 20 years, this is a difference of approximately 2 years.

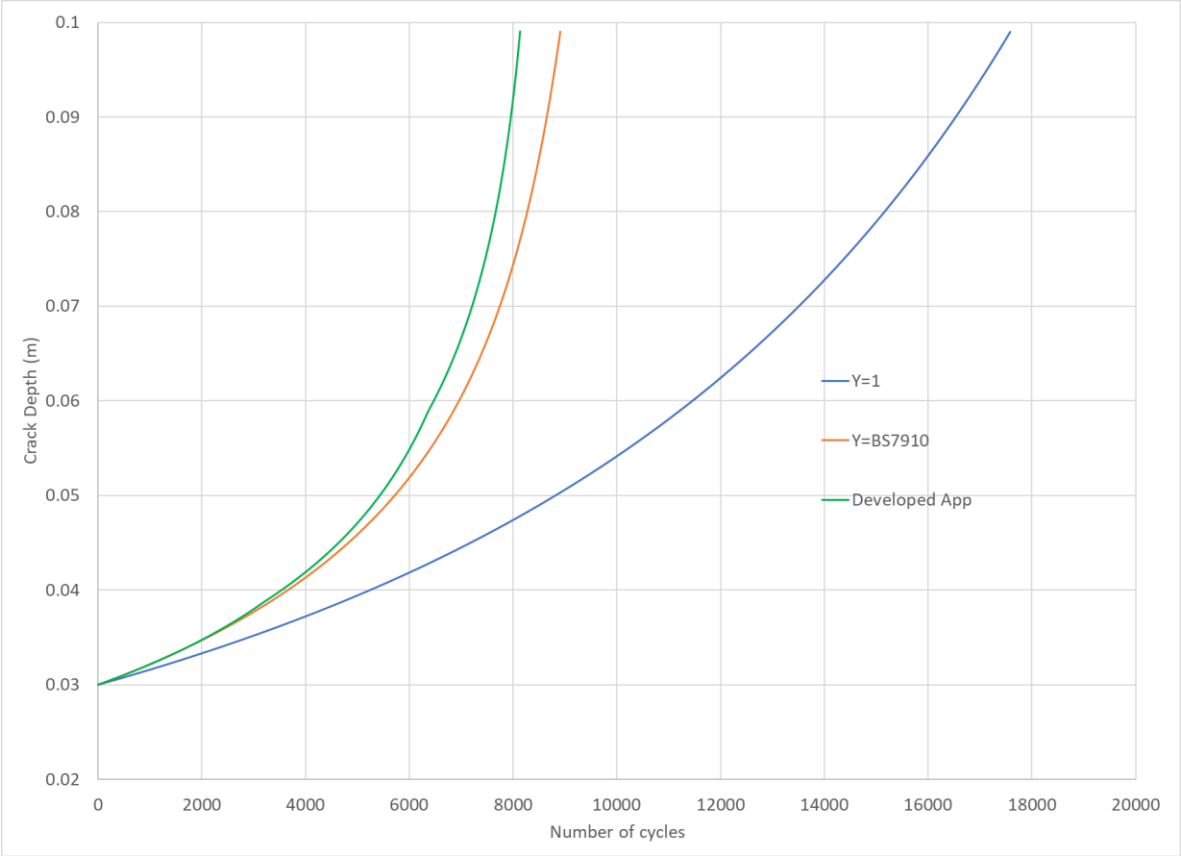


**Figure 9.1 – Crack Growth Estimation for different approaches**

# 10 CASE STUDY 2

The capability of the developed application is illustrated though a second case study. The aim of this thesis is to develop a structural methodology to enable lifetime extension of OWT monopiles. The purpose of this case study is to showcase the capability of developed application to assess the acceptability of a monopile with multiple cracks subject to stochastic environmental loading. It is noted that the loadcases do not include turbine loading.

This case study considers a monopile with three single planar external surface flaws oriented circumferentially. The monopile has an outer radius ($r_o$) of 4m, inner radius ($r_i$) of 3.9m, and wall thickness ($t$) of 100mm, in line with typical sizes of existing monopiles in various wind farms across Europe as reported in [23]. The fracture toughness is taken as 38 MPa√m. The yield, tensile and flow strengths are taken as 402.5MPa, 470MPa and 402.5MPa respectively. The Young's modulus is $2.1 \times 10^5$MPa.

The initial characteristics of the flaws are presented in Table 10.1. The cracks are assumed to be in the monopile in the region of the mudline. Other key properties, such as crack material parameters, are based on recommendations by BS 7910 [68]. The material parameters C and m are $7.27 \times 10^{-11}$ and 3.0 respectively are presented in Figure 10.1. The threshold stress intensity factor is 0MPa√m. The FAL is in accordance with Option 1 of BS 7910.

**Table 10.1 – Crack Characteristics**

| Crack No. | Crack Depth (mm) | Crack Centre Angle (°) | Crack Aspect Ratio |
|---|---|---|---|
| 1 | 40 | 80 | 0.3 |
| 2 | 50 | 160 | 0.2 |
| 3 | 60 | 210 | 0.4 |

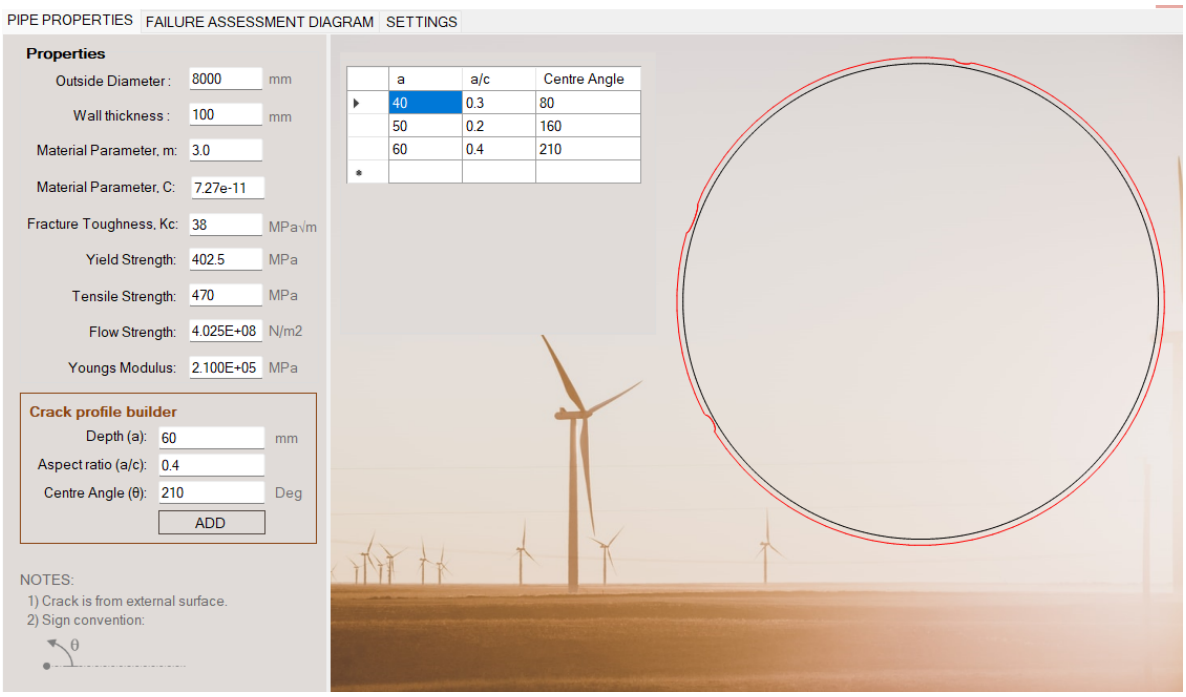


**Figure 10.1 – Crack Information**

The stress time series to be applied is generated from aero-elastic simulation of the 5MW NREL reference wind turbine [136] supported by the OC3 monopile configuration [188]. The wind and wave conditions considered are taken from the lumped scatter diagram for the Ijmuiden shallow water site presented in the Upwind design basis [32] shown in Table 10.2. Wind and wave are taken as co-directional. The wave is modelled using a JONSWAP spectrum.

**Table 10.2 – Lumped Scatter Diagram [32]**

| Load case No. | V (m/s) | TI (%) | Hs (m) | Tp (s) | Occ./year (hrs) |
|---|---|---|---|---|---|
| 1 | 2 | 29.2 | 0.91 | 5.83 | 423.9 |
| 2 | 4 | 20.4 | 0.97 | 5.65 | 1186.2 |
| 3 | 6 | 17.5 | 1.03 | 5.46 | 1437.3 |
| 4 | 8 | 16 | 1.14 | 5.39 | 1390.7 |
| 5 | 10 | 15.2 | 1.33 | 5.50 | 1379.5 |
| 6 | 12 | 14.6 | 1.57 | 5.79 | 1035.2 |
| 7 | 14 | 14.2 | 1.84 | 6.15 | 714.6 |
| 8 | 16 | 13.9 | 2.2 | 6.64 | 532.6 |
| 9 | 18 | 13.6 | 2.56 | 7.00 | 302.6 |
| 10 | 20 | 13.4 | 2.96 | 7.41 | 183.8 |
| 11 | 22 | 13.3 | 3.34 | 7.86 | 92.8 |
| 12 | 24 | 13.1 | 3.63 | 8.21 | 36.1 |
| 13 | 26 | 12.0 | 4.14 | 8.70 | 16.2 |
| 14 | 28 | 11.9 | 4.32 | 8.95 | 4.9 |
| 15 | 30 | 11.8 | 4.59 | 9.05 | 1.8 |
| 16 | 32 | 11.8 | 5.09 | 9.54 | 0.5 |
| 17 | 38 | 11.7 | 4.82 | 9.42 | 0.3 |

Each load case is simulated for 3 hours using open fast [41]. The force and moment reactions at the mudline is extracted. To simulate a year's environmental load, a randomised chain of 2920 3-hour seastates was created, with each load case only occurring the number of times expected based on its occurrence probability as shown in Table 10.2. It is noted that, although the sequence of 2920 contain all the seastates expected in a year, they are not necessarily in the correct sequence as this was not available in [32]. The estimated crack growth for a year may differ once sequence effects are included. For example, it has been observed experimentally that crack growth slows after high stress cycles. It is expected that the tool would be loaded with real sequential load time series data to determine incremental crack growth and pseudo-real time integrity assessment. The analysed chain of load cases is presented in Appendix A.

The growth of each crack is shown in Figure 10.2. The applied loading considers wind and wave loading from left to right (θ=0). Therefore, the crack initially 40mm (crack 1), centred at 80°, experiences negligible growth as it is mostly under compression. The cracks on the tensile side (cracks 2 and 3) that are initially 50mm and 60mm, grow by 4.6mm and 9.2mm respectively.

The locus of each crack is plotted on the FAD in Figure 10.3. Whilst Figure 10.2 shows the cracks on the tensile side of the monopile growing monotonously. Their respective loci on the FAD are not linear, as shown in Figure 10.4 and similarly Figure 10.5 for crack 3. The position on the FAD responds to the magnitude of the applied loads as well as the crack size. Although it is the shallower of the two cracks, crack 2 has a higher Kr value than crack 3, due to its aspect ratio and its position relative to the peak load.

The ability to perform accurate crack growth analysis whilst assessing the integrity of the cracked structure rapidly is a game-changer. Crack growth for each cycle of the load time series can be determined, thus allowing any sequencing effects to be explicitly captured. It also removes the need for load case binning, or the other workarounds typically used to quicken the conventional fatigue analysis.

The ability to analyse the OWT monopile in pseudo-real time could also form the basis of a digital twin for continuous tacking of accumulated fatigue damage. Digital twins have emerged as a novel technology in the wind energy sector that enables the design, monitoring and prediction of wind turbine performance [189]. The framework proposed in this thesis and embedded in the tool could provide the fatigue model incorporated in the global model of the wind turbine.

For a desktop fatigue analysis, the creation of a stochastic time series such as wave load train relies on seed which govern the realisation of the time series from the spectral parameters. Multiple seed realisations are often required to ensure that the maximum peak events have occurred in the analysed time series. This tool would enable the various load series for the multiple seeds to be analysed quickly.

The speed of the tool is also useful for probabilistic analysis, allowing uncertainties in crack sizes, probability of detection, and environmental parameters to be explored as recommended by Kirkemo [190, 191]. This allows a range of outcomes to be generated.

Therefore, the developed application can provide useful information that assists in operational decisions to extend the life of the monopile through protecting critical cracks.

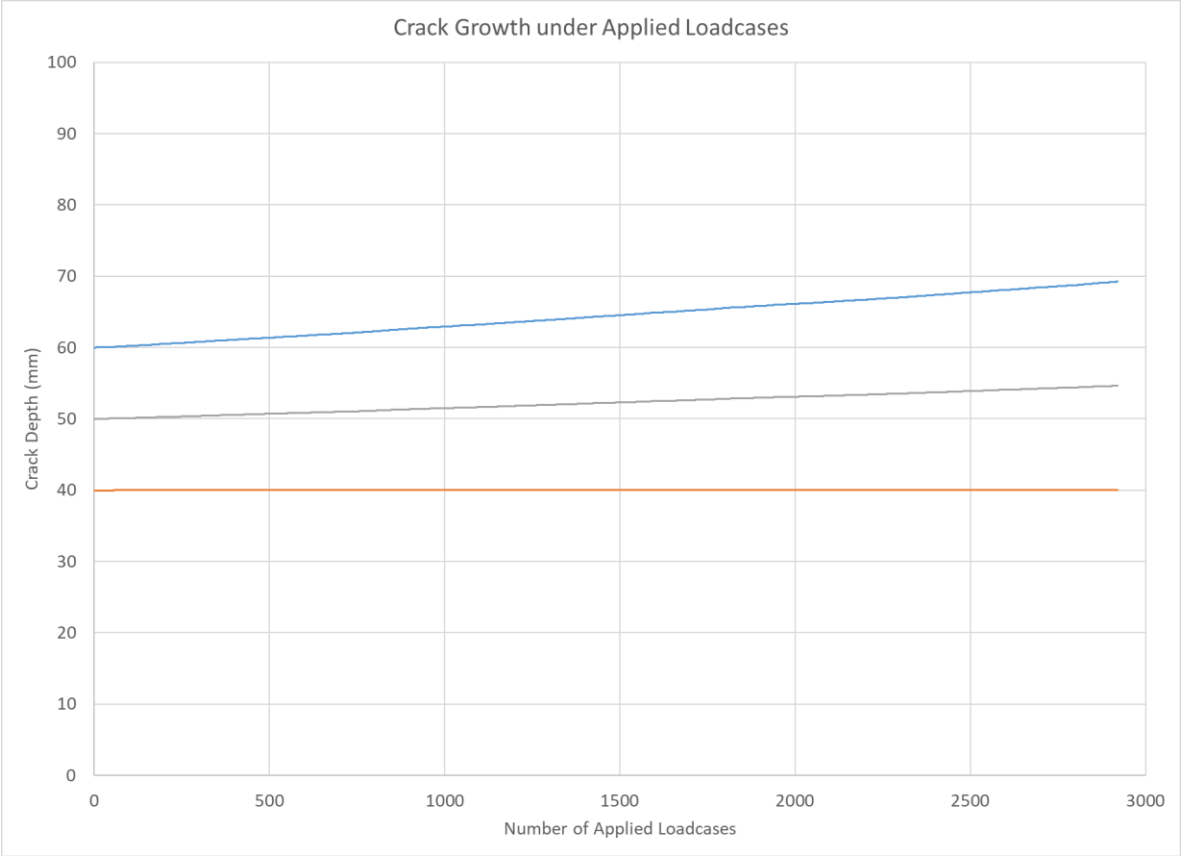


**Figure 10.2 – Crack Growth under Applied Load cases**

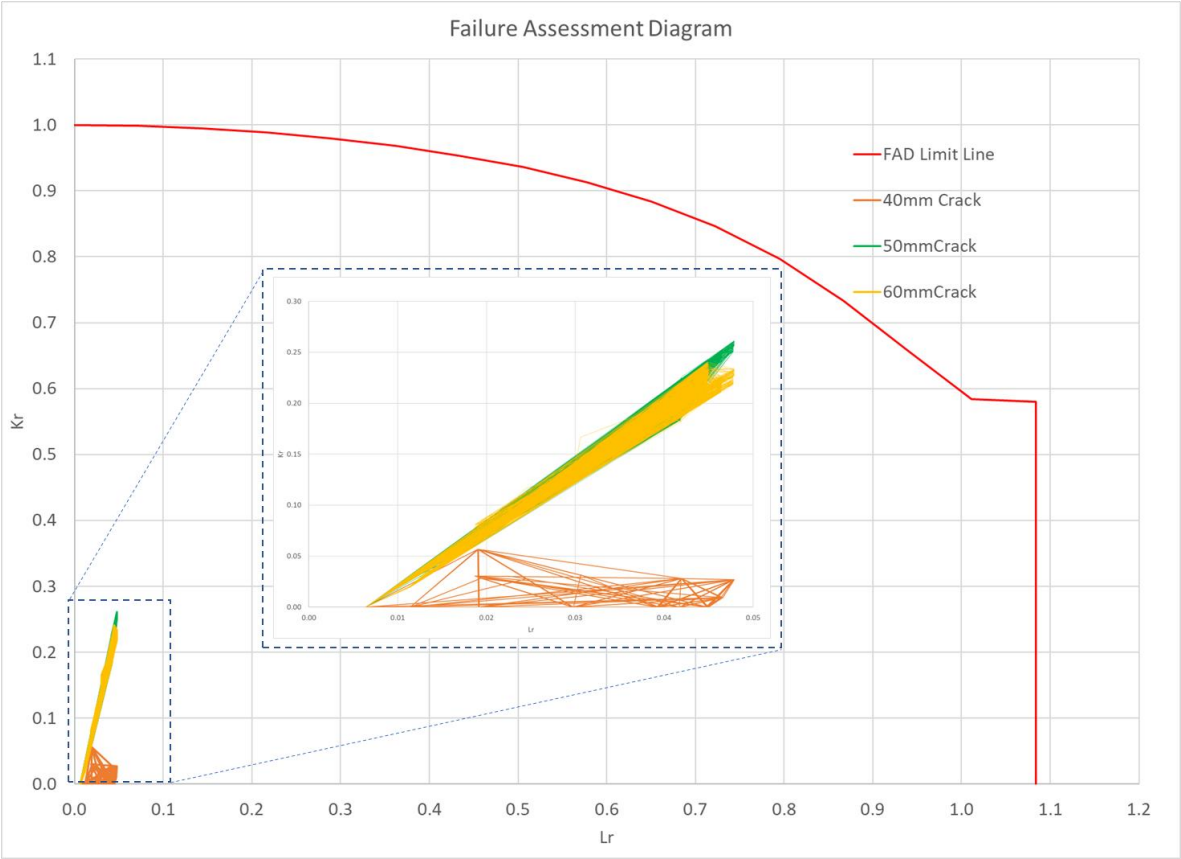


**Figure 10.3 – Failure Assessment Diagram under Applied Load cases**

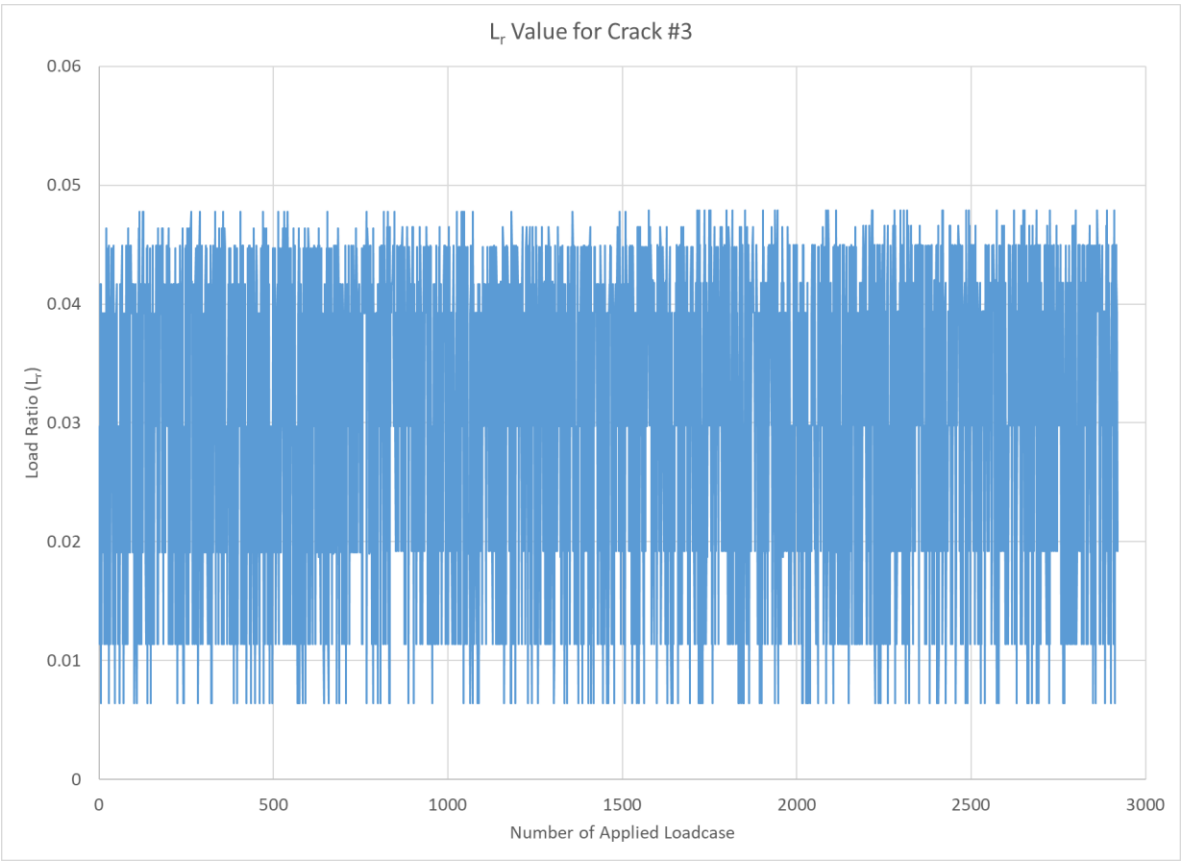


**Figure 10.4 – $L_r$ for Crack #3**

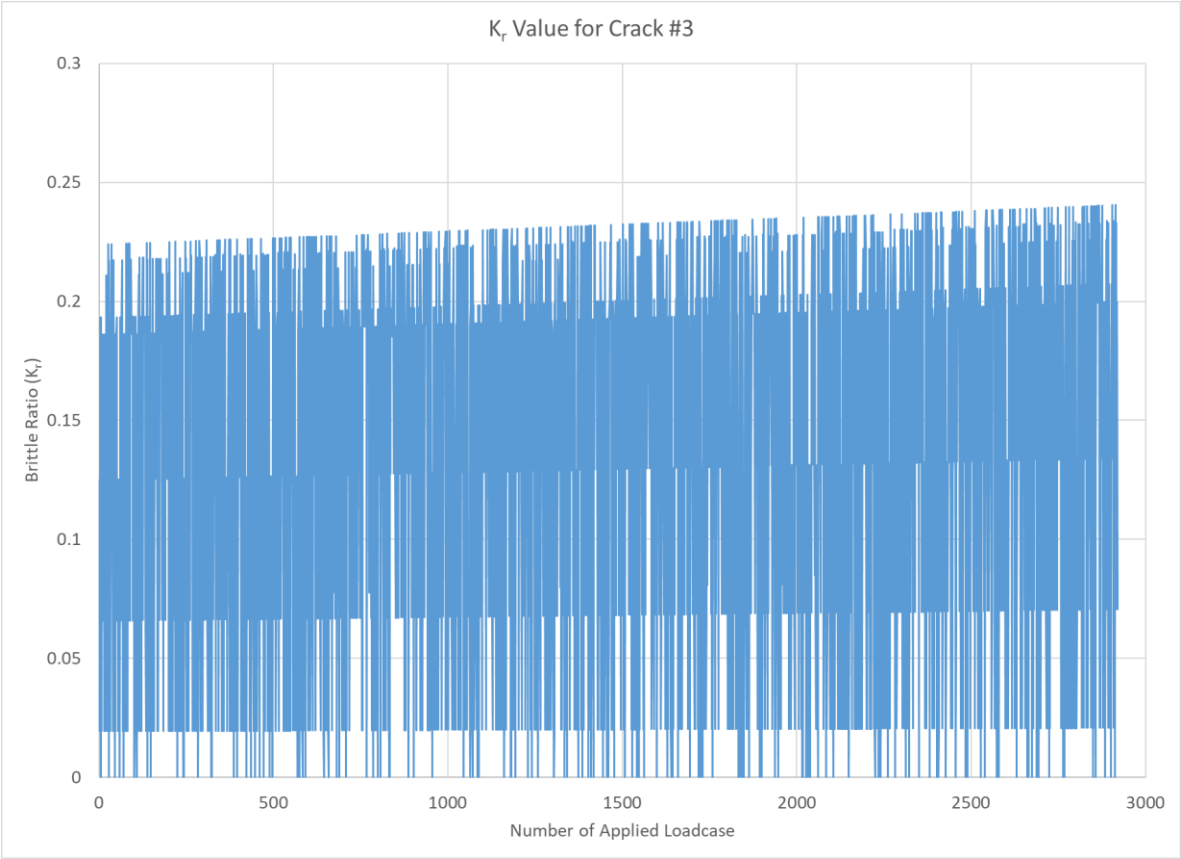


**Figure 10.5 – $K_r$ for Crack #3**

# 11 CONCLUSIONS

## 11.1 Summary and Key Findings

Monopiles are the most common type of foundation for OWT. As the early generation offshore wind farms reach the end of their design life, the wind industry needs to prepare for end-of-life decision making. Lifetime extension offers the tempting opportunity to keep operating these monopiles beyond the initial design life. In this scenario, it is necessary to prove that the monopiles have structural reserves to last the duration of the lifetime extension.

Monopiles are large, welded structures. Thus, an aged monopile is likely to already have a crack. It may actually have multiple cracks on the same plane due to manufacturing defects or loading. A framework for assessing the structural integrity of monopiles with external circumferential cracks using failure assessment diagram is provided in this thesis. The FAD depends on the calculation of stress intensity factor to assess brittle failure and plastic limit loads to assess plastic collapse.

A methodology for calculating the SIF of an OWT monopile containing a semi-elliptical external surface crack subjected to arbitrary distribution is provided in this thesis. The approach is based on the theory of weight functions. The obtained SIF is used in the calculation of crack growth and assessment of fracture. The proposed approach has some advantages over existing methodologies:

- It is significantly faster than performing finite element fracture mechanics simulation. The methodology allows near instantaneous determination of SIF.
- It provides a more appropriate estimation of SIF of OWT monopiles as it is based on FEA analysis of typical monopile sizes.

A methodology is proposed for calculating the plastic collapse (limit) bending moment load of a pipe with a circumferential flaw with an emphasis on its application for use in the assessment of cracked OWT monopile using FAD. Novel equations are derived based on theory of net section collapse (NSC) for estimating the bending plastic limit load for monopiles with multiple arbitrary cracks. The new equations have the following advantages over existing methods:

- The crack does not need to be categorised as occupying the tensile or compression zone.
- For multiple cracks, there is no need to define the span limits of each individual crack in the pipe geometry.
- The crack shape does not need to be idealised as either semi-elliptical or constant depth.
- The crack does not need to be symmetrical about the axis of the applied bending moment

Typically, monopile fatigue failure considers failure due to a dominant crack. However, this approach does not consider failure due to plastic collapse under extreme loads. The risk of plastic collapse increases with the presence of multiple cracks as simultaneous presence of multiple defects of sufficient size and density may cause a structure to lose residual strength even whilst the cracks may be individually acceptable. The assessment of multiple cracks is

inherently included in the proposed methodology for assessing limit load. For brittle failure, a first-step exploration of the interaction between co-planar, circumferential, semi-elliptical, external surface flaws located in OWT monopile. The objective is to test the interaction criteria provided in industry guideline BS 7910. The results from this work show that non-trivial interaction between cracks still exists outside of the cut-off distance. The impact of this increased interaction on fracture/fatigue analysis is still to be assessed. However, it could mean that using the interaction criteria presented in BS 7910 may miss the quicker increase in the size of a small crack in the presence of a larger crack in the region outside the interaction zone defined in BS 7910, and hence, underestimate the time to coalescence.

The various proposed methodologies were incorporated into a new application written using the Visual Basic .Net object-oriented programming language. This application demonstrates the framework through which the structural integrity of multi-cracked offshore monopiles can be assessed with the view to extending the initial lifetime.

## 11.2 Recommendations

To the author's knowledge, this thesis is the first long-term research project into the structural integrity assessment of monopiles with multiple cracks. This thesis provides a framework for these types of structural assessment. Several key issues were addressed during the course of the research work, however, there is room to improve the various processes and methodologies. Recommendations for future research work include:

1) It is assumed in this work that initially elliptical flaws remain elliptical as they grow and that the crack aspect ratio remains the same. However, it may be important to account for different growth rates at different points along the crack.

2) The interaction factors presented are for the deepest point in the crack, which typically has the largest SIF. A semi-elliptical crack in a monopile has an infinite number of points on the semi-ellipse at which SIFs can be obtained. There may be a need to study if the interaction effect is greater at other points along the crack front, for instance at the free surface. Whilst this does not affect the conclusion of the FAD (i.e. it is plotted using the largest SIF along the crack line), it may affect the change of the crack shape (aspect ratio) if the crack growth differs significantly in the circumferential direction relative to the radial direction.

3) The research work considers semi-elliptical, circumferential, external surface cracks. Future research should use the framework provided to propose similar methodologies for internal surface and embedded cracks.

4) All proposed methodologies are validated against results presented in literature and bespoke FEA. Validation against empirical data is highly desirable.

# 12 UNIQUE CONTRIBUTION

This research contributes to knowledge in a way which is novel and scientifically sound. Two scientific journals have been successfully published as well as one peer-reviewed scientific conference paper. A third paper is currently submitted to a scientific journal for review.

The goal of this thesis is to propose a fracture mechanics framework for the structural assessment OWT monopiles in terms of their operation beyond their initial design lives. The literature review revealed that there is very little research work in this area. Current approaches focus on the use of processes and methodologies from other industries or generic guidelines without any critical assessment of their suitability for OWT monopiles.

This thesis makes several unique contributions to the knowledge and understanding of fatigue assessment of OWT monopiles. Firstly, a critical examination of the state-of-the-art approach of using FAD generated using the industry standard BS 7910 found limitations in the determination of collapse ratio ($L_r$) and some lack of precision in the calculation of SIF for cylinders of typical monopile sizes. BS 7910 is a leading standard and is widely used in industry. It forms the basis of key industrial software such as CrackWISE® [192] operated by the Welding Institute. Based on the outcome of this thesis, it is clear that using this approach is potentially inaccurate for assessing OWT monopiles. Therefore, although the FAD itself is a suitable tool for assessing the acceptability of a cracked monopile, new approaches may be required for determining the brittle ($K_r$) and collapse ($L_r$) ratios needed to plot the FAD

The second major contribution of this thesis is the derivation of a new methodology for the determination of limit loads under bending for OWT monopiles. Limit loads are directly used in the calculation of $L_r$ . A key knowledge contribution of this research is that the net section collapse theory can be adapted for use with OWT monopiles. The approach allows a more accurate determination of $L_r$ compared to BS 7910 and a significantly faster determination of $L_r$ compared to conventional FEA.

The third major contribution of this thesis is the derivation of a new methodology for the determination of SIF of OWT monopiles using weight functions. Although SIF by weight functions is an established approach, this thesis clearly demonstrates that they can also be used for the analysis of monopiles. Most importantly, the research work done as part of this thesis enables the weight function approach to be used to generate SIF for OWT significantly quicker than SIF from FEA.

The various contributions discussed above were incorporated into an example application to illustrate how they may be used commercially. The ability of such a tool to perform fracture mechanics assessment of an OWT monopile was illustrated in case studies. Although the thesis considered circumferential external surface cracks, the framework developed can be imitated to generate suitable tools for other crack types. A tabular summary of the unique contributions and their value is presented in Table 12.1.

**Table 12.1 – Unique Contributions**

| Section | Contribution | Value to Knowledge |
|---|---|---|
| The use of procedure outlined in BS 7910 for the computation of FAD for cracked monopiles | • Confirmation of impreciseness in the calculation of SIF for large diameter pipes<br>• Identification of issue with the calculation of load ratio $L_r$ for deep cracks with BS 7910 approach | Issues with calculation using the procedure in BS 7910 suggest that a surface breaking defect may be identified as unacceptable based on BS 7910 when there may still be a non-trivial amount of structural residual life. The identification of this issue is beneficial to both researchers and industry |
| Determination of stress intensity factor using weight functions | • Clear demonstration that SIF determination by weight functions is suitable and accurate for OWT monopiles.<br>• A new, large library of better and more appropriate SIF reference solutions for offshore wind turbine monopiles were created as part of this thesis. | Researchers will benefit from the new wide library of reference SIF solutions for monopiles under tension and bending. These solutions can be used for future validation purpose or calculations |
| Influence of crack interaction on SIF | A test of the interaction criteria provided in BS 7910 and its application to circumferential semi-elliptical cracks in OWT monopiles. | This provides basis for further research as the results from this work show that non-trivial interaction between cracks still exists outside of the cut-off distance specified in BS 7910. |
| Estimation of monopile plastic limit loads under bending | Novel equations derived for the estimation of plastic limit loads for monopiles under bending based on the theory of net section collapse. | This provides an alternative to $L_r$ issues identified in BS 7910. It also removes the need to run computationally expensive elastic-perfectly plastic finite element simulations to determine plastic limit load for monopiles under bending. |
| VB Net application | Presented a framework for how the various methodologies may be coupled together into a user friend structural integrity tool | Researchers and industry may use this tool directly or as model for similar developments |

## 13 REFERENCES

[1] Wind Europe, "How much wind was in Europe's electricity yesterday?," February 2022 2021. Accessed: 16 June 2022. [Online]. Available: https://windeurope.org/about-wind/daily-wind-archive/2021-03-06/

[2] Wind Europe, "Wind Energy in Europe - 2021 Statistics and the outlook for 2022-2026," February 2022 2022. Accessed: 16 June 2022. [Online]. Available: https://windeurope.org/intelligence-platform/product/wind-energy-in-europe-2021-statistics-and-the-outlook-for-2022-2026/

[3] L. Ziegler, E. Gonzalez, T. Rubert, U. Smolka, and J. J. Melero, "Lifetime extension of onshore wind turbines: A review covering Germany, Spain, Denmark, and the UK," *Renewable and Sustainable Energy Reviews,* vol. 82, pp. 1261-1271, 2018.

[4] F. P. Brennan, "A framework for variable amplitude corrosion fatigue materials tests for offshore wind steel support structures," *Fatigue & Fracture of Engineering Materials & Structures,* vol. 37, no. 7, pp. 717-721, 2014.

[5] DNV GL, "DNVGL-ST-0262-lifetime extension of wind turbines," *Oslo: Det Norske Veritas,* 2017.

[6] DNV GL, "Certification of lifetime extension of wind turbines," *Service Specification DNVGL-SE-0263,* 2016.

[7] B. Pakenham, A. Ermakova, and A. Mehmanparast, "A review of life extension strategies for offshore wind farms using techno-economic assessments," *Energies,* vol. 14, no. 7, p. 1936, 2021.

[8] T. Rubert, D. McMillan, and P. Niewczas, "A decision support tool to assist with lifetime extension of wind turbines," *Renewable Energy,* vol. 120, pp. 423-433, 2018.

[9] J. S. Nielsen, L. Miller-Branovacki, and R. Carriveau, "Probabilistic and risk-informed life extension assessment of wind turbine structural components," *Energies,* vol. 14, no. 4, p. 821, 2021.

[10] G. A. R. Munoz, "Fracture mechanics approach to optimize inspection planning of offshore welds for wind turbines," 2018.

[11] T. Swift, "Damage tolerance capability," *International Journal of Fatigue,* vol. 16, no. 1, pp. 75-94, 1994.

[12] L. Ziegler, "Assessment of monopiles for lifetime extension of offshore wind turbines," *PhD, NTNU,* 2018.

[13] P. Amirafshari, F. Brennan, and A. Kolios, "A fracture mechanics framework for optimising design and inspection of offshore wind turbine support structures against fatigue failure," *Wind Energy Science,* vol. 6, no. 3, pp. 677-699, 2021.

[14] B. C. O'Kelly and M. Arshad, "Offshore wind turbine foundations–analysis and design," in *Offshore Wind Farms*: Elsevier, 2016, pp. 589-610.

[15] X. Wu *et al.*, "Foundations of offshore wind turbines: A review," *Renewable and Sustainable Energy Reviews,* vol. 104, pp. 379-393, 2019.

[16] M. Muskulus and G. Stewart, "A review and comparison of floating offshore wind turbine model experiments," 2016.

[17] G. Nogueira, F. A. Gomes, E. Dorscheidt, and G. B. Ellwanger, "Design and fatigue assessment of gravity base foundations for offshore wind turbines," *Proceedings of XLI CILAMCE,* 2020.

[18] M. B. Zaaijer, "Comparison of monopile, tripod, suction bucket and gravity base design for a 6 MW turbine," 2003.

[19] I. W. Chen, B.-L. Wong, Y.-H. Lin, S.-W. Chau, and H.-H. Huang, "Design and analysis of jacket substructures for offshore wind turbines," *Energies,* vol. 9, no. 4, p. 264, 2016.

[20] N. Nikolaos, "Deep water offshore wind technologies," *University of Strathclyde, Glasgow,* 2004.

[21] A. Ho, A. Mbistrova, and G. Corbetta, "The European offshore wind industry-key trends and statistics 2015," *Brussels, Belgium,* 2016.

[22] DNV GL, "DNVGL-ST-0126: Support structures for wind turbines," *Oslo, Norway: DNV,* 2016.
[23] L. Arany, S. Bhattacharya, J. Macdonald, and S. J. Hogan, "Design of monopiles for offshore wind turbines in 10 steps," *Soil Dynamics and Earthquake Engineering,* vol. 92, pp. 126-152, 2017.
[24] C. LeBlanc, G. T. Houlsby, and B. W. Byrne, "Response of stiff piles in sand to long-term cyclic lateral loading," *Géotechnique,* vol. 60, no. 2, pp. 79-90, 2010.
[25] D. Kallehave, B. W. Byrne, C. LeBlanc Thilsted, and K. K. Mikkelsen, "Optimization of monopiles for offshore wind turbines," *Philosophical Transactions of the Royal Society A: Mathematical, Physical and Engineering Sciences,* vol. 373, no. 2035, p. 20140100, 2015.
[26] B. K. Gupta and D. Basu, "Offshore wind turbine monopile foundations: Design perspectives," *Ocean Engineering,* vol. 213, p. 107514, 2020.
[27] F. Brennan and I. Tavares, "Fatigue design of offshore steel mono-pile wind substructures," *Proceedings of the Institution of Civil Engineers-Energy,* vol. 167, no. 4, pp. 196-202, 2014.
[28] B. W. Byrne *et al.*, "PISA: new design methods for offshore wind turbine monopiles," *Revue Française de Géotechnique,* no. 158, p. 3, 2019.
[29] *Loads and site conditions for wind turbines*, DNV GL, 2016.
[30] I. E. C. Tc88-Mt, "Iec 61400-3: Wind turbines–part 1: Design requirements," *International Electrotechnical Commission, Geneva,* vol. 64, 2005.
[31] A. Natarajan, M. H. Hansen, and S. Wang, "Design Load Basis for Offshore Wind Turbines: DTU Wind Energy Report No. E-0133," 2016.
[32] T. Fischer, W. E. De Vries, and B. Schmidt, "UpWind design basis (WP4: Offshore foundations and support structures)," 2010.
[33] C. International Electrotechnical, "Wind turbine generator systems-part 1: Safety requirements," *IEC 61400-1,* 1999.
[34] J. Van Der Tempel, "Design of support structures for offshore wind turbines," 2006.
[35] K. Hasselmann *et al.*, "Measurements of wind-wave growth and swell decay during the Joint North Sea Wave Project (JONSWAP)," *Ergaenzungsheft zur Deutschen Hydrographischen Zeitschrift, Reihe A,* 1973.
[36] L. Ziegler, S. Voormeeren, S. Schafhirt, and M. Muskulus, "Design clustering of offshore wind turbines using probabilistic fatigue load estimation," *Renewable Energy,* vol. 91, pp. 425-433, 2016.
[37] F. Vorpahl, H. Schwarze, T. Fischer, M. Seidel, and J. Jonkman, "Offshore wind turbine environment, loads, simulation, and design," *Wiley Interdisciplinary Reviews: Energy and Environment,* vol. 2, no. 5, pp. 548-570, 2013.
[38] M. Seidel, "Wave induced fatigue loads on monopiles-new approaches for lumping of scatter tables and site specific interpolation of fatigue loads," 2014.
[39] T. Fischer and W. D. Vries, "Final report 4.1: integration of support structure and wind turbine design," ed: UpWin, 2011.
[40] DNV GL, "Bladed User Manual," ed: DNV GL Oslo, Norway, 2016.
[41] J. M. Jonkman and M. L. Buhl, *FAST user's guide*. National Renewable Energy Laboratory Golden, CO, USA, 2005.
[42] M. L. Wymore, J. E. Van Dam, H. Ceylan, and D. Qiao, "A survey of health monitoring systems for wind turbines," *Renewable and Sustainable Energy Reviews,* vol. 52, pp. 976-990, 2015.
[43] W. Udo and Y. Muhammad, "Data-Driven Predictive Maintenance of Wind Turbine Based on SCADA Data," *IEEE Access,* vol. 9, pp. 162370-162388, 2021.
[44] E. Gonzalez, J. Tautz-Weinert, J. J. Melero, and S. J. Watson, "Statistical evaluation of SCADA data for wind turbine condition monitoring and farm assessment," 2018, vol. 1037: IOP Publishing, 3 ed., p. 032038.
[45] O. Emmanuel, J. P. Ruscoe, J. C. Side, R. E. Harris, S. A. Kerr, and C. R. Bullen, "An overview of recent technologies on wave and current measurement in coastal and marine applications," *Journal of Oceanography and Marine Science,* vol. 1, no. 1, pp. 001-010, 2010.

[46] G. B. Rossi *et al.*, "Measurement of Sea Waves," *Sensors,* vol. 22, no. 1, 2022, doi: 10.3390/s22010078.
[47] P. Faulkner, P. Cutter, and A. Owens, "Structural health monitoring systems in difficult environments—offshore wind turbines," 2012, pp. 1-7.
[48] T. Brown, A. Rimmer, and E. Palmer, "Wind Europe 2017 PO. 209 Monitoring Offshore Monopile Fatigue."
[49] M. Martinez-Luengo, A. Kolios, and L. Wang, "Structural health monitoring of offshore wind turbines: A review through the Statistical Pattern Recognition Paradigm," *Renewable and Sustainable Energy Reviews,* vol. 64, pp. 91-105, 2016.
[50] L. Ziegler, N. Cosack, A. Kolios, and M. Muskulus, "Structural monitoring for lifetime extension of offshore wind monopiles: Verification of strain-based load extrapolation algorithm," *Marine Structures,* vol. 66, pp. 154-163, 2019.
[51] M. Henkel, W. Weijtjens, and C. Devriendt, "Fatigue Stress Estimation for Submerged and Sub-Soil Welds of Offshore Wind Turbines on Monopiles Using Modal Expansion," *Energies,* vol. 14, no. 22, p. 7576, 2021.
[52] A. Iliopoulos, W. Weijtjens, D. Van Hemelrijck, and C. Devriendt, "Fatigue assessment of offshore wind turbines on monopile foundations using multi-band modal expansion," *Wind Energy,* vol. 20, no. 8, pp. 1463-1479, 2017.
[53] N. Noppe, K. Tatsis, E. Chatzi, C. Devrient, and W. Weijtjens, "Fatigue stress estimation of offshore wind turbine using a Kalman filter in combination with accelerometers," 2018: KU Leuven, Department of Mechanical Engineering, pp. 4693-6701.
[54] C. Bouty, S. Schafhirt, L. Ziegler, and M. Muskulus, "Lifetime extension for large offshore wind farms: Is it enough to reassess fatigue for selected design positions?," *Energy Procedia,* vol. 137, pp. 523-530, 2017.
[55] C. Loraux and E. Brühwiler, "The use of long term monitoring data for the extension of the service duration of existing wind turbine support structures," 2016, vol. 753: IOP Publishing, 7 ed., p. 072023.
[56] H. Ma, J. Yang, and L. Chen, "Numerical analysis of the long-term performance of offshore wind turbines supported by monopiles," *Ocean engineering,* vol. 136, pp. 94-105, 2017.
[57] R. I. Stephens, A. Fatemi, R. R. Stephens, and H. O. Fuchs, *Metal fatigue in engineering*. John Wiley & Sons, 2000.
[58] DNV GL, "DNVGL-RP-C203: Fatigue design of offshore steel structures," *DNV GL, Oslo, Norway,* 2016.
[59] T. Endo, "Damage evaluation of metals for random or varying loading," 1974, vol. 1: The Society of Material Science, Japan, pp. 371-380.
[60] I. Rychlik, "A new definition of the rainflow cycle counting method," *International journal of fatigue,* vol. 9, no. 2, pp. 119-121, 1987.
[61] G. Katsikogiannis, J. M. Hegseth, and E. E. Bachynski-Polić, "Application of a lumping method for fatigue design of monopile-based wind turbines using fully coupled and simplified models," *Applied Ocean Research,* vol. 120, p. 102998, 2022.
[62] J. C. Newman Jr, "FASTRAN-2: A fatigue crack growth structural analysis program," *NASA STI/recon technical report N,* vol. 92, p. 30964, 1992.
[63] O. E. Wheeler, "Spectrum loading and crack growth," *Journal of Basic Engineering,* no. 94, pp. 181-186, 1972.
[64] T. L. Anderson, "Fracture mechanics-fundamentals and applications," *NASA STI/Recon Technical Report A,* vol. 92, 1991.
[65] D. Gross, "Some remarks on the history of fracture mechanics," in *The History of Theoretical, Material and Computational Mechanics-Mathematics Meets Mechanics and Engineering*: Springer, 2014, pp. 195-209.
[66] R. O. Ritchie and D. Liu, *Introduction to fracture mechanics*. Elsevier, 2021.
[67] P. Paris and F. Erdogan, "A critical analysis of crack propagation laws," 1963.

[68] British Standards Institution, "BS 7910: 2013+ A1: 2015 Guide to methods for assessing the acceptability of flaws in metallic structures," *BSI Standard Publication,* 2015.
[69] J. C. Newman, *Stress-intensity factor equations for cracks in three-dimensional finite bodies subjected to tension and bending loads*. Langley Research Center, National Aeronautics and Space Administration, 1984.
[70] H. Tada, P. C. Paris, and G. R. Irwin, "The stress analysis of cracks," *Handbook, Del Research Corporation,* vol. 34, p. 635, 1973.
[71] D. P. Rooke and D. J. Cartwright, "Compendium of stress intensity factors," *Procurement Executive, Ministry of Defence. H. M. S. O. 1976, 330 p(Book).* 1976.
[72] G. C. Sih, P. C. Paris, and F. Erdogan, "Crack-tip, stress-intensity factors for plane extension and plate bending problems," 1962.
[73] Y. Murakami and L. M. Keer, "Stress intensity factors handbook, vol. 3," 1993.
[74] R6, "Assessment of the integrity of structures containing defects," *British Energy Generation, Report R/H/R6, Revision 4,* 2001.
[75] J. C. Newman Jr and I. S. Raju, "Analyses of surface cracks in finite plates under tension or bending loads," NATIONAL AERONAUTICS AND SPACE ADMINISTRATION HAMPTON VA LANGLEY RESEARCH …, 1979.
[76] J. C. Newman and I. S. Raju, "Stress-intensity factor equations for cracks in three-dimensional finite bodies," 1983 1983: ASTM International.
[77] M. Bocher, A. Mehmanparast, J. Braithwaite, and M. Shafiee, "New shape function solutions for fracture mechanics analysis of offshore wind turbine monopile foundations," *Ocean Engineering,* vol. 160, pp. 264-275, 2018.
[78] A. Fajuyigbe and F. Brennan, "Fitness-for-purpose assessment of cracked offshore wind turbine monopile," *Marine Structures,* vol. 77, p. 102965, 2021.
[79] S. M. Russ *et al.*, "Zencrack User's Manual, Version 7.1," ed: Zentech International, Ltd., Camberley, Surrey, UK, 2003.
[80] L. L. C. Quest Reliability, "FEA Crack User's Manual," 2009.
[81] J. M. Melenk and I. Babuška, "The partition of unity finite element method: basic theory and applications," *Computer methods in applied mechanics and engineering,* vol. 139, no. 1-4, pp. 289-314, 1996.
[82] C. A. Duarte and J. T. Oden, "Hp clouds-a meshless method to solve boundary-value Problem. Technical Report TICAM," ed: University of Texas at Austin, 1995.
[83] T. Belytschko and T. Black, "Elastic crack growth in finite elements with minimal remeshing," *International journal for numerical methods in engineering,* vol. 45, no. 5, pp. 601-620, 1999.
[84] N. Moës, J. Dolbow, and T. Belytschko, "A finite element method for crack growth without remeshing," *International journal for numerical methods in engineering,* vol. 46, no. 1, pp. 131-150, 1999.
[85] J. E. Dolbow, *An extended finite element method with discontinuous enrichment for applied mechanics*. Northwestern university, 1999.
[86] J. Dolbow, N. Moës, and T. Belytschko, "Discontinuous enrichment in finite elements with a partition of unity method," *Finite elements in analysis and design,* vol. 36, no. 3-4, pp. 235-260, 2000.
[87] N. Sukumar, N. Moës, B. Moran, and T. Belytschko, "Extended finite element method for three-dimensional crack modelling," *International journal for numerical methods in engineering,* vol. 48, no. 11, pp. 1549-1570, 2000.
[88] T. Belytschko, N. Moës, S. Usui, and C. Parimi, "Arbitrary discontinuities in finite elements," *International Journal for Numerical Methods in Engineering,* vol. 50, no. 4, pp. 993-1013, 2001.
[89] E. Budyn, G. Zi, N. Moës, and T. Belytschko, "A method for multiple crack growth in brittle materials without remeshing," *International journal for numerical methods in engineering,* vol. 61, no. 10, pp. 1741-1770, 2004.

[90] K. Agathos, S. P. A. Bordas, and E. Chatzi, "Improving the conditioning of XFEM/GFEM for fracture mechanics problems through enrichment quasi-orthogonalization," *Computer Methods in Applied Mechanics and Engineering,* vol. 346, pp. 1051-1073, 2019.

[91] S. A. Kanth, A. S. Lone, G. A. Harmain, and A. Jameel, "Elasto plastic crack growth by XFEM: a review," *Materials Today: Proceedings,* vol. 18, pp. 3472-3481, 2019.

[92] DNV GL, "DNVGL-RP-C210: Probabilistic Methods for Planning of Inspection for Fatigue Cracks in Offshore Structures," *Det Norske Veritas & Germanischer Lloyd SE: Oslo, Norway,* 2015.

[93] I. Hadley, "3 - Fracture assessment methods for welded structures," in *Fracture and Fatigue of Welded Joints and Structures*, K. A. Macdonald Ed.: Woodhead Publishing, 2011, pp. 60-90.

[94] S. e. E. Eren, I. Hadley, and K. Nikbin, "Differences in the Assessment of Plastic Collapse in BS 7910: 2005 and R6/FITNET FFS Procedures," 2011, vol. 44519, pp. 791-818.

[95] R. A. Ainsworth, M. Gintalas, M. K. Sahu, J. Chattopadhyay, and B. K. Dutta, "Application of failure assessment diagram methods to cracked straight pipes and elbows," *International Journal of Pressure Vessels and Piping,* vol. 148, pp. 26-35, 2016.

[96] K. Kouzoumis, I. Hadley, and M. Mostafavi, "Validation of BS 7910 fracture assessment procedures; wide plates and cylinders," *International Journal of Pressure Vessels and Piping,* vol. 190, p. 104309, 2021.

[97] P. W. Tan, C. A. Bigelow, and J. G. Bakuckas Jr, "Widespread fatigue damage assessment approach," WILLIAM J HUGHES TECHNICAL CENTER ATLANTIC CITY NJ, 2003.

[98] Y. Bombardier, M. Liao, and G. Renaud, "Fracture mechanics modelling of multiple site damage scenarios," 2009.

[99] G. A. Ruiz-Muñoz, "Method to analyse multiple site damage fatigue before and after crack coalescence," *Engineering Fracture Mechanics,* vol. 188, pp. 416-430, 2018.

[100] W. R. Hendricks, "The Aloha Airlines accident—a new era for aging aircraft," in *Structural integrity of aging airplanes*: Springer, 1991, pp. 153-165.

[101] D. M. Dawson and B. J. Brooks, *The Esso Longford gas plant accident: report of the Longford Royal Commission*. Government Printer, South Africa, 1999.

[102] R. Jones, D. Peng, and S. Pitt, "Assessment of multiple flat elliptical cracks with interactions," *Theoretical and applied fracture mechanics,* vol. 38, no. 3, pp. 281-291, 2002.

[103] Z. D. Jiang, J. Petit, and G. Bezine, "Stress intensity factors of two parallel 3d surface cracks," *Engineering fracture mechanics,* vol. 40, no. 2, pp. 345-354, 1991.

[104] X. B. Lin and R. A. Smith, "Fatigue growth analysis of interacting and coalescing surface defects," *International journal of fracture,* vol. 85, no. 3, pp. 283-299, 1997.

[105] W. O. Soboyejo, K. Kishimoto, R. A. Smith, and J. F. Knott, "A study of the interaction and coalescence of two coplanar fatigue cracks in bending," *Fatigue & Fracture of Engineering Materials & Structures,* vol. 12, no. 3, pp. 167-174, 1989.

[106] K. a. Kishimoto, W. O. Soboyejo, J. F. Knott, and R. A. Smith, "A numerical investigation of the interaction and coalescence of twin coplanar semi-elliptical fatigue cracks," *International Journal of Fatigue,* vol. 11, no. 2, pp. 91-96, 1989.

[107] H. Dündar and A. O. Ayhan, "Three-dimensional fracture and fatigue crack propagation analysis in structures with multiple cracks," *Computers & Structures,* vol. 158, pp. 259-273, 2015.

[108] R. J. Price and J. Trevelyan, "Boundary element simulation of fatigue crack growth in multi-site damage," *Engineering Analysis with Boundary Elements,* vol. 43, pp. 67-75, 2014.

[109] Y. J. Liu, Y. X. Li, and W. Xie, "Modeling of multiple crack propagation in 2-D elastic solids by the fast multipole boundary element method," *Engineering Fracture Mechanics,* vol. 172, pp. 1-16, 2017.

[110] E. Pierres, M.-C. Baietto, and A. Gravouil, "Experimental and numerical analysis of fretting crack formation based on 3D X-FEM frictional contact fatigue crack model," *Comptes Rendus Mécanique,* vol. 339, no. 7-8, pp. 532-551, 2011.

[111] L. Ziegler and M. Muskulus, "Fatigue reassessment for lifetime extension of offshore wind monopile substructures," 2016, vol. 753: IOP Publishing, 9 ed., p. 092010.
[112] J. F. Barbosa, J. A. F. O. Correia, R. C. S. Freire Junior, S.-P. Zhu, and A. M. P. De Jesus, "Probabilistic SN fields based on statistical distributions applied to metallic and composite materials: State of the art," *Advances in Mechanical Engineering,* vol. 11, no. 8, p. 1687814019870395, 2019.
[113] A. Jacob, J. Oliveira, A. Mehmanparast, F. Hosseinzadeh, J. Kelleher, and F. Berto, "Residual stress measurements in offshore wind monopile weldments using neutron diffraction technique and contour method," *Theoretical and Applied Fracture Mechanics,* vol. 96, pp. 418-427, 2018.
[114] A. Mehmanparast, F. Brennan, and I. Tavares, "Fatigue crack growth rates for offshore wind monopile weldments in air and seawater: SLIC inter-laboratory test results," *Materials & Design,* vol. 114, pp. 494-504, 2017.
[115] X. B. Lin and R. A. Smith, "Fatigue growth prediction of internal surface cracks in pressure vessels," 1998.
[116] I. S. Raju and J. C. Newman Jr, "Stress-intensity factors for internal and external surface cracks in cylindrical vessels," 1982.
[117] B. Standard, "BS 7910: 2013+ A1: 2015 Guide to methods for assessing the acceptability of flaws in metallic structures," *London, UK: BSI Stand Publ,* 2015.
[118] A. P. I. API, "579-1/ASME FFS-1: Fitness-for-service," *The American Society of Mechanical Engineers,* 2007.
[119] I. Hadley, "BS 7910: 2013 in brief," *International Journal of Pressure Vessels and Piping,* vol. 165, pp. 263-269, 2018.
[120] Y.-H. Zhang and M. Doré, "Fatigue crack growth assessment using BS 7910: 2013-Background and recommended developments," *International Journal of Pressure Vessels and Piping,* vol. 168, pp. 79-86, 2018.
[121] V. Igwemezie, A. Mehmanparast, and A. Kolios, "Materials selection for XL wind turbine support structures: A corrosion-fatigue perspective," *Marine Structures,* vol. 61, pp. 381-397, 2018.
[122] En, "Eurocode 3: Design of steel structures: General rules and rules for buildings," ed: CEN, European Committee for Standardization Brussels, 2005.
[123] F. Bozkurt and E. Schmidová, "Fracture Toughness Evaluation of S355 Steel Using Circumferentially Notched Round Bars," *Periodica Polytechnica Transportation Engineering,* vol. 47, no. 2, pp. 91-95, 2019.
[124] *Section III: Rules for construction of nuclear facility components*, ASME, New York, 2015.
[125] S.-X. Wu, "Shape change of surface crack during fatigue growth," *Engineering Fracture Mechanics,* vol. 22, no. 5, pp. 897-913, 1985.
[126] J. Toribio, J.-C. Matos, and B. González, "Aspect ratio evolution in embedded, surface, and corner cracks in finite-thickness plates under tensile fatigue loading," *Applied Sciences,* vol. 7, no. 7, p. 746, 2017.
[127] *User Manual*. (2016). SIMULIA.
[128] W. Brocks and I. Scheider, "Numerical aspects of the path-dependence of the J-integral in incremental plasticity," *GKSS Forschungszentrum, Geesthacht,* vol. 1, pp. 1-33, 2001.
[129] *ASME Boiler and Pressure Code*, ASME, 1995.
[130] D. Mackenzie and H. Li, "A plastic load criterion for inelastic design by analysis," 2006.
[131] D. G. Moffat, M.-F. Hsieh, and M. Lynch, "An assessment of ASME III and CEN TC54 methods of determining plastic and limit loads for pressure system components," *The Journal of Strain Analysis for Engineering Design,* vol. 36, no. 3, pp. 301-312, 2001.
[132] M. R. Booth, "Applying Finite Element Based Limit Load Analysis Methods to Structures Under Dynamic Loads," 2014 2014, vol. 45981: American Society of Mechanical Engineers, p. V001T01A005.

[133] Y.-J. Kim, D.-J. Shim, K. Nikbin, Y.-J. Kim, S.-S. Hwang, and J.-S. Kim, "Finite element based plastic limit loads for cylinders with part-through surface cracks under combined loading," *International Journal of Pressure Vessels and Piping,* vol. 80, no. 7-8, pp. 527-540, 2003.

[134] I. E. C. Iec, "61400-3, Wind Turbines-Part 3: Design Requirements for Offshore Wind Turbines," *International Electrotechnical Commission, Geneva,* 2009.

[135] A. Morató, S. Sriramula, N. Krishnan, and J. Nichols, "Ultimate loads and response analysis of a monopile supported offshore wind turbine using fully coupled simulation," *Renewable Energy,* vol. 101, pp. 126-143, 2017.

[136] J. Jonkman, S. Butterfield, W. Musial, and G. Scott, "Definition of a 5-MW reference wind turbine for offshore system development," National Renewable Energy Lab.(NREL), Golden, CO (United States), 2009.

[137] F. M. Burdekin, B. Talei-Faz, F. P. Brennan, and W. D. Dover, "Experimental validation of the ultimate strength of brace members with circumferential cracks," *OFFSHORE TECHNOLOGY REPORT-HEALTH AND SAFETY EXECUTIVE OTO,* 2002.

[138] M. F. Kanninen *et al.*, "Mechanical fracture predictions for sensitized stainless steel piping with circumferential cracks," Battelle Columbus Labs., 1976.

[139] S. Rahman and G. Wilkowski, "Net-section-collapse analysis of circumferentially cracked cylinders—part I: arbitrary-shaped cracks and generalized equations," *Engineering fracture mechanics,* vol. 61, no. 2, pp. 191-211, 1998.

[140] F. Iwamatsu, K. Miyazaki, K. Saito, T. Hamanaka, and Y. Takahashi, "Estimation of Maximum Load for Pipes With Multiple Circumferential Flaws by Limit Load Analysis," 2011, vol. 44519, pp. 503-510.

[141] K. Hasegawa, K. Saito, F. Iwamatsu, and K. Miyazaki, "Prediction of fully plastic failure stresses for pipes with multiple circumferential flaws," 2007, vol. 42797, pp. 415-419.

[142] F. Iwamatsu, K. Miyazaki, K. Saito, and K. Hasegawa, "Experimental Estimation of Fully Plastic Collapse Stresses for Pipes With Three Circumferential Flaws," 2009, vol. 43642, pp. 223-227.

[143] Y. Li, K. Hasegawa, K. Onizawa, and N. G. Cofie, "Prediction of collapse stress for pipes with arbitrary multiple circumferential surface flaws," *Journal of pressure vessel technology,* vol. 132, no. 6, 2010.

[144] Y. Li, K. Azuma, and K. Hasegawa, "Failure bending moment of pipes containing multiple circumferential flaws with complex shape," *International Journal of Pressure Vessels and Piping,* vol. 171, pp. 305-310, 2019.

[145] Y. Lei and P. J. Budden, "Limit load solutions for thin-walled cylinders with circumferential cracks under combined internal pressure, axial tension and bending," *The Journal of Strain Analysis for Engineering Design,* vol. 39, no. 6, pp. 673-683, 2004.

[146] Ş. E. Eren, T. London, Y. Yang, and I. Hadley, "Validation of plastic collapse assessments using BS 7910: 2013 and R6 procedures," 2013, vol. 55645: American Society of Mechanical Engineers, p. V01BT01A027.

[147] H. F. Bueckner, "Novel principle for the computation of stress intensity factors," *Zeitschrift fuer Angewandte Mathematik & Mechanik,* vol. 50, no. 9, 1970.

[148] J. R. Rice, "Some remarks on elastic crack-tip stress fields," *International Journal of Solids and Structures,* vol. 8, no. 6, pp. 751-758, 1972.

[149] H. J. Petroski and J. D. Achenbach, "Computation of the weight function from a stress intensity factor," *Engineering Fracture Mechanics,* vol. 10, no. 2, pp. 257-266, 1978.

[150] T. Fett, "Limitations of the Petroski-Achenbach procedure demonstrated for a simple load case," *Engineering fracture mechanics,* vol. 29, no. 6, pp. 713-716, 1988.

[151] X. R. Wu, "On the influence of reference load case on the crack face weight functions," *International journal of fracture,* vol. 48, no. 3, pp. 179-192, 1991.

[152] T. Fett, C. Mattheck, and D. Munz, "On the calculation of crack opening displacement from the stress intensity factor," *Engineering Fracture Mechanics,* vol. 27, no. 6, pp. 697-715, 1987.

[153] G. Shen and G. Glinka, "Determination of weight functions from reference stress intensity factors," *Theoretical and applied fracture mechanics,* vol. 15, no. 3, pp. 237-245, 1991.
[154] G. Shen and G. Glinka, "Weight functions for a surface semi-elliptical crack in a finite thickness plate," *Theoretical and Applied Fracture Mechanics,* vol. 15, no. 3, pp. 247-255, 1991.
[155] Z. Li, X. Jiang, and H. Hopman, "Surface crack growth in offshore metallic pipes under cyclic loads: A literature review," *Journal of Marine Science and Engineering,* vol. 8, no. 5, p. 339, 2020.
[156] P. Virtanen *et al.*, "SciPy 1.0: fundamental algorithms for scientific computing in Python," *Nature methods,* vol. 17, no. 3, pp. 261-272, 2020.
[157] G. C. Sih and Y. D. Lee, "Review of triaxial crack border stress and energy behavior," *Theoretical and Applied Fracture Mechanics,* vol. 12, no. 1, pp. 1-17, 1989.
[158] G. C. Sih and C. T. Li, "Initiation and growth characterization of corner cracks near circular hole," *Theoretical and Applied Fracture Mechanics,* vol. 13, no. 1, pp. 69-80, 1990.
[159] W. O. Soboyejo, J. F. Knott, M. J. Walsh, and K. R. Cropper, "Fatigue crack propagation of coplanar semi-elliptical cracks in pure bending," *Engineering Fracture Mechanics,* vol. 37, no. 2, pp. 323-340, 1990.
[160] A. Carpinteri, R. Brighenti, and S. Vantadori, "A numerical analysis on the interaction of twin coplanar flaws," *Engineering Fracture Mechanics,* vol. 71, no. 4-6, pp. 485-499, 2004.
[161] H. E. Coules, "Interaction of surface cracks subjected to non-uniform distributions of stress," *International Journal of Pressure Vessels and Piping,* vol. 157, pp. 20-29, 2017.
[162] H. E. Coules, "Flaw interaction under bending, residual stress and thermal shock loading," *Procedia Structural Integrity,* vol. 13, pp. 361-366, 2018.
[163] H. E. Coules, "Stress intensity interaction between dissimilar semi-elliptical surface cracks," *International Journal of Pressure Vessels and Piping,* vol. 146, pp. 55-64, 2016.
[164] Y. Murakami and S. Nemat-Nasser, "Growth and stability of interacting surface flaws of arbitrary shape," *Engineering Fracture Mechanics,* vol. 17, no. 3, pp. 193-210, 1983.
[165] C. J. Bayley and R. Bell, "Parametric investigation into the coalescence of coplanar fatigue cracks," *International journal of fatigue,* vol. 21, no. 4, pp. 355-360, 1999.
[166] M. Åman, K. Wada, H. Matsunaga, H. Remes, and G. Marquis, "The influence of interacting small defects on the fatigue limits of a pure iron and a bearing steel," *International journal of fatigue,* vol. 135, p. 105560, 2020.
[167] Y. Murakami and S. Nemat-Nasser, "Interacting dissimilar semi-elliptical surface flaws under tension and bending," *Engineering Fracture Mechanics,* vol. 16, no. 3, pp. 373-386, 1982.
[168] M. Kamaya, "Growth evaluation of multiple interacting surface cracks. Part I: Experiments and simulation of coalesced crack," *Engineering Fracture Mechanics,* vol. 75, no. 6, pp. 1336-1349, 2008.
[169] M. Kamaya, E. Miyokawa, and M. Kikuchi, "Growth prediction of two interacting surface cracks of dissimilar sizes," *Engineering Fracture Mechanics,* vol. 77, no. 16, pp. 3120-3131, 2010.
[170] J.-F. Wen, Y. Zhan, S.-T. Tu, and F.-Z. Xuan, "A combination rule for multiple surface cracks based on fatigue crack growth life," *AIMS Materials Science,* vol. 3, no. 4, pp. 1649-1664, 2016.
[171] T. H. Leek and I. C. Howard, "An examination of methods of assessing interacting surface cracks by comparison with experimental data," *International Journal of Pressure Vessels and Piping,* vol. 68, no. 2, pp. 181-201, 1996.
[172] B. Bezensek, J. Sharples, I. Hadley, and H. Pisarski, "The History of BS 7910 Flaw Interaction Criteria," in *Proceedings of the ASME 2011 Pressure Vessels and Piping Conference . Volume 1: Codes and Standards*, Baltimore, Maryland, USA, 2011, vol. 44519: ASME, pp. 837-843.
[173] Z.-J. Zeng, S.-H. Dai, and Y.-M. Yang, "Analysis of surface cracks using the line-spring boundary element method and the virtual crack extension technique," *International journal of fracture,* vol. 60, no. 2, pp. 157-167, 1993.

[174] J. R. Rice and N. Levy, "The part-through surface crack in an elastic plate," 1972.
[175] A. Fajuyigbe and F. Brennan, "Estimating stress intensity factor for semi elliptical circumferential cracks in offshore wind turbine monopiles using weight functions," in *Ageing and Life Extension of Offshore Facilities*, 2022, pp. 158-164.
[176] T. Altan and F. W. Boulger, "Flow stress of metals and its application in metal forming analyses," 1973.
[177] R. A. Ainsworth, J. K. Sharples, and S. D. Smith, "Effects of residual stresses on fracture behaviour—experimental results and assessment methods," *The Journal of Strain Analysis for Engineering Design,* vol. 35, no. 4, pp. 307-316, 2000.
[178] K. Sedighian, J. Mosayebnejac, H. Zakerhaghighi, and H. Ehsasi, "The effect of residual stresses on the fracture behaviour of a cracked body under mixed mode loading," *Procedia Engineering,* vol. 10, pp. 3273-3278, 2011.
[179] V. Ratan and A. M. Shirahatti, "Study of the interaction of residual stress and applied loading on fracture," 2019, vol. 2148: AIP Publishing LLC, 1 ed., p. 030032.
[180] A. A. Oyeniran and D. S. Aziaka, "Residual Stress Consideration in Fatigue Damage of Offshore Wind Turbine Monopiles: To Be or Not to Be?," *World Journal of Mechanics,* vol. 10, no. 04, p. 39, 2020.
[181] R. G. Forman, V. Shivakumar, J. W. Cardinal, L. C. Williams, and P. C. McKeighan, "Fatigue crack growth database for damage tolerance analysis," 2005.
[182] A. Fajuyigbe and F. Brennan, "A simplified formula for calculating the limit load of cracked offshore wind turbine monopile under bending," *Marine Structures,* vol. 83, p. 103164, 2022.
[183] B. Bezensek, Y. Li, K. Hasegawa, and P. H. Hoang, "Inclusion of Torsion Loads in Section XI Flaw Evaluation Procedures for Pipes Containing Circumferential Planar Surface Crack-Like Flaws on the Basis of Limit Load Analysis," *Journal of pressure vessel technology,* vol. 134, no. 3, 2012.
[184] Y. Li, K. Hasegawa, P. H. Hoang, and B. Bezensek, "Prediction method for plastic collapse of pipes subjected to combined bending and torsion moments," 2010, vol. 49200, pp. 81-87.
[185] S. Arun and T. Fongsamootr, "Collapse load analysis for circumferentially cracked cylinder subjected to combined torsion and bending moments," 2018, vol. 192: EDP Sciences, p. 02024.
[186] K. Lesny and J. Wiemann, "Design aspects of monopiles in German offshore wind farms," 2005: AA Balkema Publishing, pp. 383-389.
[187] L. Ziegler, S. Schafhirt, M. Scheu, and M. Muskulus, "Effect of load sequence and weather seasonality on fatigue crack growth for monopile-based offshore wind turbines," *Energy Procedia,* vol. 94, pp. 115-123, 2016.
[188] J. Jonkman and W. Musial, "Offshore code comparison collaboration (OC3) for IEA Wind Task 23 offshore wind technology and deployment," National Renewable Energy Lab.(NREL), Golden, CO (United States), 2010.
[189] H. Solman, J. K. Kirkegaard, M. Smits, B. Van Vliet, and S. Bush, "Digital twinning as an act of governance in the wind energy sector," *Environmental Science & Policy,* vol. 127, pp. 272-279, 2022.
[190] F. Kirkemo, "Applications of probabilistic fracture mechanics to offshore structures," 1988.
[191] J. Stutzmann, L. Ziegler, and M. Muskulus, "Fatigue crack detection for lifetime extension of monopile-based offshore wind turbines," *Energy Procedia,* vol. 137, pp. 143-151, 2017.
[192] *CrackWise®*. (2022). The Welding Institute.

## APPENDIX A – LOAD CASE CHAIN FOR CASE STUDY 2

2-4-4-6-1-6-2-5-3-5-5-3-5-2-5-5-4-4-2-4-9-3-4-3-2-2-7-1-8-2-2-2-3-5-7-4-5-4-2-5-8-6-4-4-1-4-2-5-5-5-6-3-4-4-2-4-
12-3-1-4-6-4-3-4-6-8-3-5-2-3-1-5-2-4-4-2-8-7-2-5-2-2-9-7-3-3-7-7-3-8-6-8-5-5-6-6-3-6-5-5-1-2-4-6-13-5-5-1-1-4-2-
5-9-3-10-2-2-6-6-3-2-5-3-6-10-3-10-6-5-5-6-5-3-2-3-2-7-1-8-3-5-6-3-2-2-4-7-1-3-5-2-3-8-2-3-4-2-3-5-4-4-4-8-11-8-
6-3-2-9-2-8-3-6-5-5-8-6-5-11-3-9-6-9-2-3-3-6-4-3-3-5-6-6-8-5-4-4-6-9-2-5-7-4-2-2-3-2-6-4-2-2-5-6-6-6-3-4-7-2-4-6-
4-2-4-1-6-12-2-6-5-2-8-4-3-6-2-6-5-9-3-1-2-1-2-4-3-3-7-4-8-2-9-4-5-2-2-5-9-5-3-5-7-9-10-6-11-5-2-2-4-4-6-2-4-3-6-
7-3-3-2-6-8-6-1-3-3-6-7-10-3-2-5-6-8-4-3-2-4-3-4-5-3-4-6-6-8-3-3-7-3-2-5-6-5-5-6-2-6-6-8-4-1-1-2-6-5-8-3-6-5-4-
10-8-2-5-4-5-5-7-4-3-5-2-9-7-7-4-3-4-6-2-9-2-5-10-4-2-3-4-9-7-3-3-4-4-3-3-2-4-6-5-6-7-2-3-7-2-2-4-5-5-6-2-6-6-2-
1-8-2-8-4-4-5-2-7-1-6-2-6-5-4-5-6-6-5-10-3-2-4-5-8-8-2-6-5-5-2-6-3-2-4-2-1-4-4-3-7-6-8-5-8-2-4-7-1-6-3-7-4-4-5-3-
2-9-5-5-1-5-2-4-8-6-2-4-4-3-5-3-5-1-5-3-4-7-3-3-3-8-5-10-1-3-4-9-2-8-4-11-9-5-3-8-6-2-8-2-6-1-2-2-3-4-4-3-2-2-1-
5-7-3-7-6-5-3-7-3-2-3-4-5-6-3-4-10-2-4-7-5-4-3-11-3-7-4-5-5-9-3-2-2-10-5-5-7-9-7-2-2-3-5-10-5-3-3-2-7-5-2-7-6-6-
4-5-5-12-2-9-4-5-4-2-8-2-3-2-4-3-1-4-1-5-9-1-1-7-3-2-3-6-3-3-5-2-1-4-7-2-3-5-9-1-6-3-3-5-7-7-4-2-9-7-2-3-6-2-6-7-
6-5-5-3-2-7-4-5-5-8-7-6-2-2-7-3-5-3-6-8-3-9-13-15-8-6-3-2-5-7-3-3-3-5-3-3-2-1-6-5-5-2-4-4-7-2-10-2-4-2-1-4-3-7-4-
6-3-5-7-2-4-3-5-5-12-8-5-5-8-3-3-8-7-4-1-6-5-9-6-4-1-4-6-6-6-6-5-3-3-2-4-6-5-3-4-2-4-4-8-1-6-2-4-6-6-5-4-5-8-2-2-
5-3-5-3-8-6-5-3-4-4-8-6-3-4-4-3-6-3-9-4-7-5-3-5-5-5-6-5-3-4-5-3-5-3-7-2-2-6-6-5-8-7-5-5-8-8-6-10-1-5-9-7-7-5-5-6-
12-8-11-8-4-3-6-2-2-3-1-9-4-4-5-4-4-2-5-2-5-3-4-4-1-6-5-6-4-6-7-1-3-4-8-8-11-7-8-4-2-10-2-8-5-3-5-6-2-5-9-7-3-
10-2-4-1-4-1-9-4-5-5-6-6-6-11-6-8-4-4-10-5-5-4-3-5-3-5-5-8-5-5-3-7-5-7-4-6-8-5-3-7-7-9-11-4-3-6-3-7-2-3-5-2-4-5-
5-9-5-4-4-1-4-7-11-4-5-6-6-4-4-3-9-3-4-9-1-6-5-3-5-3-4-4-2-5-7-3-11-6-3-5-6-3-9-2-8-5-4-3-5-2-5-4-7-4-6-3-7-6-7-
5-8-9-6-8-2-7-2-2-3-2-2-5-8-7-2-3-4-1-4-3-3-6-5-2-6-2-5-2-8-4-5-3-3-2-4-2-7-4-9-4-3-6-6-5-2-4-4-5-3-5-6-8-6-6-8-7-
2-14-4-7-3-2-5-2-9-5-7-3-3-4-5-5-5-3-2-3-3-5-8-6-4-2-3-2-2-5-3-10-6-4-5-6-2-3-7-7-7-2-5-2-3-6-10-4-10-11-4-1-10-
3-2-4-6-7-5-3-3-2-7-7-3-12-3-3-3-1-5-6-8-4-3-5-2-1-10-4-6-3-2-4-4-5-3-3-2-5-1-12-2-6-1-1-5-6-3-4-4-5-3-3-3-2-7-4-
6-6-6-6-5-4-5-2-3-6-6-6-7-4-6-3-6-3-7-5-7-5-7-3-5-3-2-7-7-5-3-8-3-4-3-6-2-7-6-2-6-3-2-4-4-6-2-2-3-11-3-4-5-2-6-3-
9-7-4-1-3-4-4-7-5-2-8-8-4-7-6-6-6-4-6-3-5-3-1-1-10-7-2-5-3-4-2-6-8-3-3-3-1-8-5-11-4-7-6-4-5-2-5-5-4-6-6-4-5-4-2-
6-9-3-3-3-5-4-4-4-2-4-7-9-6-7-6-3-1-8-4-3-8-9-5-6-2-3-1-4-9-5-7-6-4-6-2-4-2-6-2-9-4-8-5-4-1-12-5-3-7-3-5-2-6-7-4-
5-9-4-4-3-3-5-6-11-2-2-8-5-2-7-3-5-2-8-5-9-8-2-5-3-7-2-6-3-5-11-3-2-4-1-1-2-6-6-8-3-4-4-4-5-3-4-9-6-4-6-6-5-7-13-
11-2-5-2-8-4-5-6-3-6-1-2-6-2-5-2-3-1-3-7-3-7-6-3-5-6-2-5-5-7-4-4-5-10-8-3-6-8-6-2-7-3-3-4-3-2-4-3-7-3-1-5-5-5-4-
4-5-7-2-4-7-1-6-4-11-2-8-6-8-4-3-6-7-4-7-3-4-7-1-2-7-8-2-7-9-4-7-1-3-4-5-3-4-1-5-4-7-7-6-6-6-5-5-4-6-2-6-6-2-5-3-
4-11-8-6-2-2-3-3-5-1-6-2-5-4-2-6-8-3-5-4-3-1-4-5-3-1-3-5-6-5-8-8-6-7-2-6-3-2-2-6-4-1-3-3-5-6-5-3-5-4-6-9-8-4-5-4-
3-5-10-6-2-6-3-5-3-3-4-7-4-2-3-6-4-1-8-10-4-8-6-5-6-4-6-6-3-7-6-3-8-6-7-3-2-8-1-4-7-5-2-5-2-3-5-4-3-2-5-1-9-2-3-
6-9-1-5-2-9-6-5-6-7-3-6-7-4-2-5-1-3-7-5-3-4-5-7-5-4-6-5-7-6-10-4-6-9-6-4-8-6-2-4-3-5-11-5-3-2-6-3-5-3-3-3-4-1-4-
8-5-7-5-4-5-3-4-9-8-2-3-3-4-4-7-6-5-3-3-6-4-2-3-11-5-9-3-1-4-3-2-5-3-6-7-4-4-2-1-4-5-4-1-2-2-3-3-4-3-5-4-4-6-4-8-
5-7-6-1-7-6-7-3-8-2-2-7-4-9-2-2-8-9-6-7-3-3-4-4-6-6-5-7-4-7-3-4-2-5-3-4-1-4-4-11-7-6-5-4-3-7-4-4-5-3-2-4-2-4-6-3-
5-8-10-6-2-4-1-10-7-8-1-2-6-2-1-4-3-2-1-6-2-5-10-4-8-4-5-2-3-6-4-13-5-5-4-4-10-4-4-10-6-3-7-3-2-2-1-6-6-4-6-9-7-
2-5-5-3-6-7-5-11-7-2-5-4-4-4-5-9-7-11-5-3-9-5-7-5-3-5-8-8-5-3-6-6-3-10-3-7-2-2-2-9-7-5-2-2-2-3-4-7-6-10-2-2-3-3-
3-4-7-3-4-3-2-4-7-4-5-2-3-1-1-4-9-5-6-6-1-9-2-2-8-5-1-3-1-2-3-10-5-3-4-3-2-5-9-2-5-8-8-5-1-6-5-3-6-3-4-5-8-7-9-8-
5-5-5-5-3-5-5-4-4-8-5-4-2-4-2-4-5-2-1-4-4-6-3-1-3-5-2-10-6-3-7-4-6-2-6-5-3-5-3-6-2-5-7-3-8-4-5-5-5-8-5-7-4-9-2-4-
5-6-8-5-7-1-10-7-2-7-7-5-3-10-3-1-2-2-4-5-3-5-2-3-6-5-5-9-5-13-6-3-3-4-4-5-5-4-3-5-3-6-9-6-8-3-2-6-8-3-3-3-2-4-4-
4-4-3-4-8-3-3-2-4-8-4-5-4-6-8-3-4-5-3-4-2-4-3-6-6-4-3-2-5-1-8-1-8-7-3-5-5-3-4-5-3-1-3-6-1-1-4-4-4-3-4-1-4-4-4-3-5-
8-4-8-6-6-4-4-14-8-3-3-2-4-2-2-2-3-1-7-7-5-6-5-4-3-4-5-8-7-4-6-9-5-2-3-3-6-7-5-4-10-1-7-2-3-4-10-7-6-3-4-2-3-6-4-
2-4-3-2-5-3-1-7-2-8-2-8-8-3-10-4-12-7-4-2-4-6-2-7-7-8-3-3-2-3-4-2-8-3-8-2-4-8-2-5-3-2-4-5-7-2-4-2-4-5-1-3-7-3-3-
3-5-8-5-2-4-7-7-5-6-4-7-2-2-9-3-7-2-2-4-2-5-5-3-3-3-2-6-2-5-5-6-4-2-5-5-9-5-17-4-7-4-6-7-9-4-2-3-2-5-5-4-3-9-4-2-
6-2-4-2-7-10-5-7-10-4-7-2-3-8-2-1-4-3-6-2-8-3-2-8-2-1-6-2-6-8-5-1-4-2-5-5-8-6-2-2-5-9-6-4-5-2-3-5-5-3-11-9-1-4-2-
2-2-2-7-12-4-3-5-3-6-6-9-3-3-6-4-10-1-9-5-5-2-3-4-5-4-3-5-5-4-6-3-10-5-3-6-7-8-2-2-6-3-10-4-2-6-4-1-5-2-4-4-10-
2-2-3-9-6-1-5-3-4-9-8-8-5-4-16-2-6-4-5-3-5-3-7-5-8-4-5-5-8-7-4-8-1-5-4-9-4-8-8-4-4-3-3-7-7-3-4-3-4-3-2-6-7-2-3-6-
6-4-7-5-3-7-7-1-5-3-7-6-6-8-2-5-4-3-3-3-2-11-5-6-3-5-7-3-8-1-2-9-1-2-3-3-4-3-6-3-7-7-3-10-2-3-10-3-3-4-4-5-6-1-3-
3-4-3-4-3-5-5-4-5-5-9-9-9-2-6-5-8-2-7-4-4-5-5-6-7-8-3-1-3-7-6-4-5-6-9-7-5-5-3-8-4-2-2-11-2-6-7-2-5-5-4-4-5-6-3-1-
10-8-5-2-1-3-3-5-5-10-5-9-3-2-8-5-4-11-8-4-5-3-5-8-6-7-2-9-4-5-6-6-3-3-6-2-4-2-3-5-6-4-1-3-2-3-5-5-4-5-5-5-5-3-3-
1-8-7-7-7-5-3-6-4-6-8-3-5-4-5-6-5-6-3-2-3-7-7-8-8-6-5-2-12-11-2-6-4-1-10-2-4-4-6-3-1-7-7-5-3-3-3-3-9-7-4-5-3-4-9-
5-4-5-2-6-2-3-3-4-3-4-2-4-8-5-5-4-7-5-4-5-5-2-4-4-7-6-7-10-2-7-5-3-8-6-1-3-4-5-5-5-5-8-4-4-7-2-4-4-9-4-2-4-6-10-
4-9-9-10-3-5-2-3-4-7-5-1-3-1-1-6-3-9-3-6-4-6-7-3-5-1-9-3-2-5-3-7-4-6-7-8-6-10-1-3-5-4-8-4-1-4-4-4-8-2-6-5-5-5-3-
3-3-5-3-3-3-7-8-7-4-3-2-3-3-9-2-4-7-1-6-2-10-5-5-11-5-7-3-6-4-4-5-3-8-4-4-5-4-3-9-5-3-6-7-7-4-5-5-6-5-4-6-8-2-6-
6-3-5-1-6-2-3-1-4-4-4-7-4-2-2-6-2-2-3-4-7-4-3-2-6-3-6-2-4-4-9-2-7-5-4-9-2-9-5-10-2-2-2-3-3-3-4-8-6-6-8-3-8-3-3-5-
6-6-2-7-8-6-2-4-5-7-4-4-5-6-6-2-4-7-6-2-8-8-6-9-4-12-3-7-2-4-5-4-7-1-6-7-2-3-3-7-3-1-4-7-8-10-7-5-5-5-6-7-2-8-2-
5-4-5-6-6-7-5-2-3-5-4-5-3-1-4-4-9-4-10-3-8-4-2-8-2-6-3-2-4-1-4-6-4-7-5-8-5-2-4-10-8-1-6-7-3-8-11-5-3-3

## APPENDIX B– VARIABLE CRACK DEPTH PROFILE

| Crack Angle (°) | Crack Depth (mm) | Crack Angle (°) | Crack Depth (mm) | Crack Angle (°) | Crack Depth (mm) | Crack Angle (°) | Crack Depth (mm) |
|---|---|---|---|---|---|---|---|
| 0.358 | 55.171 | 79.68 | 0 | 180.48 | 0 | 281.28 | 0 |
| 0.714 | 50.228 | 80.16 | 0 | 180.96 | 0 | 281.76 | 0 |
| 1.07 | 45.171 | 80.64 | 0 | 181.44 | 0 | 282.24 | 0 |
| 1.424 | 40 | 81.12 | 0 | 181.92 | 0 | 282.72 | 0 |
| 1.712 | 45.112 | 81.6 | 0 | 182.4 | 0 | 283.2 | 0 |
| 2 | 50.15 | 82.08 | 0 | 182.88 | 0 | 283.68 | 0 |
| 2.289 | 55.113 | 82.56 | 0 | 183.36 | 0 | 284.16 | 0 |
| 2.58 | 60 | 83.04 | 0 | 183.84 | 0 | 284.64 | 0 |
| 2.884 | 55.124 | 83.52 | 0 | 184.32 | 0 | 285.12 | 0 |
| 3.188 | 50.165 | 84 | 0 | 184.8 | 0 | 285.6 | 0 |
| 3.49 | 45.124 | 84.48 | 0 | 185.28 | 0 | 286.08 | 0 |
| 3.792 | 40 | 84.96 | 0 | 185.76 | 0 | 286.56 | 0 |
| 4.043 | 45.086 | 85.44 | 0 | 186.24 | 0 | 287.04 | 0 |
| 4.295 | 50.114 | 85.92 | 0 | 186.72 | 0 | 287.52 | 0 |
| 4.548 | 55.086 | 86.4 | 0 | 187.2 | 0 | 288 | 0 |
| 4.801 | 60 | 86.88 | 0 | 187.68 | 0 | 288.48 | 0 |
| 5.229 | 55.244 | 87.36 | 0 | 188.16 | 0 | 288.96 | 0 |
| 5.654 | 50.325 | 87.84 | 0 | 188.64 | 0 | 289.44 | 0 |
| 6.079 | 45.243 | 88.32 | 0 | 189.12 | 0 | 289.92 | 0 |
| 6.502 | 40 | 88.8 | 0 | 189.6 | 0 | 290.4 | 0 |
| 6.737 | 50.025 | 89.28 | 0 | 190.08 | 0 | 290.88 | 0 |
| 6.974 | 60 | 89.76 | 0 | 190.56 | 0 | 291.36 | 0 |
| 7.451 | 55.305 | 90.24 | 0 | 191.04 | 0 | 291.84 | 0 |
| 7.927 | 50.406 | 90.72 | 0 | 191.52 | 0 | 292.32 | 0 |
| 8.402 | 45.304 | 91.2 | 0 | 192 | 0 | 292.8 | 0 |
| 8.874 | 40 | 91.68 | 0 | 192.48 | 0 | 293.28 | 0 |
| 9.362 | 45.323 | 92.16 | 0 | 192.96 | 0 | 293.76 | 0 |
| 9.851 | 50.432 | 92.64 | 0 | 193.44 | 0 | 294.24 | 0 |
| 10.342 | 55.324 | 93.12 | 0 | 193.92 | 0 | 294.72 | 0 |
| 10.835 | 60 | 93.6 | 0 | 194.4 | 0 | 295.2 | 0 |
| 11.194 | 55.173 | 94.08 | 0 | 194.88 | 0 | 295.68 | 0 |
| 11.553 | 50.23 | 94.56 | 0 | 195.36 | 0 | 296.16 | 0 |
| 11.91 | 45.172 | 95.04 | 0 | 195.84 | 0 | 296.64 | 0 |
| 12.266 | 40 | 95.52 | 0 | 196.32 | 0 | 297.12 | 0 |
| 12.501 | 45.075 | 96 | 0 | 196.8 | 0 | 297.6 | 0 |
| 12.738 | 50.101 | 96.48 | 0 | 197.28 | 0 | 298.08 | 0 |
| 12.975 | 55.076 | 96.96 | 0 | 197.76 | 0 | 298.56 | 0 |
| 13.213 | 60 | 97.44 | 0 | 198.24 | 0 | 299.04 | 0 |
| 13.772 | 55.418 | 97.92 | 0 | 198.72 | 0 | 299.52 | 0 |
| 14.33 | 50.557 | 98.4 | 0 | 199.2 | 0 | 300 | 60 |
| 14.886 | 45.417 | 98.88 | 0 | 199.68 | 0 | 300.339 | 55.154 |
| 15.439 | 40 | 99.36 | 0 | 200.16 | 0 | 300.677 | 50.204 |

| Crack Angle (°) | Crack Depth (mm) | Crack Angle (°) | Crack Depth (mm) | Crack Angle (°) | Crack Depth (mm) | Crack Angle (°) | Crack Depth (mm) |
|---|---|---|---|---|---|---|---|
| 16.173 | 45.731 | 99.84 | 0 | 200.64 | 0 | 301.014 | 45.153 |
| 16.909 | 50.977 | 100.32 | 0 | 201.12 | 0 | 301.349 | 40 |
| 17.648 | 55.734 | 100.8 | 0 | 201.6 | 0 | 301.558 | 45.059 |
| 18.388 | 60 | 101.28 | 0 | 202.08 | 0 | 301.768 | 50.079 |
| 18.792 | 57.647 | 101.76 | 0 | 202.56 | 0 | 301.978 | 55.059 |
| 19.196 | 55.149 | 102.24 | 0 | 203.04 | 0 | 302.189 | 60 |
| 19.598 | 52.504 | 102.72 | 0 | 203.52 | 0 | 302.605 | 55.232 |
| 20 | 49.715 | 103.2 | 0 | 204 | 0 | 303.021 | 50.309 |
| 20.315 | 47.42 | 103.68 | 0 | 204.48 | 0 | 303.435 | 45.231 |
| 20.63 | 45.036 | 104.16 | 0 | 204.96 | 0 | 303.848 | 40 |
| 20.945 | 42.562 | 104.64 | 0 | 205.44 | 0 | 304.156 | 45.129 |
| 21.258 | 40 | 105.12 | 0 | 205.92 | 0 | 304.466 | 50.173 |
| 21.689 | 45.252 | 105.6 | 0 | 206.4 | 0 | 304.777 | 55.13 |
| 22.121 | 50.336 | 106.08 | 0 | 206.88 | 0 | 305.089 | 60 |
| 22.554 | 55.253 | 106.56 | 0 | 207.36 | 0 | 305.437 | 55.162 |
| 22.989 | 60 | 107.04 | 0 | 207.84 | 0 | 305.784 | 50.216 |
| 23.348 | 55.173 | 107.52 | 0 | 208.32 | 0 | 306.13 | 45.162 |
| 23.707 | 50.23 | 108 | 0 | 208.8 | 0 | 306.475 | 40 |
| 24.064 | 45.172 | 108.48 | 0 | 209.28 | 0 | 306.592 | 45.019 |
| 24.42 | 40 | 108.96 | 0 | 209.76 | 0 | 306.71 | 50.025 |
| 24.71 | 45.114 | 109.44 | 0 | 210.24 | 0 | 306.828 | 55.019 |
| 25.001 | 50.153 | 109.92 | 0 | 210.72 | 0 | 306.946 | 60 |
| 25.293 | 55.115 | 110.4 | 0 | 211.2 | 0 | 307.222 | 55.102 |
| 25.586 | 60 | 110.88 | 0 | 211.68 | 0 | 307.497 | 50.136 |
| 25.901 | 55.133 | 111.36 | 0 | 212.16 | 0 | 307.772 | 45.102 |
| 26.215 | 50.177 | 111.84 | 0 | 212.64 | 0 | 308.045 | 40 |
| 26.528 | 45.132 | 112.32 | 0 | 213.12 | 0 | 308.358 | 45.133 |
| 26.84 | 40 | 112.8 | 0 | 213.6 | 0 | 308.672 | 50.178 |
| 27.454 | 45.512 | 113.28 | 0 | 214.08 | 0 | 308.987 | 55.134 |
| 28.07 | 50.684 | 113.76 | 0 | 214.56 | 0 | 309.303 | 60 |
| 28.688 | 55.514 | 114.24 | 0 | 215.04 | 0 | 309.502 | 55.053 |
| 29.308 | 60 | 114.72 | 0 | 215.52 | 0 | 309.701 | 50.071 |
| 29.61 | 55.122 | 115.2 | 0 | 216 | 0 | 309.899 | 45.053 |
| 29.912 | 50.163 | 115.68 | 0 | 216.48 | 0 | 310.097 | 40 |
| 30.212 | 45.122 | 116.16 | 0 | 216.96 | 0 | 310.307 | 40.06 |
| 30.511 | 40 | 116.64 | 0 | 217.44 | 0 | 310.518 | 40.08 |
| 30.997 | 45.32 | 117.12 | 0 | 217.92 | 0 | 310.728 | 40.06 |
| 31.484 | 50.428 | 117.6 | 0 | 218.4 | 0 | 310.939 | 40 |
| 31.973 | 55.322 | 118.08 | 0 | 218.88 | 0 | 311.271 | 45.15 |
| 32.464 | 60 | 118.56 | 0 | 219.36 | 0 | 311.604 | 50.2 |
| 33.022 | 55.417 | 119.04 | 0 | 219.84 | 0 | 311.939 | 55.15 |
| 33.579 | 50.555 | 119.52 | 0 | 220.32 | 0 | 312.274 | 60 |
| 34.134 | 45.416 | 120 | 0 | 220.8 | 0 | 312.617 | 55.157 |
| 34.687 | 40 | 120.48 | 0 | 221.28 | 0 | 312.959 | 50.209 |

| Crack Angle (°) | Crack Depth (mm) | Crack Angle (°) | Crack Depth (mm) | Crack Angle (°) | Crack Depth (mm) | Crack Angle (°) | Crack Depth (mm) |
|---|---|---|---|---|---|---|---|
| 34.866 | 45.044 | 120.96 | 0 | 221.76 | 0 | 313.3 | 45.157 |
| 35.045 | 50.058 | 121.44 | 0 | 222.24 | 0 | 313.639 | 40 |
| 35.226 | 55.044 | 121.92 | 0 | 222.72 | 0 | 313.927 | 45.113 |
| 35.406 | 60 | 122.4 | 0 | 223.2 | 0 | 314.216 | 50.151 |
| 35.522 | 55.018 | 122.88 | 0 | 223.68 | 0 | 314.506 | 55.113 |
| 35.638 | 50.024 | 123.36 | 0 | 224.16 | 0 | 314.797 | 60 |
| 35.753 | 45.018 | 123.84 | 0 | 224.64 | 0 | 315.071 | 55.1 |
| 35.868 | 40 | 124.32 | 0 | 225.12 | 0 | 315.344 | 50.133 |
| 36.091 | 45.068 | 124.8 | 0 | 225.6 | 0 | 315.615 | 45.1 |
| 36.316 | 50.091 | 125.28 | 0 | 226.08 | 0 | 315.886 | 40 |
| 36.541 | 55.068 | 125.76 | 0 | 226.56 | 0 | 316.332 | 45.27 |
| 36.767 | 60 | 126.24 | 0 | 227.04 | 0 | 316.779 | 50.361 |
| 37.579 | 56.137 | 126.72 | 0 | 227.52 | 0 | 317.228 | 55.271 |
| 38.389 | 51.685 | 127.2 | 0 | 228 | 0 | 317.678 | 60 |
| 39.196 | 46.645 | 127.68 | 0 | 228.48 | 0 | 318.227 | 55.403 |
| 40 | 41.022 | 128.16 | 0 | 228.96 | 0 | 318.774 | 50.536 |
| 40.034 | 40.768 | 128.64 | 0 | 229.44 | 0 | 319.319 | 45.401 |
| 40.069 | 40.513 | 129.12 | 0 | 229.92 | 0 | 319.863 | 40 |
| 40.103 | 40.257 | 129.6 | 0 | 230.4 | 0 | 319.897 | 40.257 |
| 40.137 | 40 | 130.08 | 0 | 230.88 | 0 | 319.931 | 40.513 |
| 40.681 | 45.401 | 130.56 | 0 | 231.36 | 0 | 319.966 | 40.768 |
| 41.226 | 50.536 | 131.04 | 0 | 231.84 | 0 | 320 | 41.022 |
| 41.773 | 55.403 | 131.52 | 0 | 232.32 | 0 | 320.804 | 46.645 |
| 42.322 | 60 | 132 | 0 | 232.8 | 0 | 321.611 | 51.685 |
| 42.772 | 55.271 | 132.48 | 0 | 233.28 | 0 | 322.421 | 56.137 |
| 43.221 | 50.361 | 132.96 | 0 | 233.76 | 0 | 323.233 | 60 |
| 43.668 | 45.27 | 133.44 | 0 | 234.24 | 0 | 323.459 | 55.068 |
| 44.114 | 40 | 133.92 | 0 | 234.72 | 0 | 323.684 | 50.091 |
| 44.385 | 45.1 | 134.4 | 0 | 235.2 | 0 | 323.909 | 45.068 |
| 44.656 | 50.133 | 134.88 | 0 | 235.68 | 0 | 324.132 | 40 |
| 44.929 | 55.1 | 135.36 | 0 | 236.16 | 0 | 324.362 | 50.024 |
| 45.203 | 60 | 135.84 | 0 | 236.64 | 0 | 324.594 | 60 |
| 45.494 | 55.113 | 136.32 | 0 | 237.12 | 0 | 324.955 | 50.058 |
| 45.784 | 50.151 | 136.8 | 0 | 237.6 | 0 | 325.313 | 40 |
| 46.073 | 45.113 | 137.28 | 0 | 238.08 | 0 | 325.866 | 45.416 |
| 46.361 | 40 | 137.76 | 0 | 238.56 | 0 | 326.421 | 50.555 |
| 46.7 | 45.157 | 138.24 | 0 | 239.04 | 0 | 326.978 | 55.417 |
| 47.041 | 50.209 | 138.72 | 0 | 239.52 | 0 | 327.536 | 60 |
| 47.383 | 55.157 | 139.2 | 0 | 240 | 0 | 328.027 | 55.322 |
| 47.726 | 60 | 139.68 | 0 | 240.48 | 0 | 328.516 | 50.428 |
| 48.061 | 55.15 | 140.16 | 0 | 240.96 | 0 | 329.003 | 45.32 |
| 48.396 | 50.2 | 140.64 | 0 | 241.44 | 0 | 329.489 | 40 |
| 48.729 | 45.15 | 141.12 | 0 | 241.92 | 0 | 329.788 | 45.122 |
| 49.061 | 40 | 141.6 | 0 | 242.4 | 0 | 330.088 | 50.163 |

| Crack Angle (°) | Crack Depth (mm) | Crack Angle (°) | Crack Depth (mm) | Crack Angle (°) | Crack Depth (mm) | Crack Angle (°) | Crack Depth (mm) |
|---|---|---|---|---|---|---|---|
| 49.272 | 40.06 | 142.08 | 0 | 242.88 | 0 | 330.39 | 55.122 |
| 49.482 | 40.08 | 142.56 | 0 | 243.36 | 0 | 330.692 | 60 |
| 49.693 | 40.06 | 143.04 | 0 | 243.84 | 0 | 331.312 | 55.514 |
| 49.903 | 40 | 143.52 | 0 | 244.32 | 0 | 331.93 | 50.684 |
| 50.101 | 45.053 | 144 | 0 | 244.8 | 0 | 332.546 | 45.512 |
| 50.299 | 50.071 | 144.48 | 0 | 245.28 | 0 | 333.16 | 40 |
| 50.498 | 55.053 | 144.96 | 0 | 245.76 | 0 | 333.472 | 45.132 |
| 50.697 | 60 | 145.44 | 0 | 246.24 | 0 | 333.785 | 50.177 |
| 51.013 | 55.134 | 145.92 | 0 | 246.72 | 0 | 334.099 | 55.133 |
| 51.328 | 50.178 | 146.4 | 0 | 247.2 | 0 | 334.414 | 60 |
| 51.642 | 45.133 | 146.88 | 0 | 247.68 | 0 | 334.707 | 55.115 |
| 51.955 | 40 | 147.36 | 0 | 248.16 | 0 | 334.999 | 50.153 |
| 52.228 | 45.102 | 147.84 | 0 | 248.64 | 0 | 335.29 | 45.114 |
| 52.503 | 50.136 | 148.32 | 0 | 249.12 | 0 | 335.58 | 40 |
| 52.778 | 55.102 | 148.8 | 0 | 249.6 | 0 | 335.936 | 45.172 |
| 53.054 | 60 | 149.28 | 0 | 250.08 | 0 | 336.293 | 50.23 |
| 53.172 | 55.019 | 149.76 | 0 | 250.56 | 0 | 336.652 | 55.173 |
| 53.29 | 50.025 | 150.24 | 0 | 251.04 | 0 | 337.011 | 60 |
| 53.408 | 45.019 | 150.72 | 0 | 251.52 | 0 | 337.446 | 55.253 |
| 53.525 | 40 | 151.2 | 0 | 252 | 0 | 337.879 | 50.336 |
| 53.87 | 45.162 | 151.68 | 0 | 252.48 | 0 | 338.311 | 45.252 |
| 54.216 | 50.216 | 152.16 | 0 | 252.96 | 0 | 338.742 | 40 |
| 54.563 | 55.162 | 152.64 | 0 | 253.44 | 0 | 339.055 | 42.562 |
| 54.911 | 60 | 153.12 | 0 | 253.92 | 0 | 339.37 | 45.036 |
| 55.223 | 55.13 | 153.6 | 0 | 254.4 | 0 | 339.685 | 47.42 |
| 55.534 | 50.173 | 154.08 | 0 | 254.88 | 0 | 340 | 49.715 |
| 55.844 | 45.129 | 154.56 | 0 | 255.36 | 0 | 340.402 | 52.504 |
| 56.152 | 40 | 155.04 | 0 | 255.84 | 0 | 340.804 | 55.149 |
| 56.565 | 45.231 | 155.52 | 0 | 256.32 | 0 | 341.208 | 57.647 |
| 56.979 | 50.309 | 156 | 0 | 256.8 | 0 | 341.612 | 60 |
| 57.395 | 55.232 | 156.48 | 0 | 257.28 | 0 | 342.106 | 57.21 |
| 57.811 | 60 | 156.96 | 0 | 257.76 | 0 | 342.599 | 54.203 |
| 58.022 | 55.059 | 157.44 | 0 | 258.24 | 0 | 343.091 | 50.977 |
| 58.232 | 50.079 | 157.92 | 0 | 258.72 | 0 | 343.582 | 47.534 |
| 58.442 | 45.059 | 158.4 | 0 | 259.2 | 0 | 344.072 | 43.875 |
| 58.651 | 40 | 158.88 | 0 | 259.68 | 0 | 344.561 | 40 |
| 58.986 | 45.153 | 159.36 | 0 | 260.16 | 0 | 345.114 | 45.417 |
| 59.323 | 50.204 | 159.84 | 0 | 260.64 | 0 | 345.67 | 50.557 |
| 59.661 | 55.154 | 160.32 | 0 | 261.12 | 0 | 346.228 | 55.418 |
| 60 | 60 | 160.8 | 0 | 261.6 | 0 | 346.787 | 60 |
| 60.48 | 0 | 161.28 | 0 | 262.08 | 0 | 347.025 | 55.076 |
| 60.96 | 0 | 161.76 | 0 | 262.56 | 0 | 347.262 | 50.101 |
| 61.44 | 0 | 162.24 | 0 | 263.04 | 0 | 347.499 | 45.075 |
| 61.92 | 0 | 162.72 | 0 | 263.52 | 0 | 347.734 | 40 |

| Crack Angle (°) | Crack Depth (mm) | Crack Angle (°) | Crack Depth (mm) | Crack Angle (°) | Crack Depth (mm) | Crack Angle (°) | Crack Depth (mm) |
|---|---|---|---|---|---|---|---|
| 62.4 | 0 | 163.2 | 0 | 264 | 0 | 348.09 | 45.172 |
| 62.88 | 0 | 163.68 | 0 | 264.48 | 0 | 348.447 | 50.23 |
| 63.36 | 0 | 164.16 | 0 | 264.96 | 0 | 348.806 | 55.173 |
| 63.84 | 0 | 164.64 | 0 | 265.44 | 0 | 349.165 | 60 |
| 64.32 | 0 | 165.12 | 0 | 265.92 | 0 | 349.658 | 55.324 |
| 64.8 | 0 | 165.6 | 0 | 266.4 | 0 | 350.149 | 50.432 |
| 65.28 | 0 | 166.08 | 0 | 266.88 | 0 | 350.638 | 45.323 |
| 65.76 | 0 | 166.56 | 0 | 267.36 | 0 | 351.126 | 40 |
| 66.24 | 0 | 167.04 | 0 | 267.84 | 0 | 351.598 | 45.304 |
| 66.72 | 0 | 167.52 | 0 | 268.32 | 0 | 352.073 | 50.406 |
| 67.2 | 0 | 168 | 0 | 268.8 | 0 | 352.549 | 55.305 |
| 67.68 | 0 | 168.48 | 0 | 269.28 | 0 | 353.026 | 60 |
| 68.16 | 0 | 168.96 | 0 | 269.76 | 0 | 353.145 | 55.019 |
| 68.64 | 0 | 169.44 | 0 | 270.24 | 0 | 353.263 | 50.025 |
| 69.12 | 0 | 169.92 | 0 | 270.72 | 0 | 353.381 | 45.019 |
| 69.6 | 0 | 170.4 | 0 | 271.2 | 0 | 353.498 | 40 |
| 70.08 | 0 | 170.88 | 0 | 271.68 | 0 | 353.921 | 45.243 |
| 70.56 | 0 | 171.36 | 0 | 272.16 | 0 | 354.346 | 50.325 |
| 71.04 | 0 | 171.84 | 0 | 272.64 | 0 | 354.771 | 55.244 |
| 71.52 | 0 | 172.32 | 0 | 273.12 | 0 | 355.199 | 60 |
| 72 | 0 | 172.8 | 0 | 273.6 | 0 | 355.452 | 55.086 |
| 72.48 | 0 | 173.28 | 0 | 274.08 | 0 | 355.705 | 50.114 |
| 72.96 | 0 | 173.76 | 0 | 274.56 | 0 | 355.957 | 45.086 |
| 73.44 | 0 | 174.24 | 0 | 275.04 | 0 | 356.208 | 40 |
| 73.92 | 0 | 174.72 | 0 | 275.52 | 0 | 356.51 | 45.124 |
| 74.4 | 0 | 175.2 | 0 | 276 | 0 | 356.812 | 50.165 |
| 74.88 | 0 | 175.68 | 0 | 276.48 | 0 | 357.116 | 55.124 |
| 75.36 | 0 | 176.16 | 0 | 276.96 | 0 | 357.42 | 60 |
| 75.84 | 0 | 176.64 | 0 | 277.44 | 0 | 357.711 | 55.113 |
| 76.32 | 0 | 177.12 | 0 | 277.92 | 0 | 358 | 50.15 |
| 76.8 | 0 | 177.6 | 0 | 278.4 | 0 | 358.288 | 45.112 |
| 77.28 | 0 | 178.08 | 0 | 278.88 | 0 | 358.576 | 40 |
| 77.76 | 0 | 178.56 | 0 | 279.36 | 0 | 358.93 | 45.171 |
| 78.24 | 0 | 179.04 | 0 | 279.84 | 0 | 359.286 | 50.228 |
| 78.72 | 0 | 179.52 | 0 | 280.32 | 0 | 359.642 | 55.171 |
| 79.2 | 0 | 180 | 0 | 280.8 | 0 | 360 | 60 |